TGAL-87-05

COMPREHENSIVE MAGNITUDE YIELD ESTIMATION FOR NUCLEAR EXPLOSIONS: A MAXIMUM LIKELIHOOD GENERAL LINEAR MODEL (MLE-GLM88)

W.W. Chan, K.L. McLaughlin, R.-S. Jih, M.E. Marshall, and R.A. Wagner

Teledyne Geotech Alexandria Laboratories
314 Montgomery Street
Alexandria, Virginia 22314-1581

JUNE 1988

FINAL TECHNICAL REPORT: TASKS 1 and 2
ARPA ORDER NO: A05143
PROJECT TITLE: Yield Estimation and Regional Location
CONTRACT: MDA903-87C-0069

Prepared for:
DEFENSE ADVANCED RESEARCH PROJECTS AGENCY
1400 Wilson Boulevard
Arlington, VA 22209

Monitored by:
Defense Supply Service, Washington
Room 1D 245, The Pentagon
Washington, D.C. 20310

Unclassified
SECURITY CLASSIFICATION OF THIS PAGE

ADA203389

REPORT DOCUMENTATION PAGE

Form Approved
OMB No 0704-0188
Exp Date Jun 30, 1986

1a REPORT SECURITY CLASSIFICATION Unclassified	1b RESTRICTIVE MARKINGS
2a SECURITY CLASSIFICATION AUTHORITY	3 DISTRIBUTION/AVAILABILITY OF REPORT Approved for Public Release; Distribution Unlimited
2b DECLASSIFICATION/DOWNGRADING SCHEDULE	
4 PERFORMING ORGANIZATION REPORT NUMBER(S) TGAL-87-05	5 MONITORING ORGANIZATION REPORT NUMBER(S)
6a NAME OF PERFORMING ORGANIZATION Teledyne Geotech Alexandria Laboratories 6b OFFICE SYMBOL (If applicable)	7a NAME OF MONITORING ORGANIZATION Defense Supply Service, Washington
6c ADDRESS (City, State, and ZIP Code) 314 Montgomery Street Alexandria, Virginia 22314	7b ADDRESS (City, State, and ZIP Code) Room 1D245, The Pentagon Washington, D.C. 20310
8a NAME OF FUNDING/SPONSORING ORGANIZATION DARPA 8b OFFICE SYMBOL (If applicable) NMRO	9 PROCUREMENT INSTRUMENT IDENTIFICATION NUMBER MDA903-87C-0069
8c ADDRESS (City, State, and ZIP Code) 1400 Wilson Boulevard Arlington, Virginia 22209	10 SOURCE OF FUNDING NUMBERS PROGRAM ELEMENT NO. / PROJECT NO. / TASK NO / WORK UNIT ACCESSION NO

11 TITLE (Include Security Classification)
Comprehensive Magnetitude Yield Estimation for Nuclear Explosions: A Maximum Likelihood General Linear Model (MLE-GLM88)

12 PERSONAL AUTHOR(S)
W.W. Chan, K.L. McLaughlin, R-S. Jih, M.E. Marshall and R.A. Wagner

13a TYPE OF REPORT	13b TIME COVERED	14 DATE OF REPORT (Year, Month, Day)	15 PAGE COUNT
Final Technical	FROM June 87 TO June 88	June 1988	117

16 SUPPLEMENTARY NOTATION
from '19

17 COSATI CODES			18 SUBJECT TERMS (Continue on reverse if necessary and identify by block number)
FIELD	GROUP	SUB-GROUP	General Linear Model, Maximum likelihood, yield estimation, body waves,

19 ABSTRACT (Continue on reverse if necessary and identify by block number)

This study performs maximum likelihood event magnitudes and station effects for 111 nuclear explosions from more than 8 different test sites using a general linear model. The estimates are performed for the three P-wave phases "a", "b", and "max" by considering the signals, non-detection, and clipping information. The bias between a model that does not include censoring effects from non-detection and clipping is demonstrated. The maximum-likelihood magnitude estimates are performed using data for each phase individually and the three phases combined. The difference in m_b's between the phases is studied for some of the major test sites. A presumed multiple event is found to be characterized with large "max" phase amplitude compared to the "a" phase, whereas in the case of a presumed cratering event showing surficial collapse, the amplitudes for the "b" and "max" phases are smaller instead. In addition, ~~we also examined~~ the biases at several test sites that may

20 DISTRIBUTION/AVAILABILITY OF ABSTRACT	21 ABSTRACT SECURITY CLASSIFICATION
☒ UNCLASSIFIED/UNLIMITED ☐ SAME AS RPT ☐ DTIC USERS	
22a NAME OF RESPONSIBLE INDIVIDUAL Dr. Robert R. Blandford	22b TELEPHONE (Include Area Code) (202) 697-7523 22c OFFICE SYMBOL NMRO

DD FORM 1473, 84 MAR 83 APR edition may be used until exhausted
All other editions are obsolete

SECURITY CLASSIFICATION OF THIS PAGE
Unclassified

(19. continued)

exist for general linear models based on a specific test site relative to a model that contains sources from many test sites. The effects of assuming correlation among the events on the magnitude estimates using the present event-station distribution are investigated using an inter-event correlation model.

SUMMARY

This study performs maximum likelihood event magnitudes and station effects for 111 nuclear explosions from more than 8 different test sites using a general linear model. The estimates are performed for the three P-wave phases "a", "b", and "max" by considering the signals, non-detection, and clipping information. The bias between a model that does not include censoring effects from non-detection and clipping is demonstrated. The maximum-likelihood magnitude estimates are performed using data for each phase individually and the three phases combined. The difference in m_b's between the phases is studied for some of the major test sites. A presumed multiple event is found to be characterized with large "max" phase amplitude compared to the "a" phase, whereas in the case of a presumed cratering event showing surficial collapse, the amplitudes for the "b" and "max" phases are smaller instead. In addition, we also examined the biases at several test sites that may exist for general linear models based on a specific test site relative to a model that contains sources from many test sites. The effects of assuming correlation among the events on the magnitude estimates using the present event-station distribution are investigated using an inter-event correlation model.

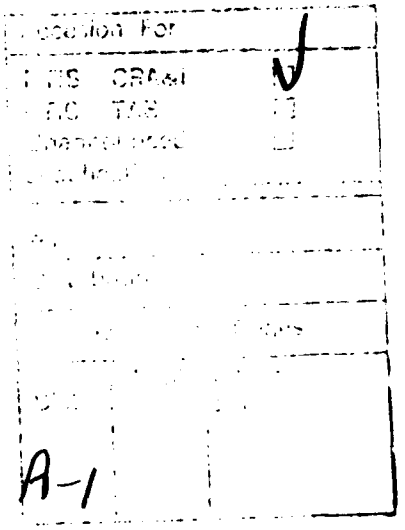

(THIS PAGE INTENTIONALLY LEFT BLANK)

TABLE OF CONTENTS

LIST OF FIGURES

LIST OF TABLES

1.0 INTRODUCTION

This study presents results of the analysis of the P-wave amplitudes for 111 explosions from over 8 major test sites world-wide as well as numerous US and foreign peaceful nuclear explosions located away from the established test sites. The data base consists of seismic measurements made from the short-period WWSSN film chips for these events. The maximum-likelihood estimation general linear model program, *MLGLM,* was developed to estimate the magnitudes for these events in a model framework. In magnitude-yield estimation studies, it is important to provide event-magnitude calibration within a large data set to give relative magnitudes between events. We report on the estimation of maximum-likelihood magnitudes and station correction terms, MLE-GLM88. This model is used to document some of the statistical biases that occur in typical processing of data for magnitude:yield estimation. In addition, we have also incorporated event-event correlation into the magnitude estimations for the large database, which involves inverting an immense matrix with the aid of a supercomputer. A maximum-likelihood estimation of the error terms is also used which proves to be more efficient and practical than the bootstrap method.

Douglas (1966) has applied the general linear model (GLM) to magnitude estimation as the least squares multiple factor program (LSMF). Heasler *et al.* (1988) have discussed the formulation of a modeling and estimation theory (GLM) and tested it on NTS data. The GLM program is widely used to calibrate a network of stations and gives estimates of the precision of relative event magnitudes for a given test site. The model assumes that the observed magnitude at each station for each event is the sum of independent event and station terms:

$$m_{ij} = E_i + S_j + \varepsilon_{ij}$$

where E_i is the i'th event magnitude, S_j is the j'th station term, and ε_{ij} is an independent normal random error with zero mean and standard deviation, σ. This linear model has been validated and solved using standard linear methods. However, traditional solutions to this system of linear equations cannot accommodate censoring information such as clipping or non-detection levels for the individual station magnitudes. Such information has been found to be relevant to the magnitude estimation problem either when events are small and low amplitude stations are excluded by non-detection, or when events are large and large magnitudes are excluded by clipping. In either case, we can use the censoring information such as $m_{ij} \leq m^d_{ij}$, or $m_{ij} \geq m^c_{ij}$, in a maximum likelihood formulation of the GLM, where m^d_{ij} is the magnitude at the lowest detectable level and m^c_{ij} is the magnitude at the critically clipped level to provide constraints to the model.

Ringdal (1977) introduced the maximum likelihood estimator (MLE) to correct for the statistical bias introduced by data censoring from non-detection. Von Seggern and Rivers (1978) extended the procedure to include data censoring by clipping. Blandford and Shumway (1982) further extended the maximum likelihood estimator to the GLM in the presence of data censoring using the expectation maximization algorithm (MLE-GLM). They simultaneously estimated event magnitudes and station corrections in a maximum likelihood sense. This MLE-GLM is to the LSMF program what the Ringdal MLE procedure is to the single event network average. The following table summarizes the inter-relationships of these estimation procedures. In the case of no censoring, the MLE-GLM reduces to the least squares linear estimation problem

(LS-GLM) and in the case of no station effects the least squares linear problem reduces to a network average.

Table 1. Inter-Relationships of Magnitude Estimators

	No station effects 1 Dimension	station effects N+M-1 Dimensions
No censoring	Network Mean	LS-GLM
Censoring	MLE	MLE-GLM

where M is the number of stations and N is the number of events.

The expectation maximization algorithm was applied to the linear estimation problem with two additional improvements by Blandford *et al.* (1984). They proposed to use a bootstrapping scheme to estimate the uncertainty for the maximum likelihood general linear model and to introduce data correlation estimates to the GLM in order to reduce the biasing effects of uneven data sampling.

The general linear model (GLM) was improved by Blandford and Shumway (1982) to relate amplitude readings, event magnitudes, and station effects to include the data censoring effects of clipping and non-detection. The technique was applied to WWSSN short-period recordings of NTS and Algerian shots in granite (Blandford and Shumway, 1982), and after corrections for pP it was concluded that there was only a small offset in magnitude between the NTS and Algerian shots. A number of other event magnitudes were also determined, and the station corrections resulting were compared to those of North (1977) with fairly good agreement.

It was noted in Blandford and Shumway (1982) that a weakness of the mathematical procedure was the assumption that readings from explosions in close proximity to each other were independent. Thus if many events were entered into the linear model from a single test site, and if those amplitudes were in fact highly correlated, then the station corrections would tend to reflect that particular path and not truly represent the average structure under the stations. Again, this could lead to inaccurate relative magnitudes between events at widely different test sites. In Blandford *et al.* (1984) this was remedied by estimating the event-event correlation and incorporating the resulting correlation matrix (regarded as *a priori*) into the theory.

A method of computing confidence intervals for this complex problem was also developed and applied by Blandford *et al.* (1984) using the bootstrap methods of Efron (1979, 1981). This becomes an attractive method for uncertainty estimation as computing power becomes less expensive and more readily available. It is an extension of the "Jackknife" method where each N-1 subset of the N data is examined in turn to test for stability of the results to subtle changes in the data set. The bootstrap procedure resamples the entire data set M times treating the data as the next best thing to an ensemble of realizations. Each resampling is used to estimate the model parameters and the ensemble of model parameters is used to estimate the stability of the final model estimate. This procedure is used to evaluate the results of the maximum likelihood estimators for the GLM rather than evaluate the multi-dimensional partial derivative matrix of the GLM's likelihood function. McLaughlin (1988) has shown how to apply the bootstrap procedure to single event maximum likelihood magnitude estimation. Of course, the bootstrap procedure has many more potential geophysical

applications than just the magnitude estimation problem.

2.0 DATA ANALYSIS

The expectation maximization (EM) algorithm (Dempster *et al.*, 1977) may be applied to solve the multi-parameter version of the maximum likelihood estimation problem originally considered by Ringdal (1977) when the errors in observing the amplitudes are uncorrelated from event to event and from station to station. This method, as has been applied by Blandford and Shumway (1982) is desirable since the log-likelihood is a non-linear function of the residuals, non-detection levels, and clipping levels. The number of unknowns (N+M-1) for the multi-parameter estimation problem is equal to one less than the sum of the number of events (N) and the number of stations (M). For problems of interest, this commonly exceeds 200 and a systematic search of a 200 dimensional solution space becomes very inefficient. The EM algorithm is an iterative technique for maximizing the log-likelihood function that reduces to the least squares solution in the event that there is no data censoring. A detailed description of the algorithm is presented in Blandford and Shumway (1982) and Blandford *et al.* (1984). The estimation procedure has been formalized in a program called *MLGLM* (see Appendix) written in FORTRAN-77 running on VAX 11/780, SUN 3/160, Celerity 12600, and Cray XP/II computer systems.

An additional problem with maximum likelihood solutions is the estimation of uncertainties of the estimated model parameters. Although this problem can be written in closed form for the least squares solution of linear problems, the same procedure would require the determination of all second order partial derivatives of the log-likelihood function. Calculation of such a large Jacobian for a non-linear function of many dimensions is highly undesirable. An alternative to this is the Bootstrap

procedure of Efron (1979, 1981). The Bootstrapping procedure has been applied to single event magnitude estimation by McLaughlin (1988) for uncertainty estimation. Using the standard deviations of the perturbing noise returned by the EM algorithm as a measure of the uncertainty in any single measurement, Jih *et al.* (1988) proposed another method to estimate the errors. In this case, the σ is scaled with the number of associated observations to infer the precision of each estimated parameter.

2.1 Data Measurement

The work of Ringdal (1977) and of von Seggern and Rivers (1978) emphasized the importance in measuring or estimating noise and clipping levels in order to be able to calculate unbiased magnitudes. In contrast to Ringdal (1986) or Lilwall (1985), we measure the non-detection threshold levels and clipping levels for each station and event. It should, however, be possible to extend this work to estimate detection thresholds and/or clipping levels for use with bulletin data such as the ISC.

In order to assure the greatest degree of commonality between stations and events in this study, we have used WWSSN short-period film data. While use of these data has been difficult in the past due to their susceptibility to either clipping or masking by system or earth noise, the advent of the ability to allow for noise and clipping within the context of a general linear model reduces these difficulties and allows the WWSSN network to be superior than others for all except the smallest events. The WWSSN network is valuable because it has had a constant instrument response over a long period of time with a good spatial distribution relative to most test sites. The following measurement procedures from Blandford *et al.* (1984) are repeated here for complete-

ness.

2.2 Film Reading Procedures Used in this Study

1. Read the "a" (zero-crossing to first peak), "b" (first peak to first trough), and "max" peak-to-trough or trough-to-peak in the first 5 seconds, in millimeters. Record readings in millimeters in the data file. Also, record gain as written on the film and as seen with particular viewer.
2. Measure period for max as peak-to-peak or zero-crossing to zero-crossing or trough-to-trough as in your judgement best reflects the period of the maximum energy.
3. If a weak signal must be measured then try to find a strong signal from the same test site and by correlation try to establish if a particular cycle is "a" or "b". In general, it is good practice to analyze events in pairs, with any weak events paired with a strong event.
4. If it is not possible to determine the exact location of the "a" or "b" cycles then the first clear down-swing is to be used to place a "noise" limit on the "b" cycle; that is, the true "b" amplitude is less than or equal to that down-swing. Apply a similar method for the "a" phase if there is a clear up-swing which cannot confidently be said to be a phase.
5. More commonly, however, there will be no clear up-swing; in this case a noise measurement must be made, and to do so search the preceding 20 seconds for the largest peak-to-trough excursion in the 1-2 Hz frequency range. (For the a phase find the largest zero-to-peak.) Often such amplitudes are less than 1 mm on WWSSN film. The period is to be recorded as 1 Hz.
6. Of course, if no arrival at all can be discerned then again a noise measurement must be made.
7. If the peak for any phase can not be found (clipped) then a conservative estimate of the clipping level must be made. To do this measure the amplitude of the largest "turning point" visible and multiply by 2. If you can be confident that the largest turning point is off the film then you could use the maximum distance to the edge of the film. If you can not discern any turning points and can not determine whether the trace is off the film in the first 5 seconds of the P arrival, then measure the largest on-scale peak-to-peak P coda that is visible. These measurements should be recorded as clipping levels.
8. In data reduction, all measurements with raw amplitudes less than 1 mm are converted to noise or non-detection levels. The predominant period, T, measured from the maximum P phase in the first 5 seconds,,,, is used to correct the amplitudes of "a", "b", and "max" for instrument response, A(T), and to calculate A(T)/T. For non-detection and clipping, the period, T, is assumed to be 1 second.

3.0 MLE-GLM88

The maximum-likelihood generalized linear model, MLE-GLM88, for event magnitude estimation is performed with 111 events as listed in Table 2. The m_b(a), and m_b(b), and m_b(max) for each of the events are listed in Table 3. The "a", "b", and "max" magnitudes for each event are treated as separate events in the model, and therefore all data from all events for all phases are used to estimate simultaneously all event magnitudes and station corrections in a maximum likelihood sense.

The events are grouped by test site: Cannikin, Longshot, and Milrow at the Amchitka test site; Salmon, Gasbuggy, Rulison, Rio Blanco, Faultless, and Shoal are U.S. shots located away from NTS; Almendro, Benham, Bilby, Bourbon, Boxcar, Cambric, Chancellor, Chartreuse, Corduroy, Handcar, Handley, Harzer, Kankakee, Mast, Nash, Piledriver, Rex, and Scotch at NTS; Beryl, Corundon, Emeraude, Grenat, Opale, Rubis, Saphir, Tourmaline, and Turquoise at the French southern Sahara test site; "dek" identifies the Degelen Eastern Kazakhstan test site; "sek" identifies the Shagan River Eastern Kazakhstan test site; "nnz" identifies the northern Novaya Zemlya test site; "snz" identifies the southern Novaya Zemlya test site; "pne" identifies one event located in the northern Urals; "azg" identifies events located near Azgir; "tu" identifies the Tuomotu test site; "raj18may74" is the Indian underground test located in Rajasthan, India; and "ch" identifies events located in southern Sinkiang, China. The number of observations indicates the number of stations for which a signal amplitude, noise level, or clipping level measurement was made. The event magnitude and station correction uncertainties were estimated using the EM algorithm. The least squares estimates LS-GLM are also listed for comparison. Although 111 events are listed for

"b" and "max" phase, 5 events had no direct observations of the "a" phase and only 106 events could be included for the "a" phase magnitude.

Table 2. MLE-GLM88 Event List

EVENT	DATE	OT	LAT	LON	H(M)	MED	m_b	NAME
1	651029	21:00:00.0	51.44N	179.18E	701	AN	5.9	LONGSHOT
2	691002	22:06:00.0	51.42N	179.18E	1219	LV	6.6	MILROW
3	711106	22:00:00.0	51.47N	179.11E	1791	BA	7.0	CANNIKIN
4	630913	13:53:00.0	37.06N	116.53W	714	TF	5.7	BILBY
5	660224	15:55:00.0	37.27N	116.43W	672	TF	4.7	REX
6	660506	15:00:00.0	37.35N	116.32W	667	RH	5.5	CHARTREUSE
7	670523	14:00:00.0	37.27N	116.37W	978	TF	5.6	SCOTCH
8	680426	15:00:00.0	37.29N	116.46W	1158	TF/RH	6.5	BOXCAR
9	680628	12:22:00.0	37.25N	116.48W	617	RH	5.3	CHATEAUGAY
10	681219	16:30:00.0	37.23N	116.47W	1402	TF	6.4	BENHAM
11	700326	19:00:00.0	37.30N	116.53W	1206	TF	6.6	HANDLEY
12	730606	13:00:00.0	37.25N	116.35W	1063	RH	6.1	ALMENDRO
13	750619	13:00:00.0	37.35N	116.32W	912	TF	6.0	MAST
14	810606	18:00:00.0	37.20N	116.33W	637	TF	5.5	HARZER
15	830901	14:00:00.0	37.27N	116.36W	-	-	5.4	CHANCELLOR
16	641105	15:00:00.0	37.17N	116.07W	403	DO	4.7	HANDCAR
17	650514	14:57:52.0	36.82N	115.97W	295	AL	4.6	CAMBRIC
18	651203	15:13:02.0	37.16N	116.05W	679	TF	5.6	CORDUROY
19	660602	15:30:00.0	37.23N	116.06W	462	GR	5.5	PILEDRIVER
20	660615	18:02:47.0	37.17N	116.05W	455	DO	4.8	KANKAKEE
21	670119	16:45:00.0	37.14N	116.14W	365	DO	5.4	NASH
22	670120	17:40:04.0	37.10N	116.00W	559	DO	5.2	BOURBON
23	631026	17:00:00.0	39.20N	118.38W	367	GR	4.8	SHOAL
24	680119	18:15:00.0	38.63N	116.21W	975	TF	6.5	FAULTLESS
25	690910	21:00:00.0	39.41N	107.95W	2575	SS/SH	4.6	RULISON
26	671210	19:30:00.0	36.68N	107.21W	1293	SH	4.8	GASBUGGY
27	730517	16:00:00.0	39.79N	108.37W	2010	SS	4.9	RIO BLANCO
28	641022	16:00:00.0	31.14N	89.57W	828	ST	4.3	SALMON

EVENT	DATE	OT	LAT	LON	m_b	TEST SITE
29	650115	05:59:58.4	49.88N	78.96E	5.8	SHAGAN RIVER
30	680619	05:05:57.4	49.96N	79.05E	5.4	SHAGAN RIVER
31	691130	03:32:57.3	49.94N	78.98E	6.0	SHAGAN RIVER
32	730723	01:22:57.8	49.98N	78.85E	6.2	SHAGAN RIVER
33	731214	07:46:57.1	50.03N	79.02E	5.8	SHAGAN RIVER
34	750427	05:36:57.2	49.94N	79.02E	5.6	SHAGAN RIVER
35	760704	02:56:57.5	49.85N	78.97E	5.8	SHAGAN RIVER
36	761207	04:56:57.5	49.87N	78.89E	5.9	SHAGAN RIVER
37	780611	02:56:57.7	49.88N	78.81E	5.7	SHAGAN RIVER
38	780915	02:36:57.3	49.91N	78.94E	6.0	SHAGAN RIVER
39	790623	02:56:57.6	49.91N	78.91E	6.2	SHAGAN RIVER
40	800914	02:42:39.3	49.97N	78.88E	5.9	SHAGAN RIVER
41	661218	04:57:57.7	49.90N	77.80E	5.6	DEGELEN
42	670226	03:57:57.6	49.77N	78.15E	5.7	DEGELEN
43	690911	04:01:57.0	49.70N	78.11E	5.0	DEGELEN
44	710425	03:32:58.0	49.82N	78.09E	5.9	DEGELEN
45	711230	06:20:57.7	49.75N	78.13E	5.6	DEGELEN
46	770329	03:56:57.7	49.79N	78.14E	4.8	DEGELEN
47	770730	01:56:58.0	49.77N	78.16E	4.8	DEGELEN
48	780326	03:56:57.6	49.73N	78.07E	5.6	DEGELEN
49	780422	03:06:57.6	49.72N	78.17E	5.3	DEGELEN

Table 2. (cont'd)

EVENT	DATE	OT	LAT	LON	m_b	TEST SITE
50	730927	06:59:58.0	70.75N	53.87E	5.7	S. NOVAYA ZEMLYA
51	731027	06:59:57.4	70.77N	54.17E	6.9	S. NOVAYA ZEMLYA
52	731027	08:21:20.7	70.89N	52.86E	4.2	S. NOVAYA ZEMLYA
53	731027	09:13:51.3	71.29N	51.87E	4.8	S. NOVAYA ZEMLYA
54	741102	04:59:56.7	70.81N	54.06E	7.0	S. NOVAYA ZEMLYA
55	751018	08:59:56.3	70.84N	53.69E	6.9	S. NOVAYA ZEMLYA
56	661027	05:57:57.7	73.40N	54.90E	6.5	N. NOVAYA ZEMLYA
57	671021	04:59:58.1	73.40N	54.80E	5.6	N. NOVAYA ZEMLYA
58	681107	10:02:05.3	73.40N	54.85E	6.0	N. NOVAYA ZEMLYA
59	691014	07:00:06.2	73.40N	54.81E	6.5	N. NOVAYA ZEMLYA
60	701014	05:59:57.1	73.31N	55.14E	6.7	N. NOVAYA ZEMLYA
61	710927	05:59:55.2	73.38N	55.10E	6.4	N. NOVAYA ZEMLYA
62	720828	05:59:56.5	73.33N	55.08E	6.3	N. NOVAYA ZEMLYA
63	730912	06:59:54.3	73.30N	55.16E	6.8	N. NOVAYA ZEMLYA
64	740829	09:59:55.5	73.36N	55.09E	6.6	N. NOVAYA ZEMLYA
65	750823	08:59:57.9	73.36N	54.64E	6.5	N. NOVAYA ZEMLYA
66	751021	11:59:57.3	73.35N	55.07E	6.6	N. NOVAYA ZEMLYA
67	761020	08:00:00.0	73.00N	55.00E	4.7	N. NOVAYA ZEMLYA
68	770901	02:59:57.5	73.37N	54.58E	5.7	N. NOVAYA ZEMLYA
69	780810	07:59:57.7	73.33N	54.79E	5.9	N. NOVAYA ZEMLYA
70	801011	07:09:57.0	73.35N	54.99E	5.8	N. NOVAYA ZEMLYA
71	811001	12:14:56.7	73.31N	54.81E	5.9	N. NOVAYA ZEMLYA
72	830818	16:09:58.6	73.38N	54.91E	5.9	N. NOVAYA ZEMLYA
73	841025	06:29:57.7	73.37N	54.96E	5.9	N. NOVAYA ZEMLYA
74	740829	14:59:59.6	67.23N	62.11E	4.7	N. URAL MTNS.
75	660422	02:58:03.0	47.90N	47.70E	4.7	AZGIR
76	711222	06:59:56.0	47.87N	48.22E	6.0	AZGIR
77	750425	04:59:57.0	47.50N	47.50E	4.8	AZGIR
78	760729	05:00:00.0	47.78N	48.12E	5.9	AZGIR
79	770930	07:00:00.0	48.80N	48.14E	4.8	AZGIR
80	781017	04:59:56.0	47.81N	48.11E	5.8	AZGIR
81	781218	07:59:56.0	47.78N	48.19E	5.9	AZGIR
82	791024	05:59:56.0	47.80N	48.15E	5.8	AZGIR
83	790714	04:59:55.0	47.81N	48.09E	5.6	AZGIR
84	790117	07:59:55.0	47.88N	48.12E	6.0	AZGIR

Table 2. (cont'd)

EVENT	DATE	OT	LAT	LON	H(M)	MED	m_b	LOCATION
85	770219	23:29:57.9	22.100S	138.760W	-	BA	4.7	MURUROA
86	770319	23:00:58.1	21.890S	138.960W	-	-	5.7	MURUROA
87	771124	16:59:58.5	21.895S	138.960W	-	-	5.8	MURUROA
88	781130	17:31:58.4	21.903S	138.975W	-	-	5.8	MURUROA
89	790725	17:56:58.3	21.892S	138.993W	-	-	6.0	MURUROA
90	800323	19:36:58.4	21.878S	139.020W	-	-	5.6	MURUROA
91	800719	23:46:58.2	21.886S	139.019W	-	-	5.7	MURUROA
92	801203	17:32:58.2	21.938S	138.961W	-	-	5.6	MURUROA
93	820725	18:01:58.1	21.864S	138.943W	-	-	5.6	MURUROA
94	830419	18:52:58.4	21.847S	138.900W	-	-	5.6	MURUROA
95	830525	17:30:58.2	21.900S	138.920W	-	-	5.9	MUROROA
96	620501	10:00:00.458	24.0630N	5.0419E	-	GR	4.7	BERYL
97	630318	10:02:00.351	24.0414N	5.0522E	-	GR	4.6	EMERAUDE
98	631020	13:00:00.011	24.0355N	5.0386E	-	GR	5.5	RUBIS
99	640214	11:00:00.347	24.0536N	5.0524E	-	GR	4.1	OPALE
100	641128	10:30:00.035	24.0419N	5.0417E	-	GR	4.2	TURQUOISE
101	650227	11:30:00.039	24.0587N	5.0312E	785	GR	5.8	SAPHIR
102	651001	10:00:00.043	24.0649N	5.0341E	-	GR	4.2	CORUNDON
103	651201	10:30:00.088	24.0437N	5.0469E	-	GR	4.6	TOURMALINE
104	660216	11:00:00.035	24.0442N	5.0412E	-	GR	4.8	GRENAT

EVENT	DATE	OT	LAT	LON	m_b	LOCATION
105	690922	16:14:58.9	41.350N	88.330E	5.2	SINKIANG
106	751027	00:59:59.0	41.430N	88.400E	4.5	SINKIANG
107	761017	05:00:00.0	41.000N	89.000E	4.6	SINKIANG
108	831006	10:00:02.8	41.570N	88.760E	5.5	SINKIANG
109	841003	05:59:57.8	41.600N	88.730E	5.3	SINKIANG
110	841219	06:00:04.2	41.680N	88.440E	4.7	SINKIANG

EVENT	DATE	OT	LAT	LON	m_b	LOCATION
111	740518	02:34:55.3	26.94N	71.70E	5.0	INDIA

	MEDIUM
AN	ANDESITE
BA	BASALT
GR	GRANITE
LV	LAVA
RH	RHYOLITE
SH	SHALE
SS	SANSTONE
ST	SALT
TF	TUFF

Table 3a. MLE-GLM88 m_b(a)

	MLE-GLM		LS-GLM		# of observations		
event	m_b	σ	m_b	σ	signal	noise	clipped
cannikin	6.411	0.040	6.416	0.036	55	2	12
milrow	5.947	0.044	5.958	0.037	51	5	0
longshot	5.056	0.038	5.362	0.046	33	39	3
faultless	5.833	0.046	5.841	0.039	47	4	1
gasbuggy	4.144	0.047	5.058	0.188	2	47	0
rio blanco	4.042	0.056	4.522	0.153	3	32	0
rulison	4.038	0.048	4.610	0.153	3	44	0
shoal	4.274	0.051	4.847	0.133	4	38	0
salmon	3.450	0.053	4.288	0.266	1	38	0
almendro	5.735	0.062	5.747	0.055	23	3	2
benham	5.785	0.046	5.871	0.043	39	11	1
bilby	5.143	0.052	5.380	0.058	21	19	0
bourbon	4.576	0.047	4.992	0.089	9	40	0
boxcar	5.833	0.054	5.945	0.052	26	10	1
cambric	4.092	0.049	4.623	0.133	4	42	0
chancellor	4.882	0.060	5.241	0.100	7	22	1
chartreuse	4.872	0.048	5.102	0.064	17	30	1
chateaugay	4.467	0.048	5.042	0.153	3	42	2
corduroy	4.972	0.057	5.180	0.071	14	19	0
handcar	4.305	0.047	4.824	0.119	5	45	0
handley	6.064	0.050	6.054	0.041	42	1	0
harzer	5.005	0.053	5.362	0.077	12	25	1
kankakee	4.334	0.046	4.976	0.108	6	45	0
mast	5.406	0.059	5.527	0.054	24	7	0
nash	4.750	0.045	5.119	0.069	15	38	0
piledriver	4.918	0.046	5.094	0.055	23	29	0
rex	3.867	0.045	4.451	0.188	2	51	0
scotch	5.068	0.048	5.215	0.058	21	26	1
azg14jul79	4.841	0.099	5.235	0.153	3	7	1
azg17jan79	5.528	0.088	5.602	0.089	9	2	3
azg17oct78	5.287	0.095	5.494	0.089	9	2	1
azg18dec78	5.379	0.095	5.682	0.108	6	4	2
azg22apr66	3.863	0.091	5.009	0.266	1	12	0
azg22dec71	5.483	0.088	5.629	0.074	13	1	0
azg24oct79	4.863	0.110	5.251	0.188	2	6	1
azg29jul76	5.105	0.045	5.444	0.055	23	26	4
azg30sep77	4.043	0.045	5.025	0.188	2	51	0

Table 3a. (cont'd)

	MLE-GLM		LS-GLM		# of observations		
event	m_b	σ	m_b	σ	signal	noise	clipped
dek11sep69	3.976	0.043	4.761	0.153	3	57	0
dek18dec66	5.253	0.040	5.459	0.041	42	25	0
dek22apr78	4.477	0.060	4.892	0.094	8	22	0
dek25apr71	5.278	0.050	5.459	0.049	30	13	0
dek26feb67	5.369	0.041	5.510	0.038	48	18	0
dek26mar78	4.965	0.058	5.235	0.069	15	17	0
dek29mar77	4.315	0.054	4.771	0.094	8	29	0
dek30dec71	5.018	0.074	5.263	0.077	12	8	0
dek30jul77	4.196	0.053	4.816	0.133	4	34	0
nnz01oct81	5.230	0.046	5.360	0.045	35	14	3
nnz01sep77	5.093	0.060	5.270	0.057	22	8	0
nnz07nov68	5.597	0.041	5.695	0.037	51	11	4
nnz10aug78	5.395	0.043	5.447	0.040	45	8	7
nnz11oct80	5.185	0.046	5.256	0.046	33	14	5
nnz12sep73	6.369	0.049	6.325	0.050	28	0	17
nnz14oct69	5.762	0.040	5.809	0.037	53	9	6
nnz14oct70	6.434	0.043	6.424	0.039	47	1	10
nnz18aug83	5.327	0.052	5.414	0.049	30	8	2
nnz20oct76	4.027	0.043	4.641	0.108	6	54	0
nnz21oct67	5.397	0.042	5.538	0.039	46	15	1
nnz21oct75	6.106	0.051	6.112	0.048	31	1	9
nnz23aug75	6.119	0.051	6.134	0.045	35	0	6
nnz25oct84	5.158	0.061	5.318	0.063	18	10	1
nnz27oct66	6.071	0.039	6.061	0.035	58	2	11
nnz27sep71	6.269	0.049	6.248	0.048	31	1	13
nnz28aug72	5.993	0.050	5.996	0.046	34	2	8
nnz29aug74	6.128	0.050	6.155	0.047	32	1	10
snz02nov74	6.504	0.051	6.440	0.053	25	0	16
snz18oct75	6.227	0.051	6.228	0.047	32	1	9
snz27oc73a	6.650	0.053	6.555	0.063	18	0	20
snz27oc73c	3.522	0.053	4.216	0.266	1	38	0
snz27sep73	5.182	0.054	5.326	0.049	29	8	0
sek04jul76	5.245	0.074	5.422	0.069	15	5	0
sek07dec76	4.990	0.076	5.451	0.084	10	9	0
sek11jun78	5.272	0.076	5.452	0.071	14	5	0
sek14dec73	5.242	0.042	5.476	0.048	31	29	1
sek14sep80	5.436	0.056	5.654	0.053	25	10	0

Table 3a. (cont'd)

	MLE-GLM		LS-GLM		# of observations		
event	m_b	σ	m_b	σ	signal	noise	clipped
sek15jan65	5.491	0.046	5.569	0.041	42	7	3
sek15sep78	5.429	0.054	5.593	0.054	24	11	2
sek19jun68	4.598	0.056	4.964	0.084	10	24	0
sek23jul73	5.740	0.051	5.788	0.041	41	1	0
sek23jun79	5.622	0.050	5.761	0.045	35	8	0
sek27apr75	4.969	0.076	5.125	0.066	16	3	0
sek30nov69	5.361	0.056	5.554	0.055	23	11	0
pne29aug74	3.998	0.049	4.567	0.108	6	39	0
ch03oct84	4.463	0.070	5.019	0.153	3	19	0
ch06oct83	4.761	0.059	5.189	0.108	6	24	1
ch17oct76	3.886	0.048	4.772	0.188	2	45	0
ch19dec84	3.972	0.091	4.563	0.266	1	12	0
ch22sep69	4.322	0.051	5.019	0.119	5	37	0
ch27oct75	4.139	0.054	4.953	0.153	3	34	0
raj18may74	4.023	0.060	4.881	0.266	1	29	0
tu03dec80	4.690	0.050	5.147	0.080	11	32	0
tu19apr83	4.991	0.069	5.202	0.077	12	11	0
tu19jul80	4.888	0.051	5.179	0.063	18	24	0
tu19mar77	5.146	0.063	5.450	0.071	14	13	0
tu23mar80	4.678	0.049	5.070	0.094	8	36	1
tu24nov77	5.043	0.057	5.348	0.064	17	16	0
tu25jul79	5.076	0.078	5.645	0.108	6	12	0
tu25jul82	4.675	0.056	5.054	0.089	9	26	0
tu25may83	5.141	0.078	5.360	0.094	8	10	0
tu30nov78	4.821	0.047	5.306	0.080	11	37	1
beryl	4.378	0.078	5.203	0.188	2	16	0
corundon	3.794	0.045	4.458	0.188	2	52	0
grenat	4.290	0.041	5.045	0.100	7	58	0
opale	3.761	0.045	5.183	0.266	1	52	0
rubis	4.810	0.048	5.149	0.061	19	29	0
saphir	5.180	0.041	5.396	0.042	40	23	0
tourmaline	4.098	0.040	4.786	0.119	5	62	0

Table 3b. MLE-GLM88 m_b(b)

event	MLE-GLM m_b	σ	LS-GLM m_b	σ	# of observations signal	noise	clipped
cannikin	6.667	0.040	6.598	0.037	51	0	18
longshot	5.432	0.038	5.537	0.036	54	18	3
milrow	6.198	0.044	6.146	0.036	54	0	2
faultless	6.158	0.046	6.128	0.038	48	1	3
gasbuggy	4.404	0.047	4.890	0.089	9	40	0
rio blanco	4.537	0.056	4.903	0.084	10	25	0
rulison	4.151	0.048	4.676	0.119	5	42	0
salmon	3.979	0.053	4.387	0.119	5	34	0
shoal	4.426	0.051	4.775	0.084	10	32	0
almendro	6.031	0.062	6.005	0.052	26	0	2
benham	6.103	0.046	6.056	0.039	46	1	4
bilby	5.407	0.052	5.459	0.046	34	6	0
bourbon	4.711	0.047	5.014	0.071	14	35	0
boxcar	6.178	0.054	6.108	0.046	33	0	4
cambric	4.341	0.049	4.660	0.084	10	36	0
chancellor	5.176	0.060	5.313	0.066	16	13	1
chartreuse	5.001	0.048	5.135	0.053	25	22	1
chateaugay	4.882	0.048	5.198	0.071	14	30	3
corduroy	5.091	0.057	5.359	0.069	15	18	0
handcar	4.496	0.047	4.719	0.071	14	36	0
handley	6.309	0.050	6.298	0.041	41	1	1
harzer	5.305	0.053	5.388	0.051	27	10	1
kankakee	4.591	0.046	4.837	0.061	19	32	0
mast	5.735	0.059	5.761	0.049	29	2	0
nash	4.914	0.045	5.085	0.052	26	27	0
piledriver	5.191	0.046	5.283	0.044	36	16	0
rex	4.372	0.045	4.669	0.077	12	41	0
scotch	5.348	0.048	5.470	0.047	32	15	1
azg14jul79	5.375	0.099	5.509	0.094	8	1	2
azg17jan79	5.880	0.088	5.885	0.084	10	0	4
azg17oct78	5.737	0.095	5.781	0.094	8	0	4
azg18dec78	5.751	0.095	5.859	0.089	9	1	2
azg22apr66	4.100	0.091	4.494	0.153	3	10	0
azg22dec71	5.835	0.088	5.879	0.074	13	0	1
azg24oct79	5.696	0.110	5.691	0.153	3	1	5
azg25apr75	3.915	0.080	4.817	0.266	1	16	0
azg29jul76	5.580	0.045	5.612	0.042	40	6	7
azg30sep77	4.579	0.045	4.976	0.069	15	37	1

Table 3b. (cont'd)

	MLE-GLM		LS-GLM		# of observations		
event	m_b	σ	m_b	σ	signal	noise	clipped
dek11sep69	4.232	0.043	4.710	0.089	9	51	0
dek18dec66	5.491	0.040	5.608	0.037	53	14	0
dek22apr78	4.781	0.060	5.051	0.064	17	13	0
dek25apr71	5.552	0.050	5.629	0.043	38	5	0
dek26feb67	5.609	0.041	5.705	0.037	52	12	2
dek26mar78	5.284	0.058	5.392	0.055	23	9	0
dek29mar77	4.710	0.054	4.953	0.061	19	18	0
dek30dec71	5.366	0.074	5.452	0.064	17	3	0
dek30jul77	4.595	0.053	4.918	0.071	14	24	0
nnz01oct81	5.492	0.046	5.511	0.041	42	4	6
nnz01sep77	5.426	0.060	5.492	0.052	26	3	1
nnz07nov68	5.845	0.041	5.842	0.035	57	2	7
nnz10aug78	5.630	0.043	5.590	0.041	41	3	16
nnz11oct80	5.445	0.046	5.472	0.041	42	5	5
nnz12sep73	6.699	0.049	6.615	0.058	21	0	24
nnz14oct69	5.960	0.040	5.979	0.036	55	5	8
nnz14oct70	6.648	0.043	6.546	0.043	39	0	19
nnz18aug83	5.531	0.052	5.567	0.049	29	6	5
nnz20oct76	4.353	0.043	4.717	0.066	16	43	1
nnz21oct67	5.595	0.042	5.685	0.037	52	9	1
nnz21oct75	6.348	0.051	6.302	0.049	29	0	12
nnz23aug75	6.381	0.051	6.339	0.049	30	0	11
nnz25oct84	5.434	0.061	5.452	0.055	23	3	3
nnz27oct66	6.306	0.039	6.255	0.036	54	1	16
nnz27sep71	6.487	0.049	6.401	0.052	26	0	19
nnz28aug72	6.254	0.050	6.200	0.047	32	0	12
nnz29aug74	6.397	0.050	6.312	0.053	25	1	17
snz02nov74	6.799	0.051	6.633	0.064	17	0	24
snz18oct75	6.519	0.051	6.427	0.052	26	0	16
snz27oc73a	6.879	0.053	6.698	0.071	14	0	24
snz27oc73b	4.007	0.054	4.340	0.108	6	31	0
snz27oc73c	3.854	0.053	4.335	0.133	4	35	0
snz27sep73	5.474	0.054	5.570	0.048	31	5	1
sek04jul76	5.609	0.074	5.690	0.063	18	1	1
sek07dec76	5.439	0.078	5.485	0.063	18	0	0
sek11jun78	5.579	0.078	5.638	0.064	17	1	0
sek14dec73	5.546	0.042	5.659	0.041	41	16	4

Table 3b. (cont'd)

	MLE-GLM		LS-GLM		# of observations		
event	m_b	σ	m_b	σ	signal	noise	clipped
sek14sep80	5.748	0.056	5.861	0.049	30	5	0
sek15jan65	5.736	0.046	5.763	0.038	48	1	3
sek15sep78	5.708	0.054	5.693	0.048	31	2	4
sek19jun68	4.999	0.056	5.104	0.052	26	7	1
sek23jul73	5.992	0.051	6.041	0.042	40	1	1
sek23jun79	5.852	0.050	5.914	0.043	39	4	0
sek27apr75	5.288	0.076	5.423	0.064	17	2	0
sek30nov69	5.757	0.056	5.803	0.046	33	1	0
pne29aug74	4.401	0.049	4.637	0.059	20	25	0
ch03oct84	4.756	0.070	5.016	0.094	8	14	0
ch06oct83	5.030	0.059	5.232	0.071	14	16	1
ch17oct76	4.142	0.048	4.745	0.119	5	42	0
ch19dec84	3.954	0.091	4.663	0.266	1	12	0
ch22sep69	4.747	0.051	4.866	0.053	25	17	0
ch27oct75	4.402	0.054	4.672	0.084	10	27	0
raj18may74	4.307	0.060	4.746	0.119	5	25	0
tu03dec80	4.982	0.050	5.197	0.054	24	19	0
tu19apr83	5.193	0.069	5.304	0.063	18	5	0
tu19feb77	4.363	0.049	4.700	0.080	11	34	0
tu19jul80	5.160	0.051	5.279	0.047	32	9	1
tu19mar77	5.445	0.063	5.534	0.058	21	6	0
tu23mar80	5.106	0.050	5.243	0.057	22	19	3
tu24nov77	5.364	0.060	5.488	0.053	25	5	0
tu25jul79	5.563	0.078	5.632	0.066	16	2	0
tu25jul82	5.035	0.056	5.200	0.058	21	14	0
tu25may83	5.446	0.078	5.458	0.069	15	3	0
tu30nov78	5.235	0.047	5.384	0.048	31	17	1
beryl	4.755	0.078	5.028	0.084	10	8	0
corundon	3.897	0.045	4.500	0.133	4	50	0
emeraude	4.218	0.051	4.795	0.100	7	34	0
grenat	4.495	0.041	4.845	0.057	22	43	0
opale	3.847	0.045	4.507	0.153	3	50	0
rubis	5.155	0.048	5.316	0.044	36	12	0
saphir	5.460	0.041	5.563	0.036	54	8	1
tourmaline	4.424	0.040	4.821	0.063	18	49	0
turqoise	3.925	0.040	4.492	0.133	4	63	0

Table 3c. MLE-GLM88 m_b(max)

	MLE-GLM		LS-GLM		# of observations		
event	m_b	σ	m_b	σ	signal	noise	clipped
cannikin	6.916	0.040	6.832	0.038	49	0	20
milrow	6.497	0.044	6.433	0.037	52	0	4
longshot	5.823	0.038	5.854	0.032	67	4	3
faultless	6.458	0.046	6.433	0.038	48	1	3
gasbuggy	4.654	0.047	5.177	0.080	11	38	0
rio blanco	4.803	0.056	5.042	0.069	15	20	0
rulison	4.524	0.048	4.915	0.084	10	37	0
shoal	4.713	0.051	5.047	0.071	14	28	0
salmon	4.183	0.053	4.503	0.108	6	33	0
almendro	6.238	0.062	6.215	0.052	26	0	2
benham	6.357	0.046	6.285	0.041	43	1	7
bilby	5.655	0.052	5.666	0.044	37	3	0
bourbon	4.897	0.047	5.199	0.063	18	31	0
boxcar	6.399	0.054	6.329	0.046	33	0	4
cambric	4.550	0.049	4.901	0.077	12	34	0
chancellor	5.329	0.060	5.503	0.066	16	13	1
chartreuse	5.242	0.048	5.338	0.048	31	16	1
chateaugay	5.063	0.048	5.399	0.064	17	28	2
corduroy	5.282	0.057	5.527	0.063	18	15	0
handcar	4.629	0.047	4.845	0.066	16	34	0
handley	6.481	0.050	6.475	0.041	41	1	1
harzer	5.527	0.053	5.545	0.048	31	6	1
kankakee	4.842	0.046	5.045	0.054	24	27	0
mast	5.971	0.059	5.990	0.049	30	1	0
nash	5.144	0.045	5.285	0.048	31	22	0
piledriver	5.431	0.046	5.500	0.043	38	13	1
rex	4.717	0.045	4.933	0.066	16	36	1
scotch	5.603	0.048	5.655	0.043	39	8	1
azg14jul79	5.705	0.099	5.747	0.084	10	0	1
azg17jan79	6.161	0.088	6.192	0.084	10	0	4
azg17oct78	6.112	0.095	6.122	0.100	7	0	5
azg18dec78	6.118	0.095	6.161	0.089	9	0	3
azg22apr66	4.181	0.091	4.657	0.153	3	10	0
azg22dec71	6.173	0.088	6.208	0.077	12	0	2
azg24oct79	5.980	0.110	5.961	0.153	3	0	6
azg25apr75	3.954	0.080	4.857	0.266	1	16	0
azg29jul76	5.865	0.045	5.891	0.041	41	5	7
azg30sep77	4.816	0.045	5.141	0.058	21	31	1

Table 3c. (cont'd)

	MLE-GLM		LS-GLM		# of observations		
event	m_b	σ	m_b	σ	signal	noise	clipped
dek11sep69	4.571	0.043	4.932	0.061	19	41	0
dek18dec66	5.704	0.040	5.764	0.035	58	8	1
dek22apr78	5.028	0.060	5.196	0.058	21	9	0
dek25apr71	5.739	0.050	5.831	0.043	38	5	0
dek26feb67	5.829	0.041	5.892	0.037	51	9	6
dek26mar78	5.505	0.058	5.581	0.052	26	6	0
dek29mar77	4.989	0.053	5.172	0.053	25	14	0
dek30dec71	5.544	0.074	5.639	0.064	17	3	0
dek30jul77	4.859	0.053	5.069	0.057	22	16	0
nnz01oct81	5.651	0.046	5.678	0.041	43	4	5
nnz01sep77	5.574	0.059	5.610	0.051	27	2	2
nnz07nov68	6.040	0.041	6.043	0.034	60	1	5
nnz10aug78	5.861	0.043	5.812	0.043	39	3	18
nnz11oct80	5.661	0.046	5.685	0.041	42	4	6
nnz12sep73	6.795	0.049	6.715	0.054	24	0	21
nnz14oct69	6.131	0.040	6.117	0.035	59	2	7
nnz14oct70	6.831	0.043	6.709	0.044	36	0	22
nnz18aug83	5.709	0.052	5.738	0.049	30	5	5
nnz20oct76	4.660	0.043	4.913	0.053	25	34	1
nnz21oct67	5.771	0.042	5.787	0.036	54	5	3
nnz21oct75	6.561	0.051	6.445	0.054	24	0	17
nnz23aug75	6.506	0.051	6.458	0.049	29	0	12
nnz25oct84	5.606	0.061	5.608	0.057	22	3	4
nnz27oct66	6.449	0.039	6.397	0.035	57	0	14
nnz27sep71	6.635	0.049	6.515	0.054	24	0	21
nnz28aug72	6.382	0.050	6.316	0.046	33	0	11
nnz29aug74	6.582	0.050	6.495	0.053	25	0	18
snz02nov74	7.021	0.051	6.792	0.077	12	0	29
snz18oct75	6.836	0.051	6.716	0.058	21	0	21
snz27oc73a	7.099	0.053	6.961	0.071	14	0	24
snz27oc73b	4.156	0.054	4.454	0.089	9	28	0
snz27oc73c	3.875	0.053	4.383	0.133	4	35	0
snz27sep73	5.717	0.054	5.783	0.046	33	3	1
sek04jul76	5.928	0.074	5.904	0.069	15	0	5
sek07dec76	5.614	0.072	5.760	0.063	18	2	1
sek11jun78	5.878	0.076	5.880	0.063	18	0	1
sek14dec73	5.773	0.042	5.819	0.039	47	8	6

Table 3c. (cont'd)

	MLE-GLM		LS-GLM		# of observations		
event	m_b	σ	m_b	σ	signal	noise	clipped
sek14sep80	5.985	0.052	6.092	0.049	29	5	6
sek15jan65	5.883	0.046	5.917	0.038	49	1	2
sek15sep78	5.899	0.054	5.866	0.048	31	1	5
sek19jun68	5.255	0.056	5.308	0.049	29	3	2
sek23jul73	6.177	0.051	6.228	0.042	40	1	1
sek23jun79	6.050	0.049	6.101	0.042	40	3	3
sek27apr75	5.531	0.072	5.614	0.061	19	1	1
sek30nov69	5.958	0.056	5.987	0.046	34	0	0
pne29aug74	4.726	0.049	4.889	0.051	27	18	0
ch03oct84	5.005	0.070	5.227	0.084	10	12	0
ch06oct83	5.245	0.059	5.393	0.064	17	13	1
ch17oct76	4.532	0.048	4.848	0.074	13	34	0
ch19dec84	4.366	0.091	4.825	0.153	3	10	0
ch22sep69	5.134	0.051	5.183	0.049	30	12	0
ch27oct75	4.590	0.054	4.877	0.077	12	25	0
raj18may74	4.565	0.060	5.047	0.100	7	23	0
tu03dec80	5.333	0.050	5.449	0.047	32	11	0
tu19apr83	5.491	0.069	5.495	0.057	22	1	0
tu19feb77	4.608	0.049	4.924	0.066	16	29	0
tu19jul80	5.515	0.051	5.510	0.043	38	2	2
tu19mar77	5.646	0.063	5.759	0.059	20	6	1
tu23mar80	5.358	0.050	5.470	0.051	27	14	3
tu24nov77	5.659	0.057	5.652	0.046	33	0	0
tu25jul79	5.856	0.078	5.838	0.063	18	0	0
tu25jul82	5.211	0.056	5.406	0.057	22	13	0
tu25may83	5.778	0.078	5.721	0.063	18	0	0
tu30nov78	5.611	0.047	5.668	0.042	40	7	2
beryl	4.995	0.078	5.237	0.077	12	6	0
corundon	4.212	0.045	4.661	0.080	11	43	0
emeraude	4.541	0.052	4.830	0.069	15	25	0
grenat	4.766	0.041	5.025	0.047	32	32	1
opale	3.889	0.045	4.603	0.153	3	50	0
rubis	5.433	0.048	5.517	0.041	42	5	1
saphir	5.729	0.041	5.769	0.037	53	5	5
tourmaline	4.643	0.040	4.976	0.051	27	40	0
turqoise	4.227	0.040	4.689	0.077	12	55	0

3.1 Censoring versus No-censoring

Figure 1 plots the GLM versus the MLE-GLM magnitudes for the complete set of events for the "a", "b", and "max" phase. The results show that in using the stations belonging to the WWSSN, there is only a small magnitude range from about 5.7 to 6.5 where ignoring the censoring effects of clipping or non-detection does not lead to biased magnitudes. For events less than m_b of 5, the GLM and MLE-GLM magnitude bias for the "a" phase may be up to a full magnitude unit. For the "b" and "max" phases, the magnitude bias between the GLM and MLE-GLM averages to be about 0.6.

If all calibration events could be selected in the magnitude range of 5.7 to 6.5 where no bias is found between GLM and MLE-GLM and if those calibration events were truly representative of the test site, then an MLE-GLM would not be necessary. However, in order to have a representative sample of explosions from a test site and a representative sample from all test sites for comparison, it rapidly becomes necessary to select events from outside this range of magnitudes. An example is the three events at Amchitka, where the WWSSN stations underwent changes in network coverage in the late 1960's between the detonations of Longshot, Milrow, and Cannikin. This reconfiguration of the network coverage may produce inconsistency in the m_b estimation which results in Longshot not being an adequate calibration event for Milrow and Cannikin.

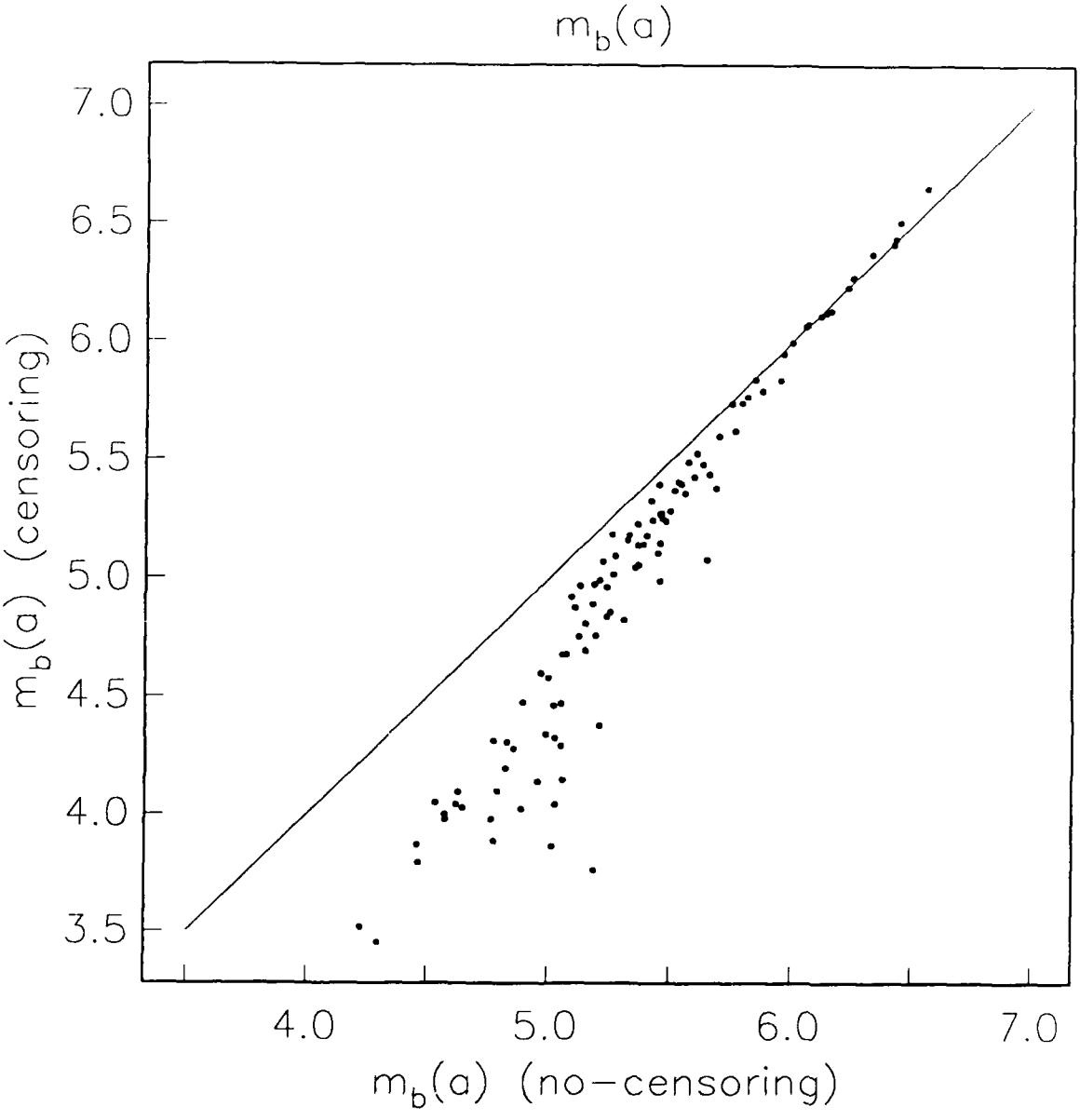

Figure 1a. m_b(a) event magnitudes from LS-GLM (no-censoring) estimates plotted against MLE-GLM (censoring) estimates for 106 explosions. Note that there is only a narrow range of magnitudes (5.7 to 6.5) for which the two sets of magnitudes are on average the same. The LS-GLM event magnitudes are too large at the lower m_b's.

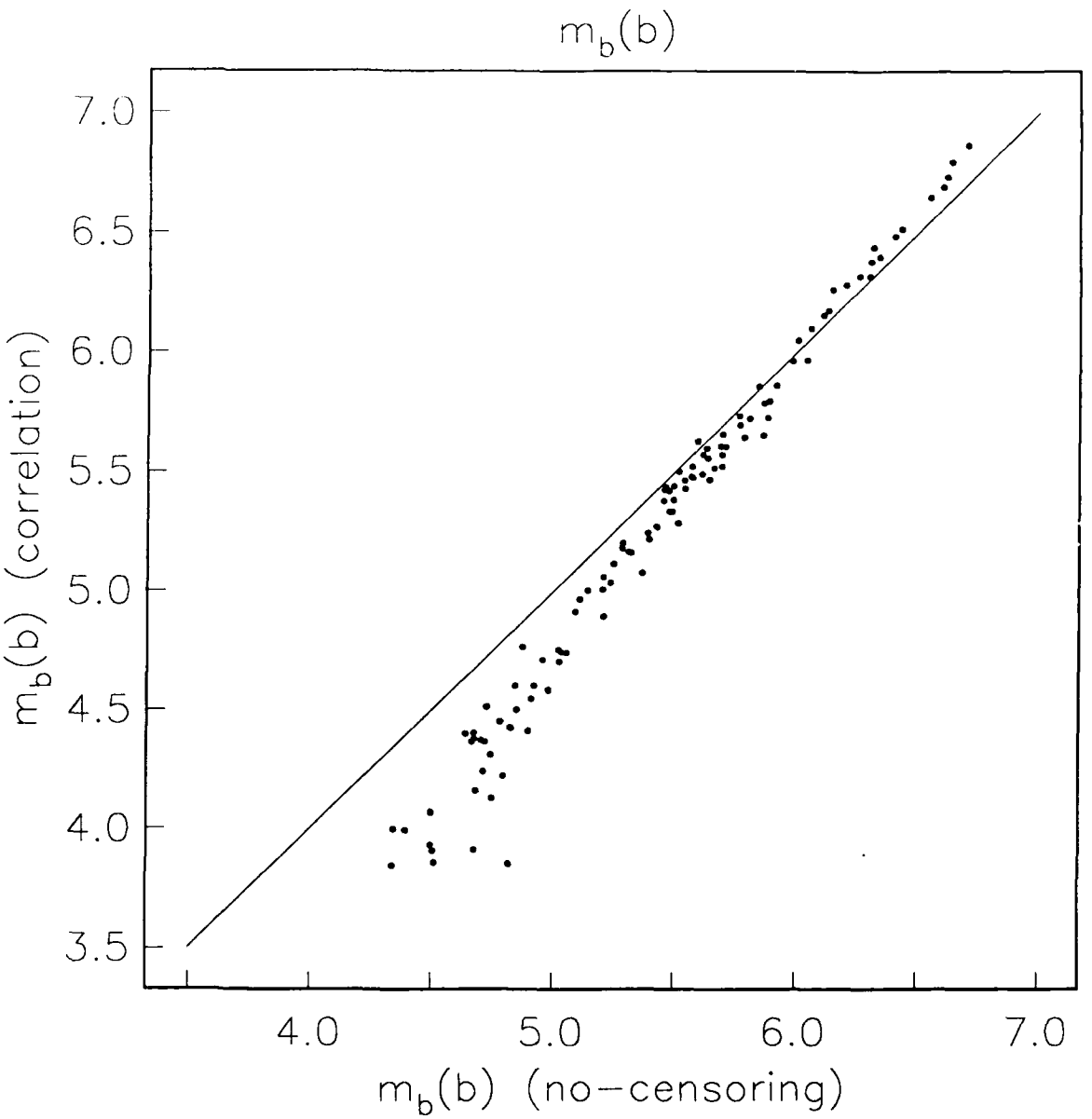

Figure 1b. m_b(b) event magnitudes from LS-GLM (no-censoring) estimates plotted against MLE-GLM (censoring) estimates for 109 explosions. Note that there is only a narrow range of magnitudes (5.5 to 6.5) for which the two sets of magnitudes are on average the same. The LS-GLM event magnitudes are too large at the lower m_b's and too small at the higher m_b's.

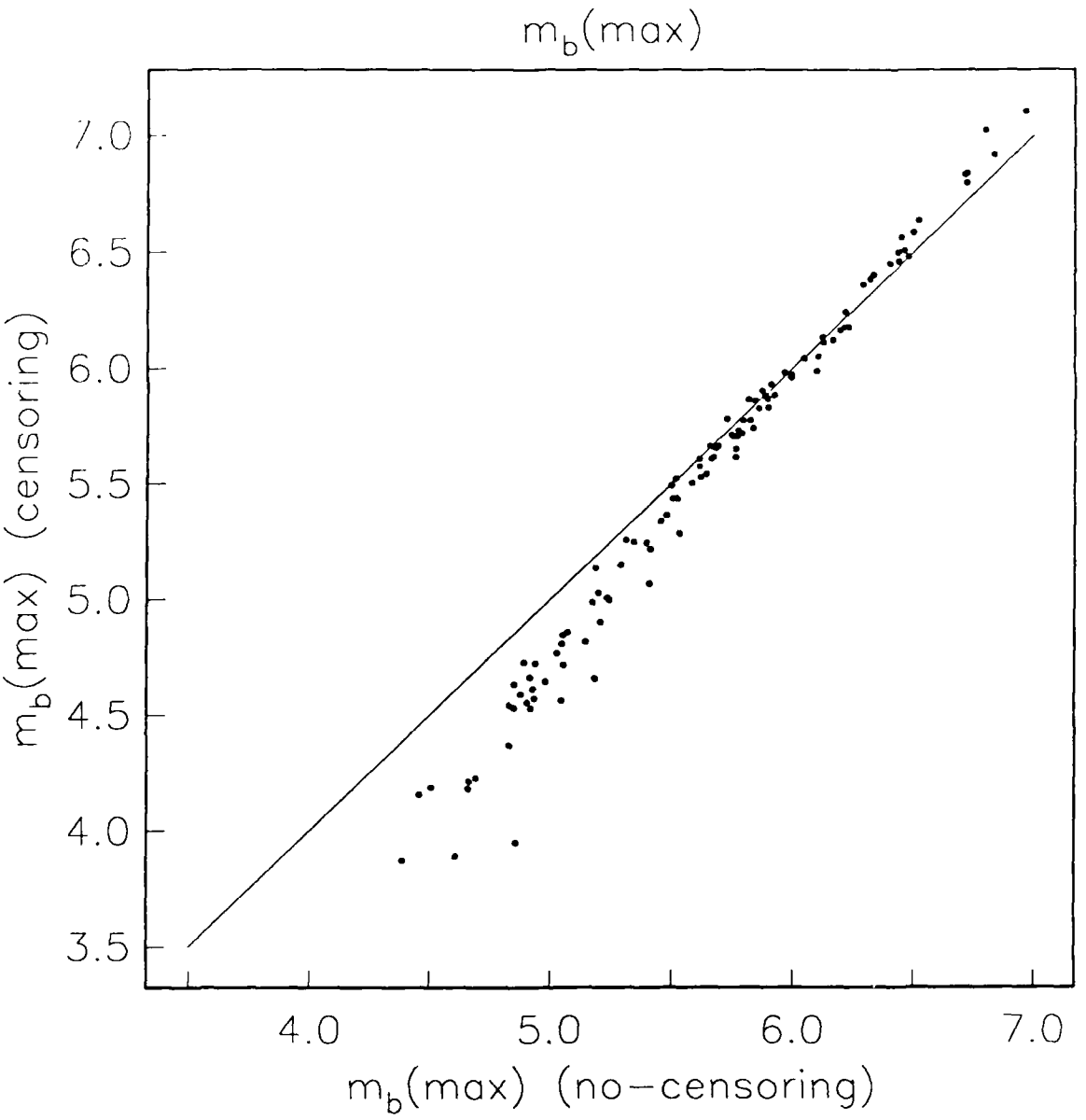

Figure 1c. m_b(max) event magnitudes from LS-GLM (no-censoring) estimates plotted against MLE-GLM (censoring) estimates for 109 explosions. Note that there is only a narrow range of magnitudes (5.5 to 6.5) for which the two sets of magnitudes are on average the same. The LS-GLM event magnitudes are too large at the lower m_b's and too small at the higher m_b's.

3.2 Phase Comparison

The GLM and MLE-GLM m_b magnitudes estimated for all events using both the censoring and non-censoring information for the three phases totaling 32,328 event-phases readings are plotted in Figures 2 and 3 respectively. In the case of GLM with no-censoring information, the m_b(a) values are on average 0.4 magnitude unit less than m_b(max) and 0.16 magnitude unit less than m_b(b) for m_b(a) over 5.3. The m_b bias between the m_b(b) and m_b(max) is 0.2. For events less than 5.3, the m_b bias decreases. The departure from the normal magnitude bias for the m_b(a) *vs* m_b(b) and m_b(a) *vs* m_b(max) may be due to the low signal detection levels for some of the lower yield events.

In the case of MLE-GLM when censoring data are included, the m_b biases between m_b(a) and other phases have increased compared to those without including the censoring information (Figure 3). The m_b bias is approximately 0.28 for m_b(a) *vs* m_b(b), 0.19 for m_b(b) *vs* m_b(max), and 0.48 for m_b(a) *vs* m_b(max). The inclusion of censoring information provides better constraints on the m_b's of the low yield events and therefore furnishes a more coherent set of magnitude relationship among the phases.

3.3 Multiple versus Single Phase Determination

The maximum-likelihood m_b estimations are performed in two different data configurations. The first one is to perform LS-GLM and MLE-GLM estimates using data for all three phases for 111 events assuming they are correlated. The other estimates are obtained by grouping the data for each individual phase for all events and

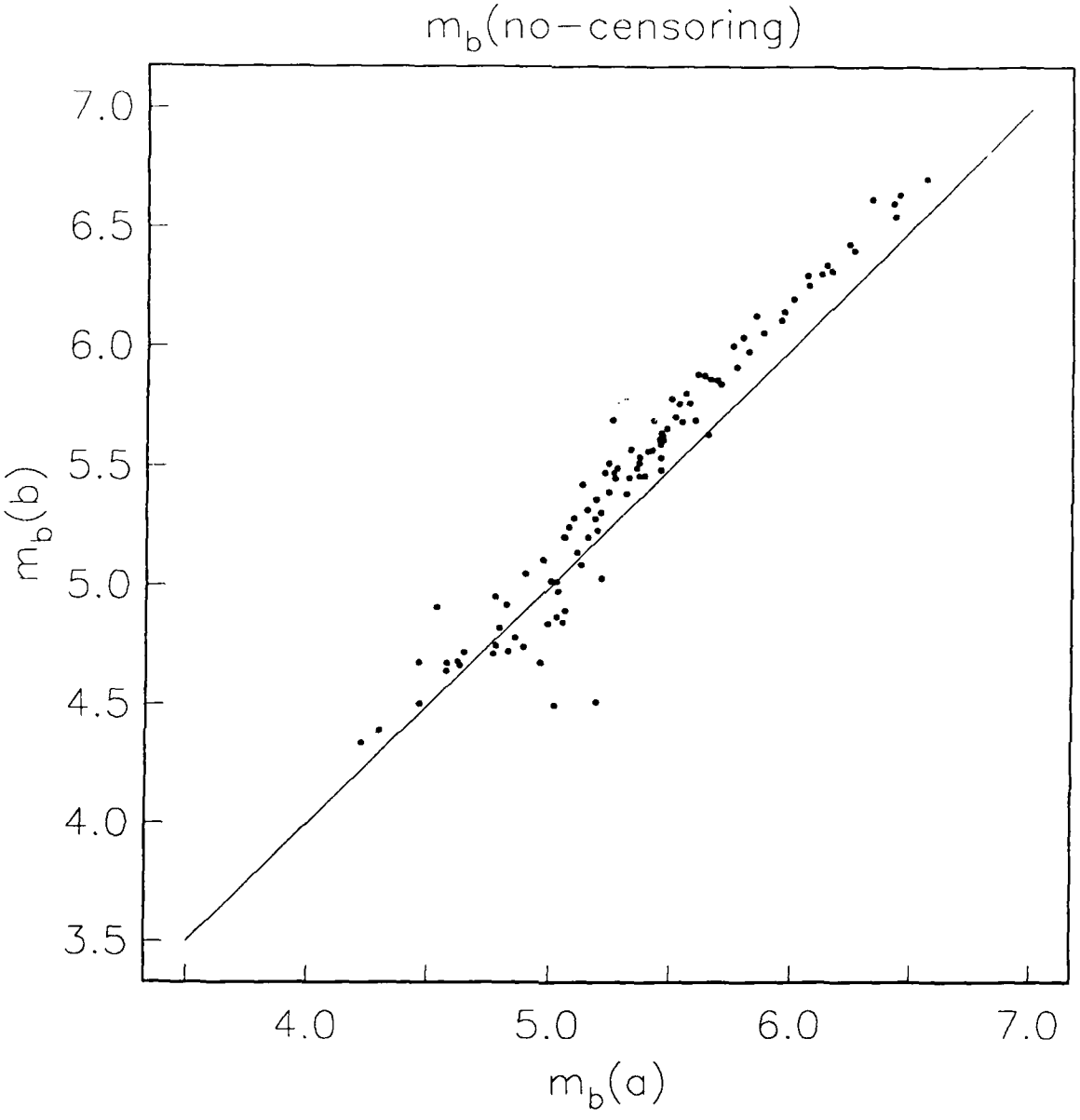

Figure 2a. LS-GLM (no-censoring) m_b's estimates for the "a" phase plotted against the "b" phase. The m_b(b)'s are on the average 0.16 magnitude unit greater than the m_b(a)'s for the larger events.

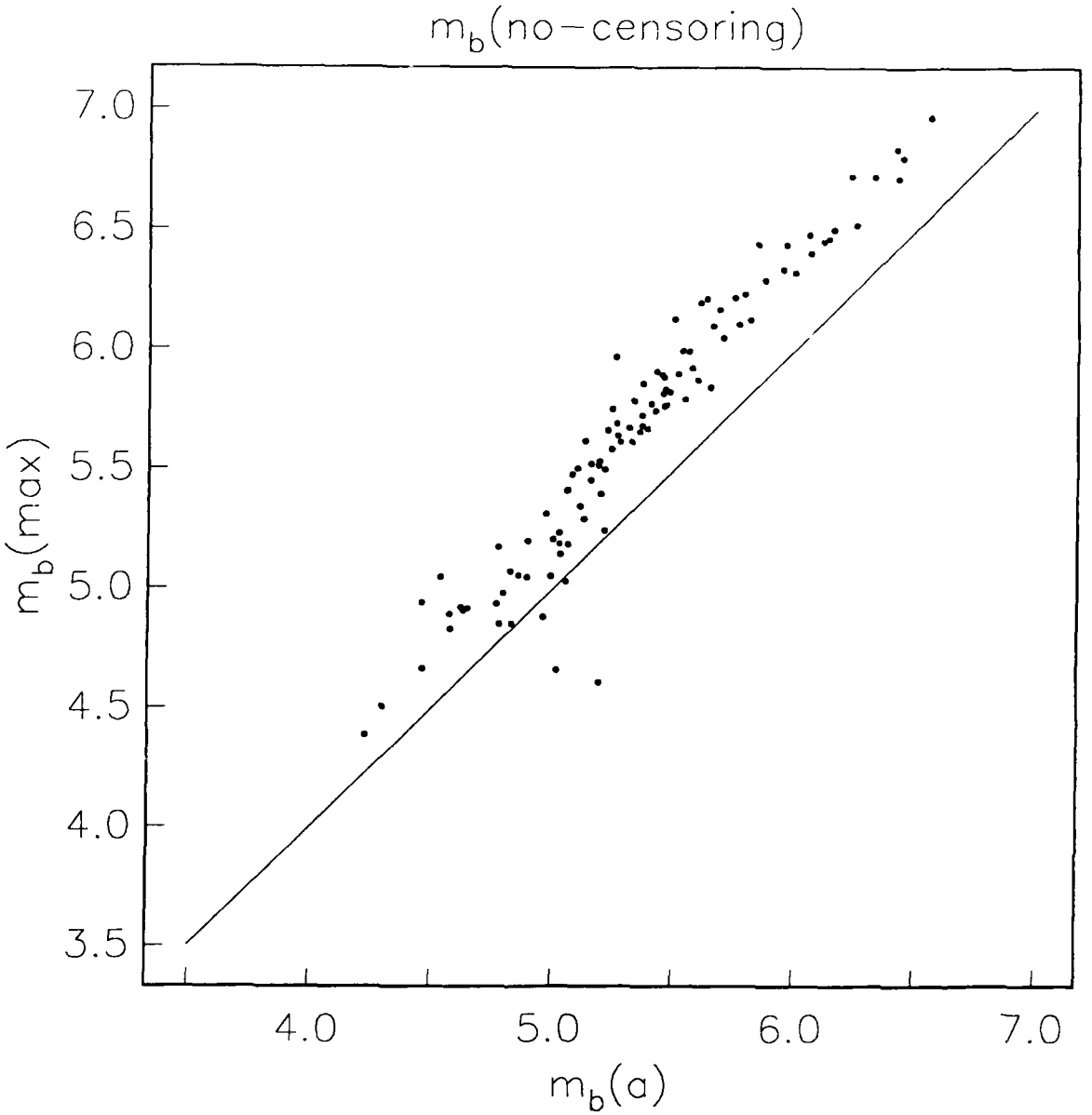

Figure 2b. LS-GLM (no-censoring) m_b's estimates for the "a" phase plotted against the "max" phase. The m_b(max)'s are on the average 0.4 magnitude unit greater than the m_b(a)'s for the larger events.

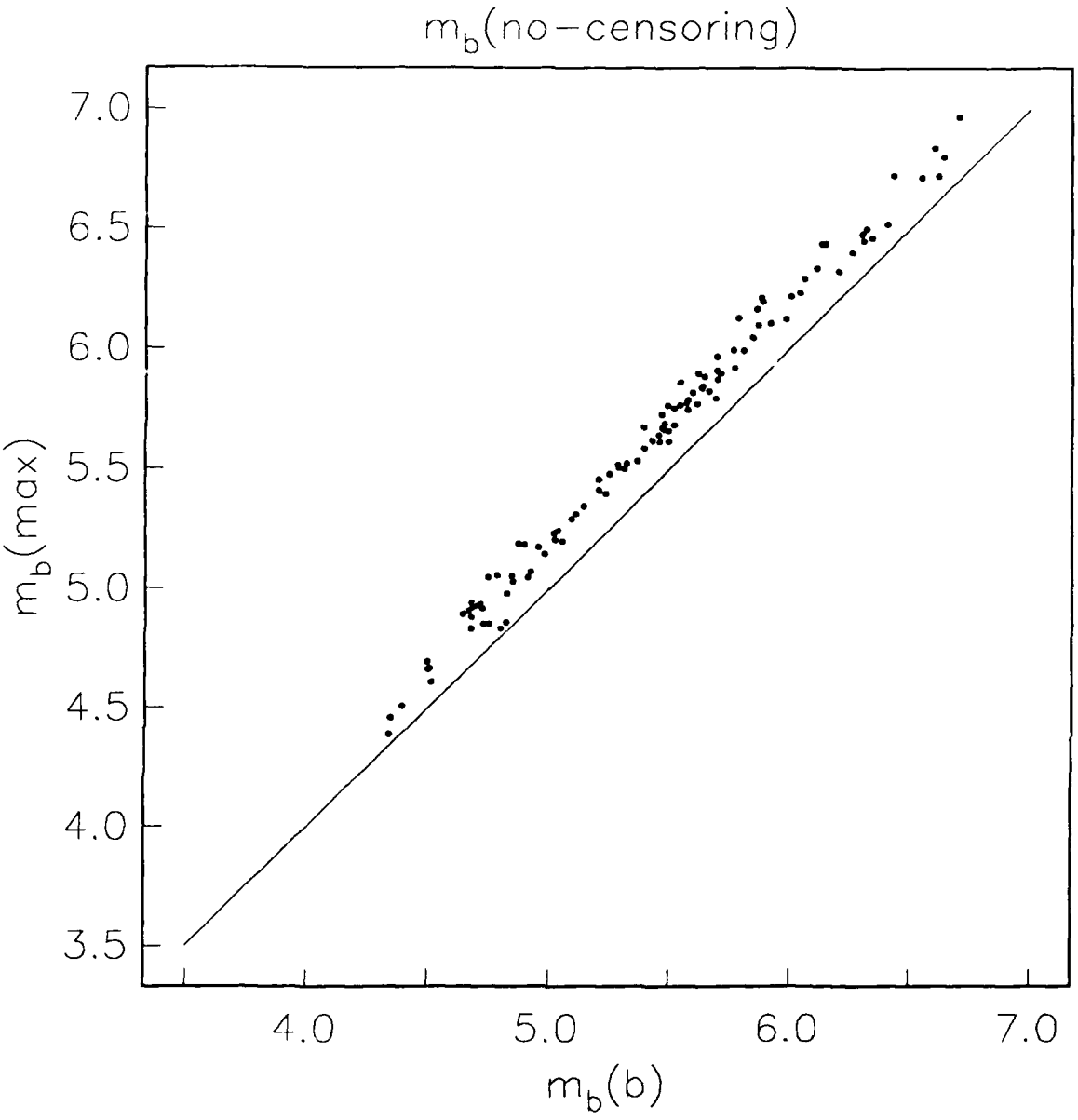

Figure 2c. LS-GLM (no-censoring) m_b's estimates for the "b" phase plotted against the "max" phase. The m_b(max)'s are on the average 0.2 magnitude unit greater than the m_b(a)'s for the larger events.

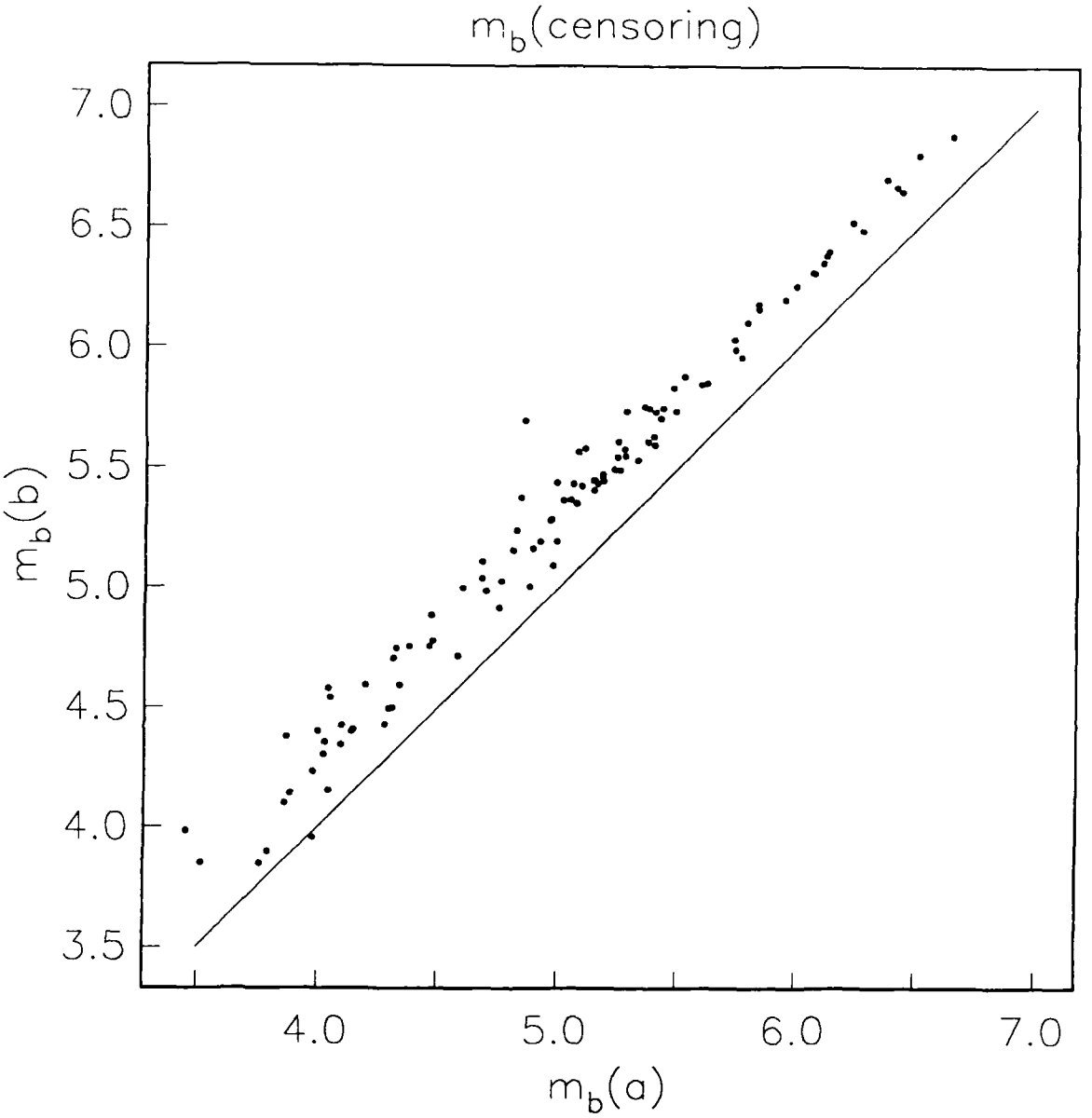

Figure 3a. MLE-GLM m_b's estimates for the "a" phase plotted against those for the "b" phase. These m_b's are derived using all three phases. The m_b(b)'s are on the average 0.28 magnitude unit greater than the m_b(a)'s.

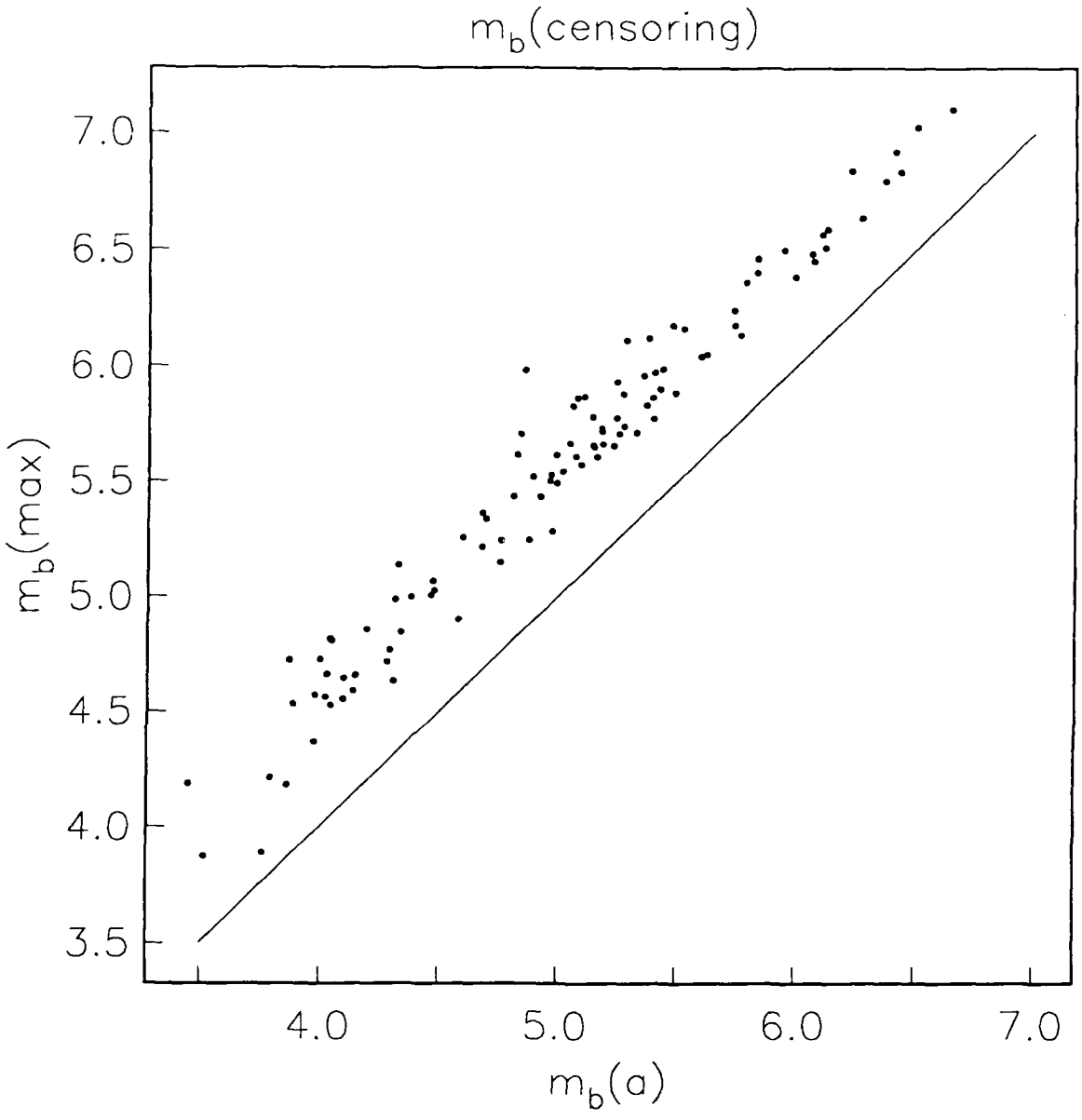

Figure 3b. MLE-GLM m_b's estimates for the "a" phase plotted against those for the "max" phase. These m_b's are derived using all three phases. The m_b(max)'s are on the average 0.48 magnitude unit greater than the m_b(a)'s.

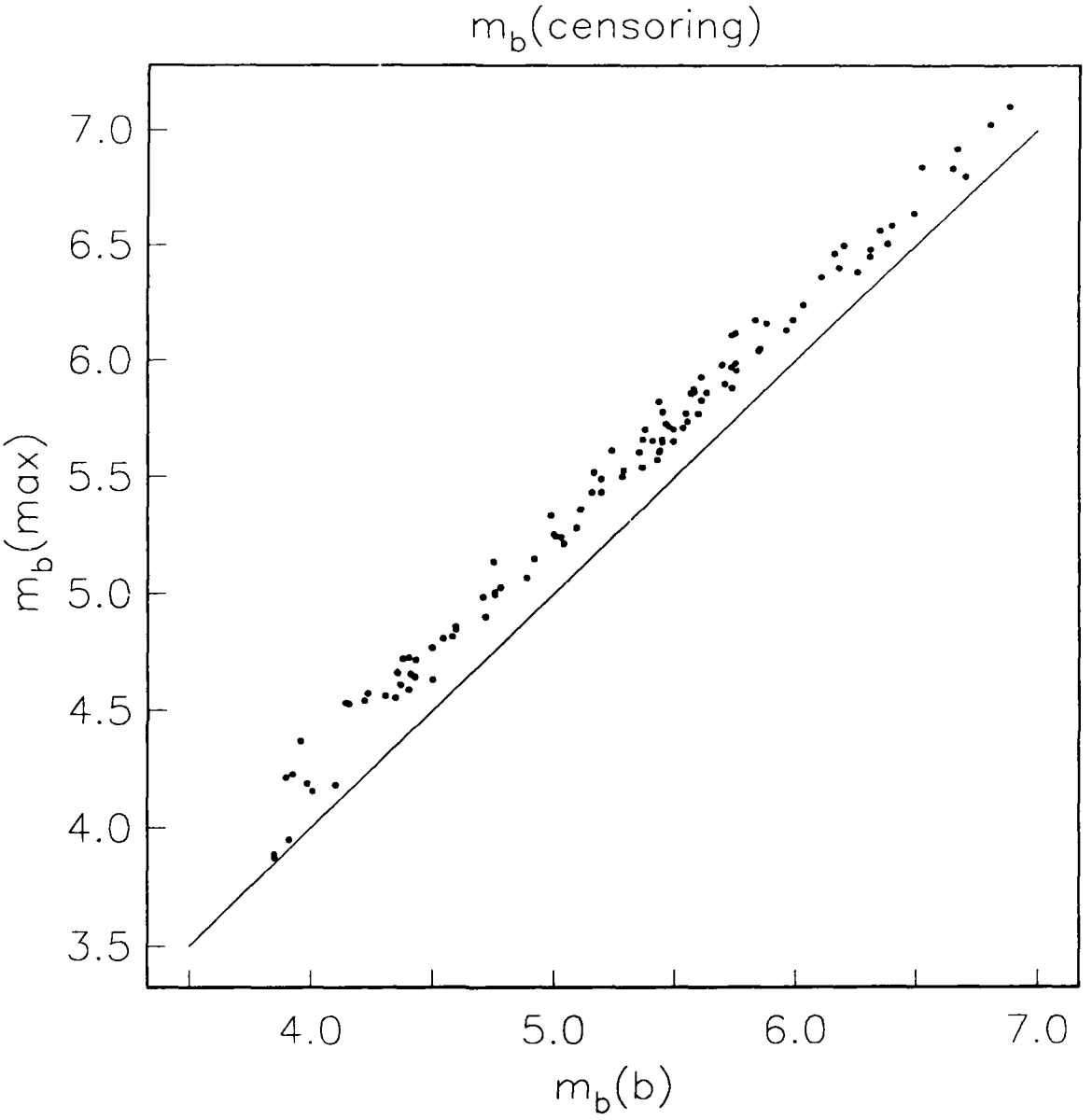

Figure 3c. MLE-GLM m_b's estimates for the "b" phase plotted against those for the "max" phase. These m_b's are derived using all three phases. The m_b(max)'s are on the average 0.19 magnitude unit greater than the m_b(a)'s.

performing three separate inversions. The results are plotted in Figures 4 and 5 for the LS-GLM and MLE-GLM respectively. When no censoring information is taken into account, the m_b(a) estimates using just the "a" phases alone are on the average higher than the m_b(a)'s obtained by inverting all three phases together (Figure 4a). On the other hand, the m_b(b)'s obtained using all phases appear to be slightly lower than those obtained using just the "b" phase (Figure 4b). There is no apparent bias between the m_b(max)'s obtained using all phases and just the "max" phase.

When censored data are taken into account, the m_b(a)'s obtained using all phases appears to be slightly lower than those obtained by using just the "a" phase for the lower yield event (Figure 5a). In the case of m_b(max), the magnitude estimates using just the "max" phase are slightly higher than those obtained using all three phases for the lower yield events (Figure 5c), inverse to the pattern for m_b(a)'s. No apparent bias is observed between the two sets of m_b(b)'s. But in all cases, the m_b biases for estimates using all phases versus those using the individual phases are small, being no more than 0.03 magnitude unit.

3.4 Station Effects

The estimation of the station terms has a controlling effect on the estimation of m_b's. The station effect is a function of the local elastic and anelastic structure near the station. A secondary dependence may be attributed to the azimuthal and incidence angle of the ray paths, due to a focusing-defocusing effect near the station. Stations corrections have been constructed by several researchers using various sets of data. Ringdal (1984) derived station corrections using nearly 40,000 P-wave amplitudes,

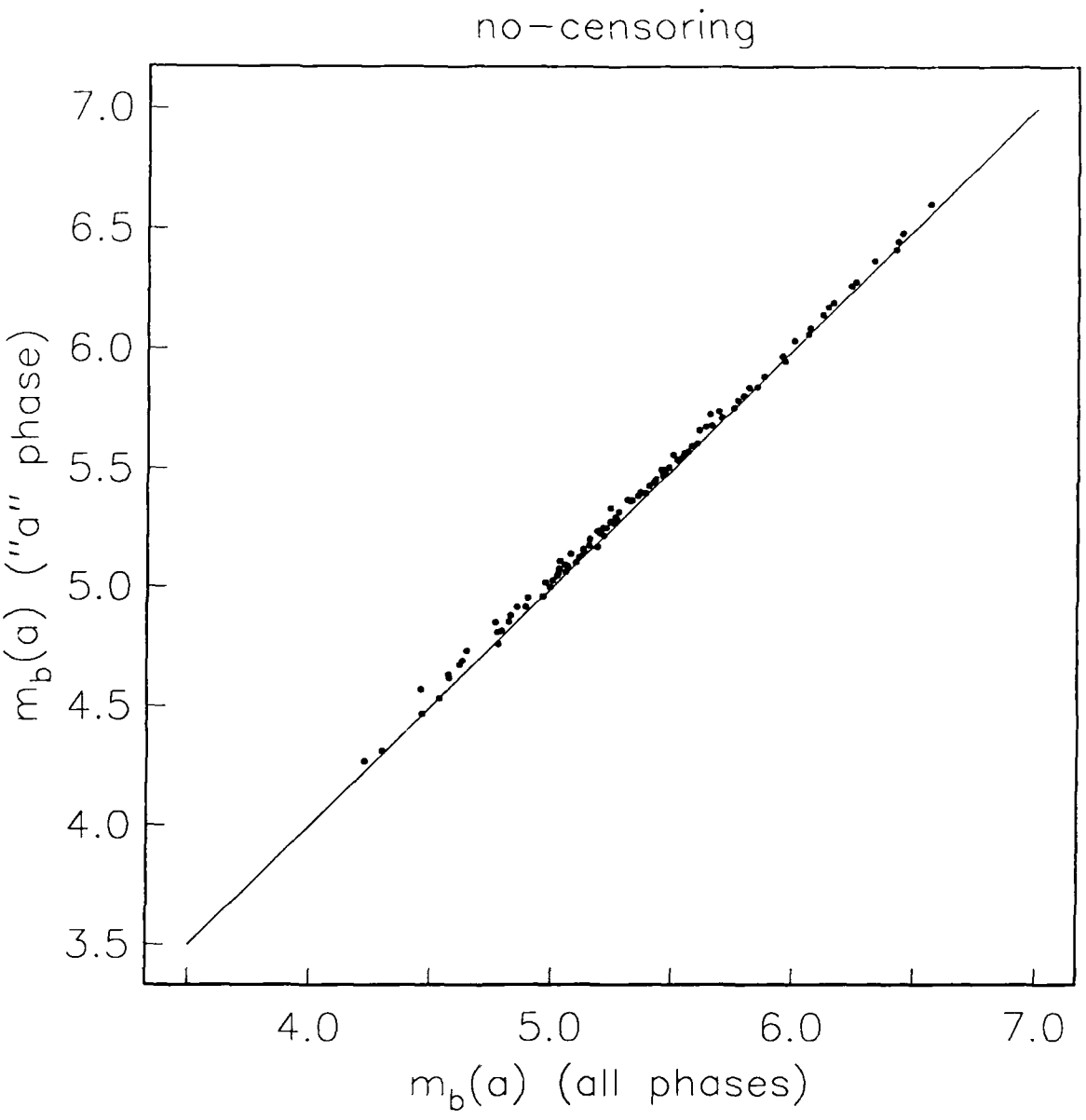

Figure 4a. LS-GLM $m_b(a)$ estimates derived from using just the "a" phase plotted versus those derived from using all three phases. The $m_b(a)$'s derived from using just the "a" phase are consistently higher.

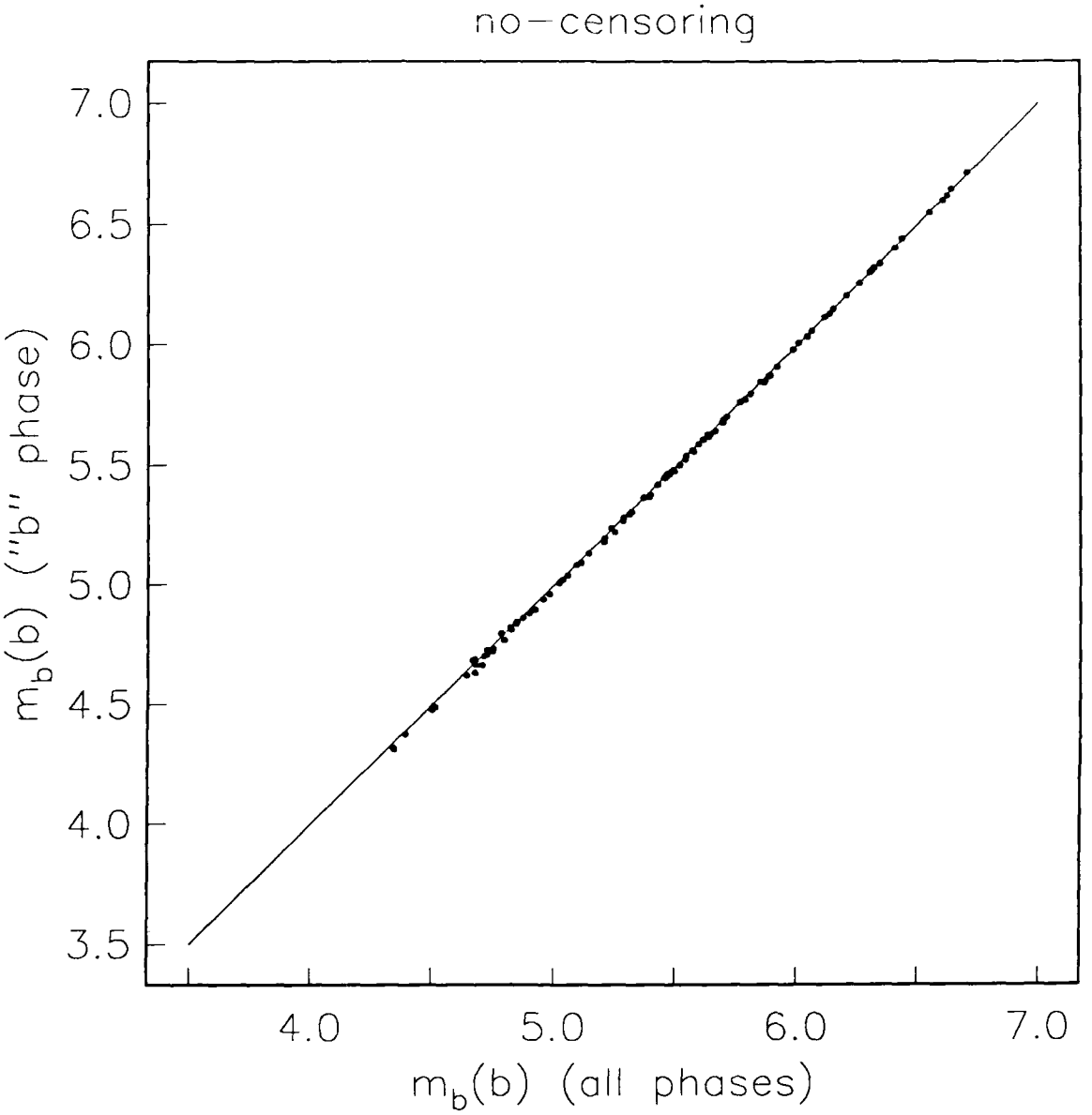

Figure 4b. LS-GLM $m_b(b)$ estimates derived from using just the "b" phase plotted versus those derived from using all three phases. These two sets of magnitudes agree very well.

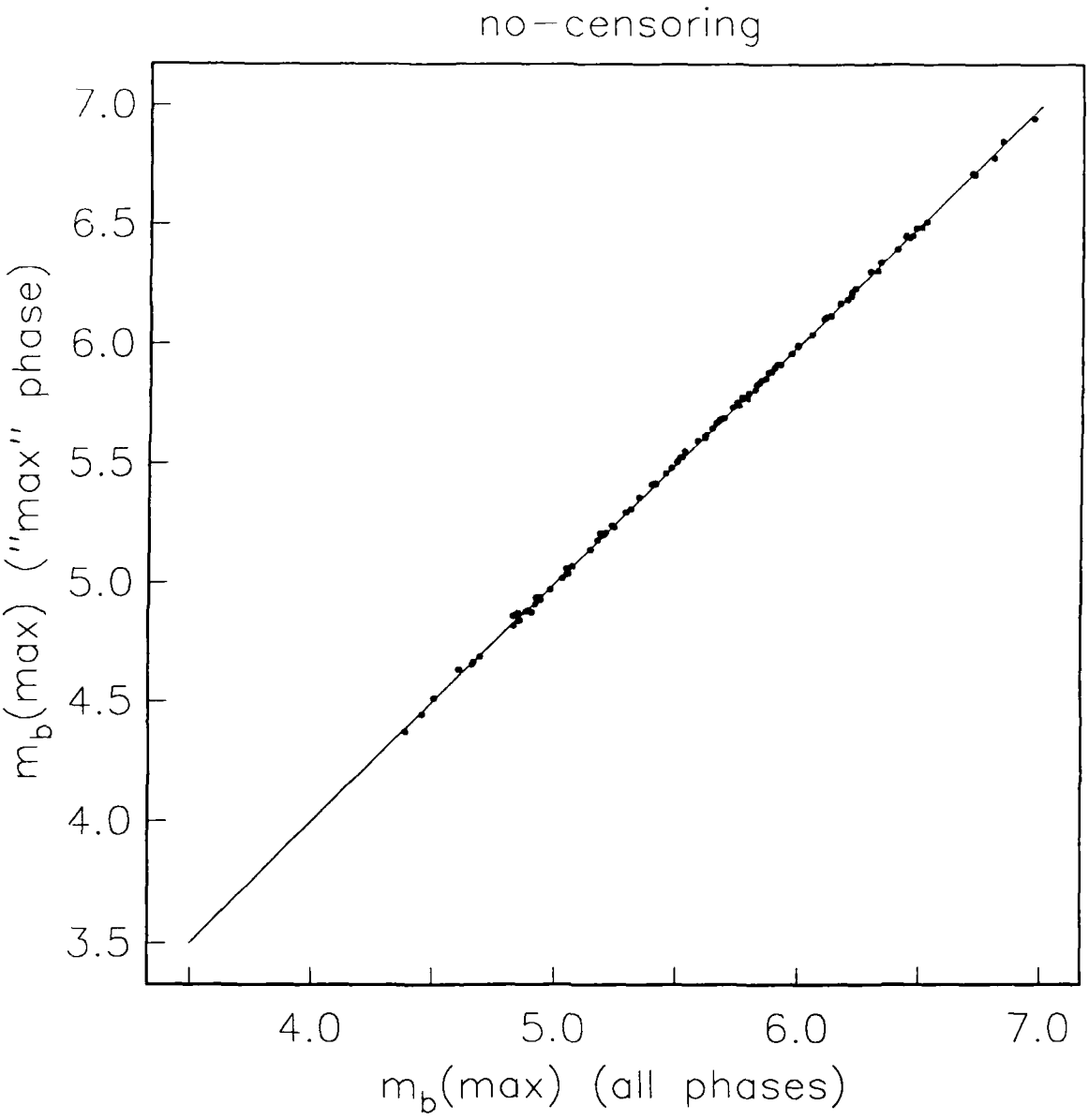

Figure 4c. LS-GLM m_b(max) estimates derived from using just the "max" phase plotted versus those derived from using all three phases. These two sets of magnitudes agree very well.

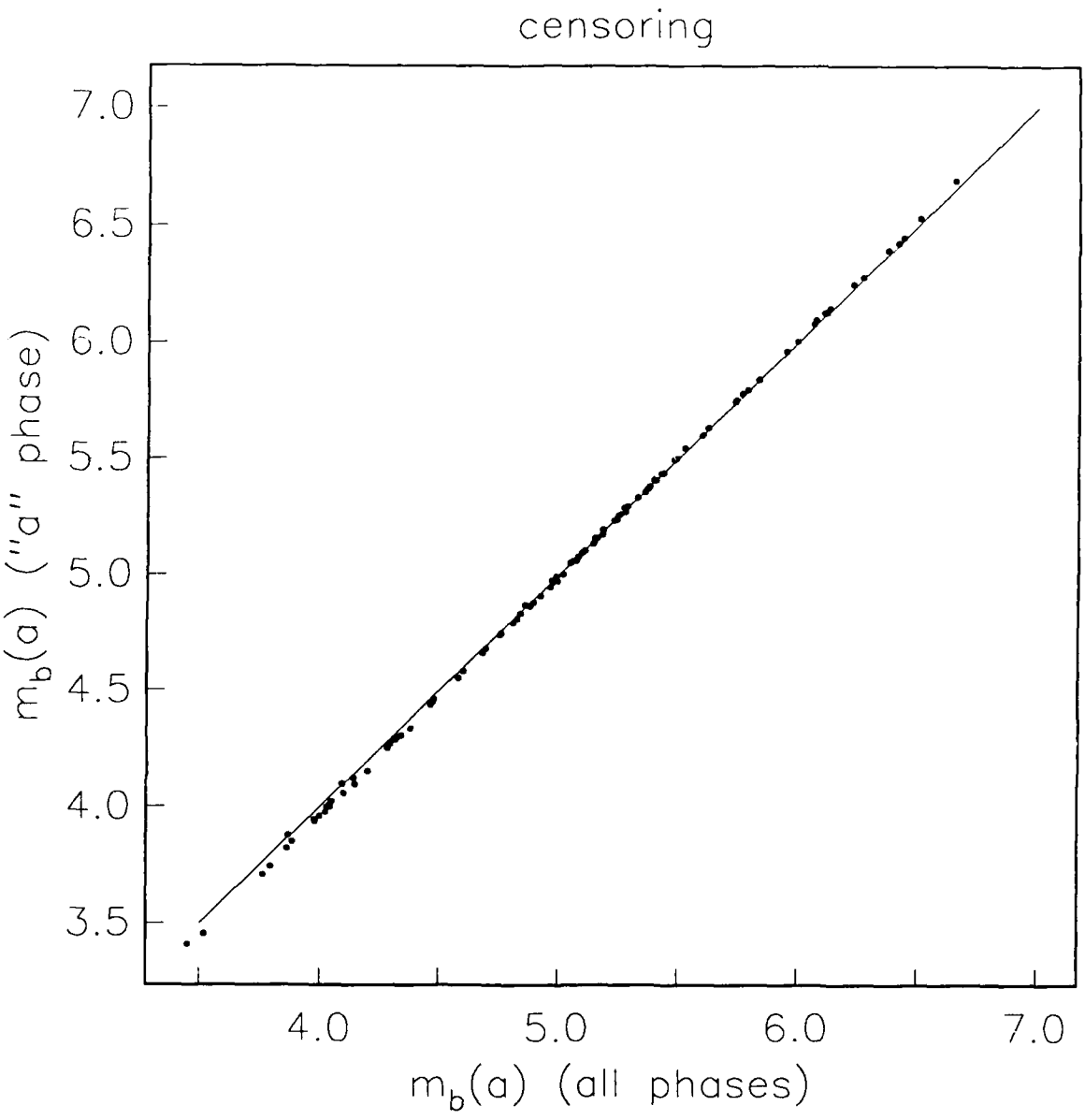

Figure 5a. MLE-GLM $m_b(a)$ estimates derived from using just the "a" phase plotted versus those derived from using all three phases. There is a slight indication that the $m_b(a)$'s for just the "a" phase are biased low towards low m_b's.

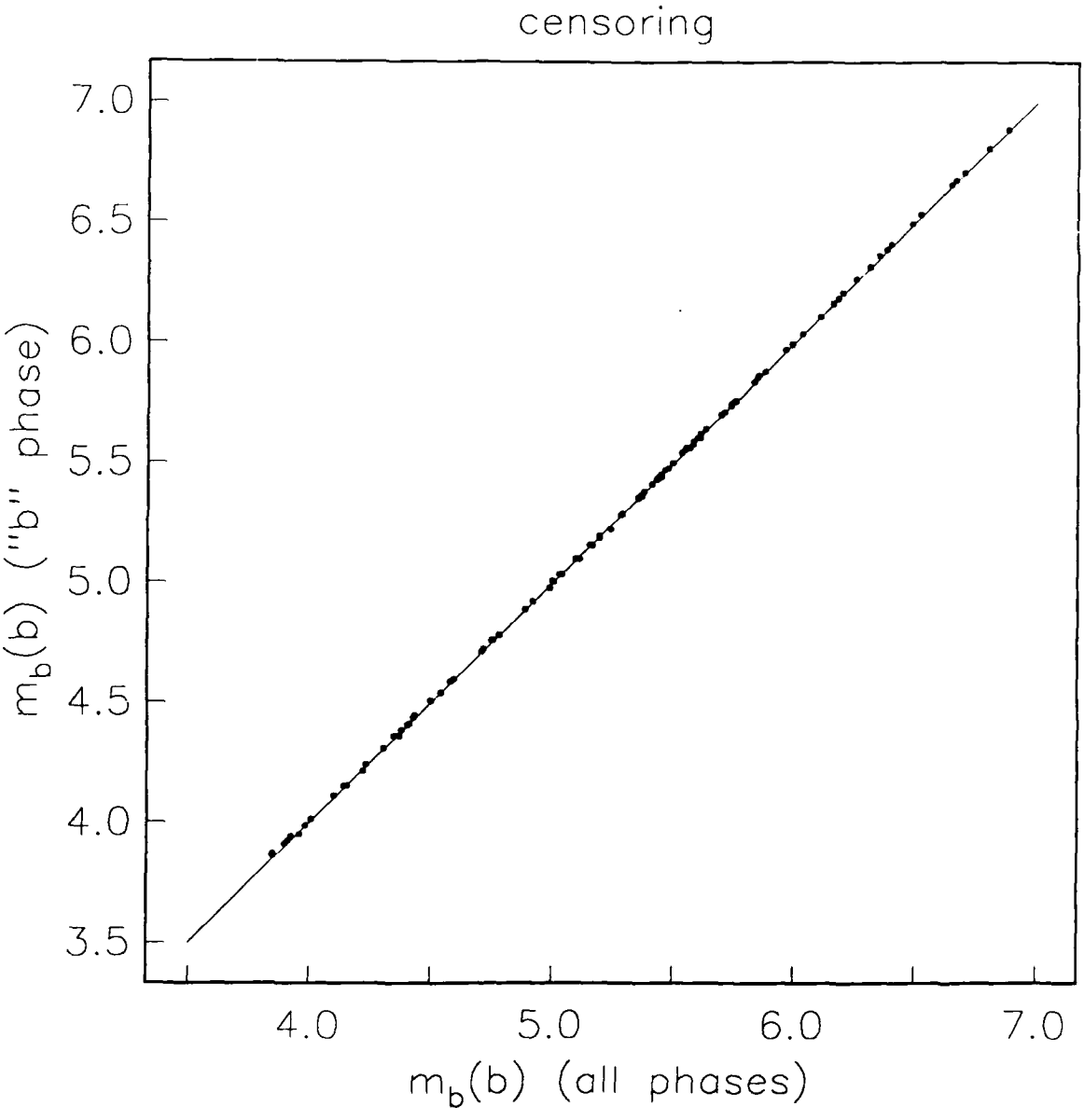

Figure 5b. MLE-GLM $m_b(a)$ estimates derived from using just the "b" phase plotted versus those derived from using all three phases. These two sets of magnitudes agree very well.

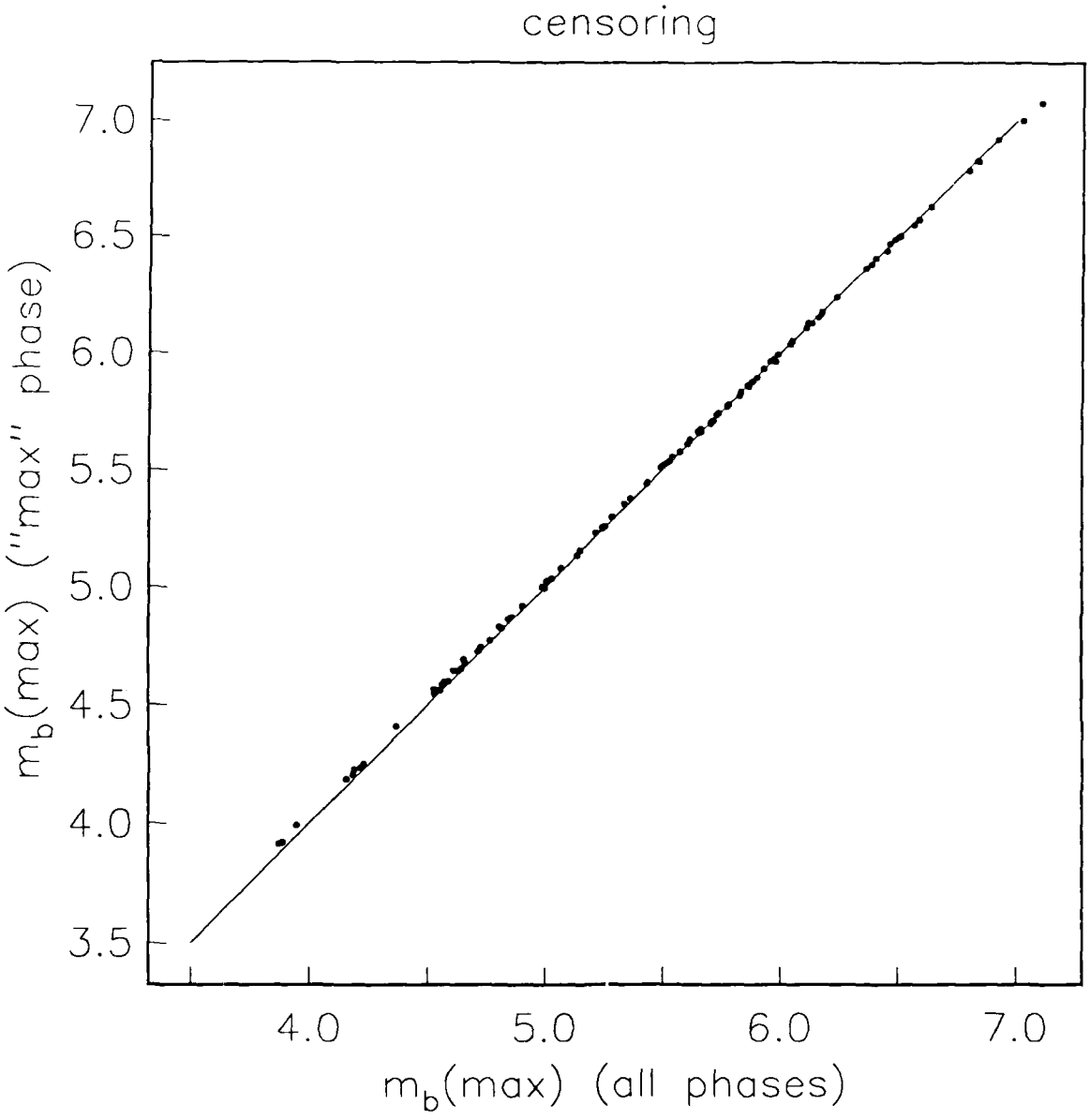

Figure 5c. MLE-GLM m_b(max) estimates derived from using just the "max" phase plotted versus those derived from using all three phases. These two sets of magnitudes agree very well.

whereas Blandford *et al.* (1984) used data from nuclear test sites to derive average station corrections.

Table 4 lists the maximum likelihood station effect estimates and their uncertainties, σ, estimated from a bootstrap procedure. The number of observations, noise level estimates, and clipping level estimates at each station are also listed. The RMS station standard deviation is 0.0279, and the RMS station effect is 0.2112. We have assumed that the station corrections for "a", "b", and "max" phases are the same. Due to the fact that the station effects were determined in a maximum likelihood sense, the censoring information, such as non-detection or clipping, levels was also taken into account. Stations that may have often clipped or not detected signals were assigned appropriate station corrections that reflected their tendency to have larger or smaller amplitudes.

The station effects pertaining to each phase are studied separately by not making the assumption that the station effects are the same for the different phases. Figure 6 plots the MLE-GLM station effects derived from each of the three phases separately. The station effects range from -0.8 to 0.6 and show quite a scatter among the different phases indicating a potential source of bias in the determination of m_b station corrections using different phases. The bias is expected since each station does not always detect each of the "a", "b", and "max" phase for an event. There is less scattering in the station effects as observed between the "a" and "b" phase (Figure 6a) compared to those between the "a" and "max" phase (Figure 6b), indicating that there is a greater common number for "a" and "b" phase observations for each event by each station than of "a" and "max" phase observations. Figure 7 plots the LS-GLM versus the

Table 4. MLE-GLM88 Station Corrections

station	MLE-GLM correction	σ	LS-GLM correction	σ	# of observations signal	noise	clipped
aae	-0.190	0.027	-0.171	0.033	66	71	16
aam	0.279	0.024	0.239	0.024	125	52	6
ade	-0.005	0.051	0.128	0.066	16	25	0
afi	-0.148	0.034	0.007	0.051	27	65	0
aku	-0.135	0.029	-0.038	0.034	62	63	0
alq	0.030	0.024	-0.099	0.022	140	22	19
alt	-0.160	0.190	-0.209	0.153	3	0	0
anp	-0.376	0.040	-0.118	0.066	16	53	0
ant	0.056	0.034	0.097	0.041	41	49	2
aqu	-0.093	0.030	-0.202	0.033	66	44	14
are	0.104	0.030	0.038	0.029	83	40	0
ath	0.356	0.134	0.253	0.119	5	1	0
atl	0.150	0.030	0.067	0.028	90	26	2
atu	0.159	0.025	0.147	0.027	94	66	14
bag	-0.020	0.025	0.026	0.025	113	52	8
bdf	-0.011	0.095	-0.060	0.084	10	2	0
bec	-0.126	0.029	-0.029	0.041	41	85	3
bhp	-0.181	0.032	0.038	0.049	30	75	0
bks	0.083	0.025	0.080	0.024	124	50	1
bla	0.155	0.024	0.047	0.023	137	39	12
bog	0.222	0.027	0.336	0.032	69	78	0
boz	0.259	0.051	-0.009	0.046	34	3	4
bul	0.094	0.026	0.021	0.024	121	28	8
car	0.153	0.026	0.127	0.028	92	59	7
ccg	-0.125	0.329	-0.657	0.266	1	0	0
chg	-0.210	0.031	-0.368	0.032	71	16	27
cmc	-0.213	0.040	-0.287	0.041	42	26	0
col	0.069	0.019	-0.040	0.018	229	45	25
cop	0.161	0.025	0.193	0.034	61	94	14
cor	0.089	0.030	0.090	0.032	71	47	3
cta	0.235	0.042	0.123	0.039	46	12	4
dag	-0.075	0.052	-0.132	0.054	24	15	1
dal	0.191	0.049	0.158	0.064	17	24	4
dav	-0.246	0.037	0.032	0.055	23	58	0
dug	-0.002	0.025	-0.148	0.022	144	16	18
eil	0.062	0.048	-0.229	0.063	18	3	27
ept	0.003	0.057	-0.117	0.049	29	2	2
esk	0.104	0.027	0.209	0.031	75	75	2
flo	0.080	0.033	-0.133	0.031	72	16	9
fvm	-0.010	0.046	-0.110	0.040	44	8	0

Table 4. (cont'd)

station	MLE-GLM correction	σ	LS-GLM correction	σ	# of observations signal	noise	clipped
gdh	-0.167	0.021	-0.151	0.023	138	110	1
geo	0.016	0.027	0.065	0.030	81	64	2
gie	-0.195	0.044	0.041	0.089	9	46	0
gol	-0.264	0.026	-0.340	0.023	130	20	9
grm	0.028	0.085	1.029	0.266	1	14	0
gsc	0.065	0.032	-0.039	0.031	73	17	16
gua	-0.247	0.022	-0.128	0.030	77	149	0
hkc	-0.107	0.028	-0.040	0.030	79	55	0
hlw	-0.009	0.033	-0.254	0.041	43	25	29
hnr	0.228	0.033	0.380	0.048	31	67	0
hon	0.043	0.085	0.132	0.108	6	9	0
ist	0.189	0.023	0.162	0.028	88	94	25
jct	0.157	0.035	0.017	0.035	59	4	24
jer	0.057	0.029	0.046	0.032	68	39	20
kbl	0.146	0.043	-0.208	0.071	14	0	46
kbs	-0.154	0.039	-0.152	0.041	42	30	0
kev	-0.141	0.024	-0.120	0.026	104	87	4
kip	0.118	0.023	0.255	0.029	84	118	0
kod	0.040	0.028	-0.023	0.030	81	29	25
kon	0.089	0.022	-0.011	0.026	108	61	63
krk	-0.348	0.095	-0.330	0.119	5	7	0
ktg	-0.273	0.029	-0.199	0.035	58	66	1
lah	0.419	0.066	0.555	0.119	5	17	3
lem	-0.507	0.031	-0.338	0.037	51	59	0
lon	-0.047	0.024	-0.138	0.023	133	38	21
lor	0.219	0.035	0.069	0.033	63	8	16
lpa	0.419	0.033	0.868	0.094	8	91	0
lpb	-0.042	0.033	-0.116	0.035	58	39	3
lps	-0.069	0.037	-0.108	0.038	50	27	3
lub	0.210	0.039	0.174	0.042	40	30	3
mal	0.052	0.030	0.005	0.030	78	37	5
man	0.343	0.060	0.288	0.058	21	8	1
mat	-0.083	0.024	-0.136	0.023	130	40	18
mds	-0.087	0.046	-0.179	0.046	33	19	0
mhi	0.356	0.110	0.291	0.119	5	2	2
mnn	0.087	0.076	-0.170	0.084	10	7	2
msh	0.170	0.042	0.221	0.046	34	19	9
mso	0.059	0.044	-0.071	0.039	46	7	2
mun	-0.038	0.043	0.087	0.050	28	31	0
nai	-0.065	0.028	-0.110	0.028	93	36	9
nat	0.067	0.045	0.138	0.051	27	27	0

Table 4. (cont'd)

	MLE-GLM		LS-GLM		# of observations		
station	correction	σ	correction	σ	signal	noise	clipped
ndi	0.108	0.028	0.028	0.027	100	23	20
nha	-0.214	0.134	-0.168	0.133	4	2	0
nil	-0.010	0.053	-0.076	0.071	14	6	18
nna	-0.163	0.032	-0.093	0.039	47	57	0
nor	-0.304	0.032	-0.247	0.034	62	45	0
nur	-0.017	0.026	-0.013	0.030	77	77	3
ogd	-0.090	0.025	-0.125	0.024	124	42	6
oxf	0.353	0.030	0.205	0.028	91	16	17
pda	0.074	0.029	0.195	0.048	31	91	3
pel	0.052	0.039	0.077	0.049	29	39	3
pmg	-0.082	0.032	-0.057	0.034	62	45	0
poo	0.006	0.026	-0.070	0.025	110	33	23
pre	-0.020	0.038	-0.118	0.038	49	28	0
pto	-0.127	0.029	-0.147	0.030	76	45	5
que	-0.410	0.031	-0.602	0.036	56	22	33
qui	0.002	0.038	0.188	0.089	9	67	0
rab	-0.152	0.028	0.072	0.043	38	104	0
rar	-0.106	0.050	0.080	0.077	12	32	0
rcd	0.484	0.050	0.373	0.051	27	14	3
riv	0.348	0.059	0.595	0.089	9	22	0
sba	-0.632	0.088	-0.320	0.188	2	12	0
scp	0.056	0.022	-0.009	0.022	148	55	18
sdb	0.070	0.037	-0.005	0.036	56	15	9
seo	-0.016	0.026	0.054	0.029	82	65	11
sha	0.343	0.028	0.358	0.030	76	65	0
shi	0.308	0.032	0.127	0.032	67	11	25
shk	-0.293	0.032	-0.069	0.042	40	68	0
shl	0.067	0.032	-0.137	0.036	55	15	34
sjg	-0.251	0.024	-0.244	0.023	129	57	0
sna	0.105	0.080	0.067	0.108	6	11	0
sng	-0.083	0.043	-0.035	0.045	35	24	1
spa	-0.759	0.074	-0.761	0.074	13	7	0
stu	0.055	0.021	0.037	0.022	142	89	20
tab	0.172	0.034	0.199	0.036	56	37	3
tau	-0.119	0.065	-0.067	0.077	12	14	0
tol	0.235	0.026	0.189	0.028	91	42	22
tri	-0.159	0.023	-0.209	0.026	105	81	17
trn	0.098	0.024	0.103	0.025	112	70	1
tuc	0.075	0.037	-0.062	0.035	57	3	21
ume	0.157	0.027	0.101	0.026	102	48	1
unm	-0.244	0.067	-0.026	0.084	10	13	1

Table 4. (cont'd)

	MLE-GLM		LS-GLM		# of observations		
station	correction	σ	correction	σ	signal	noise	clipped
upa	-0.260	0.190	-0.406	0.188	2	1	0
val	0.009	0.022	0.053	0.026	104	108	12
wel	0.131	0.074	0.393	0.094	8	12	0
wes	-0.106	0.022	-0.043	0.024	124	97	6
win	-0.193	0.049	-0.149	0.057	22	24	0

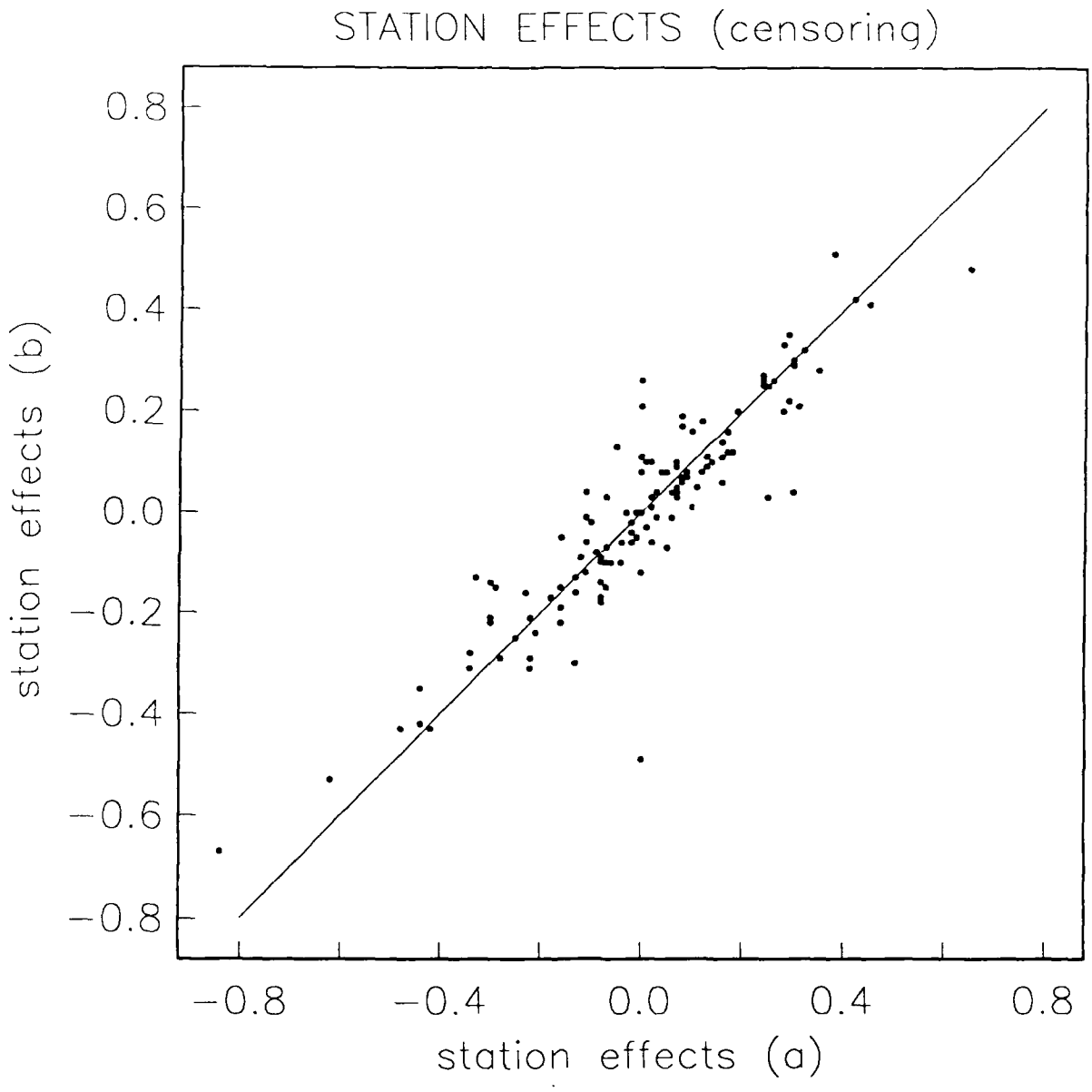

Figure 6a. MLE-GLM station effects derived using the "a" phase plotted versus those for the "b" phase. The bias between the two estimates is up to 0.2 magnitude units.

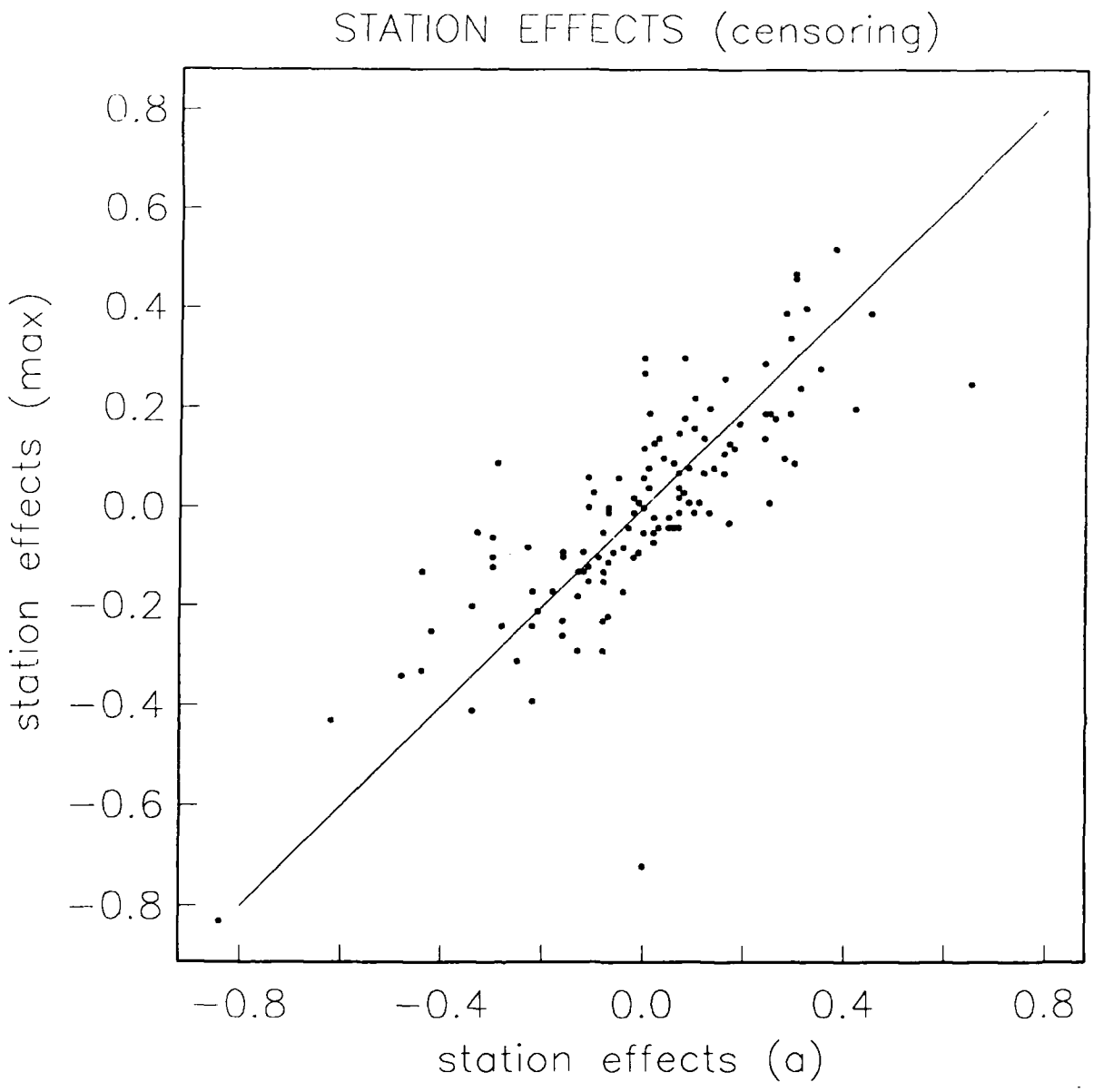

Figure 6b. MLE-GLM station effects derived using the "a" phase plotted versus those for the "max" phase. The bias between the two estimations is much higher, being up to 0.4 magnitude units.

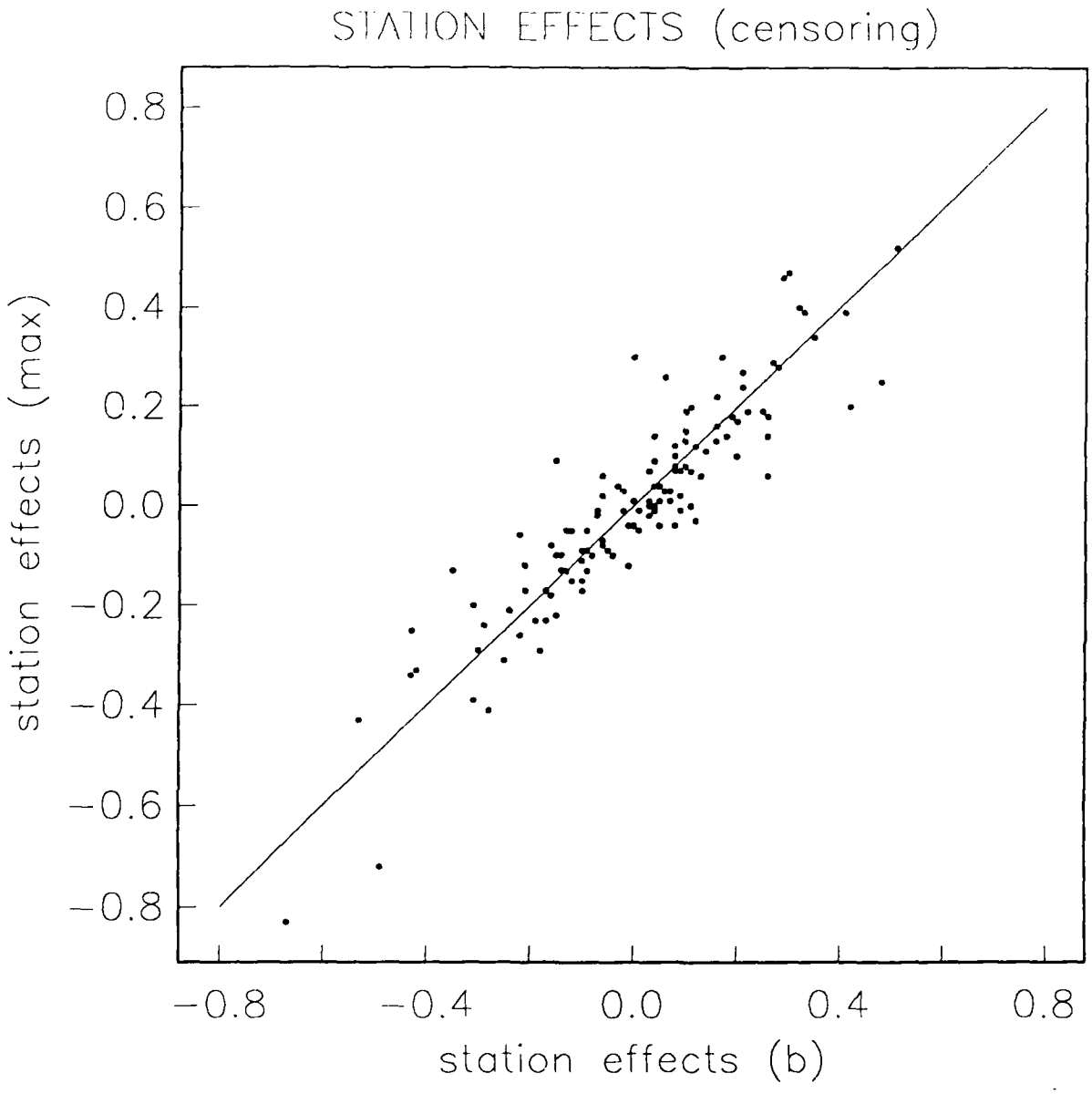

Figure 6c. MLE-GLM station effects derived using the "b" phase plotted versus those for the "max" phase. The bias between the two estimates is up to 0.2 magnitude units.

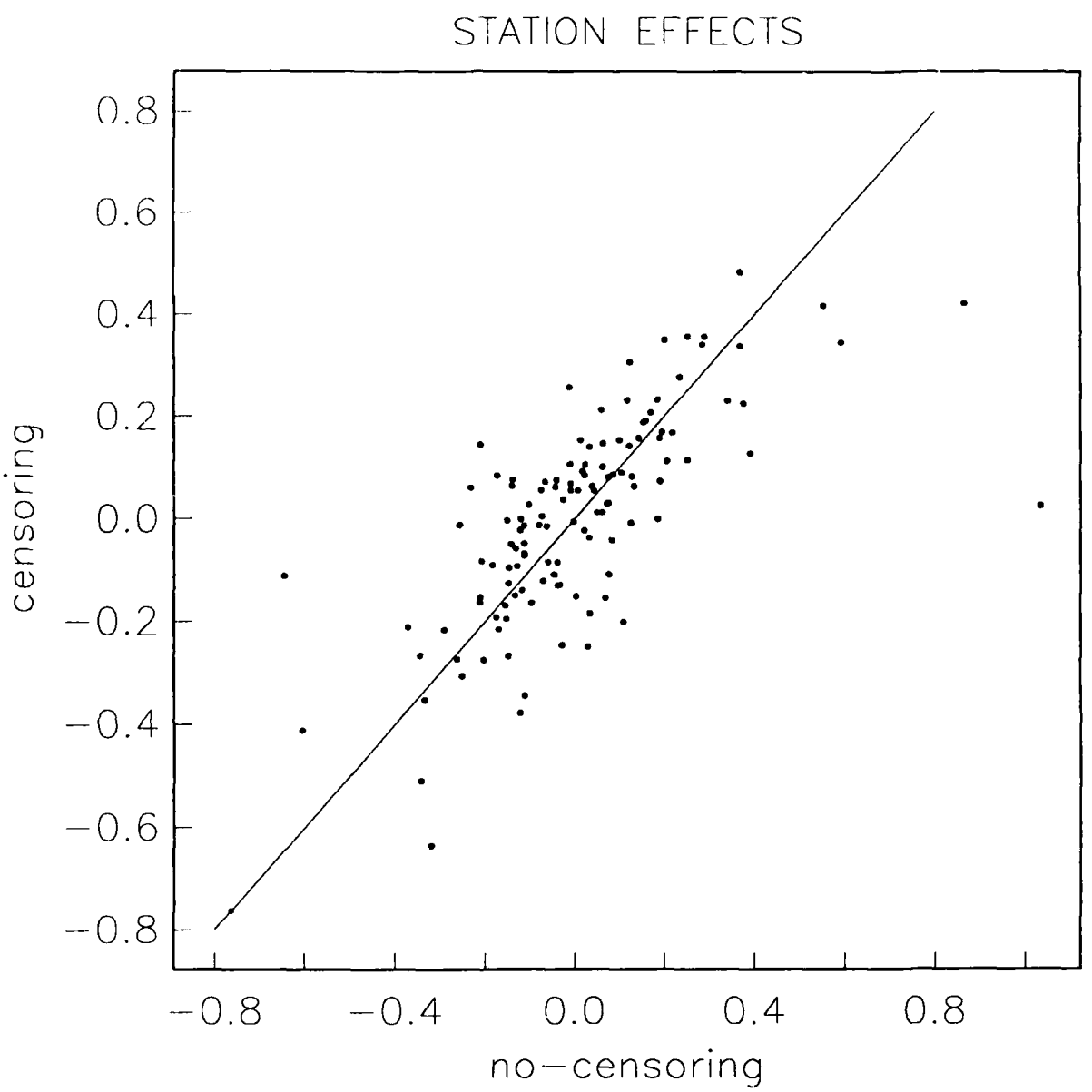

Figure 7. LS-GLM station effects versus MLE-GLM station effects for 127 WWSSN stations. Note that for most stations the difference is skewed and therefore potential for bias exists when the censoring information is ignored.

MLE-GLM station effects derived for all magnitude models. The net difference between the two data sets is by definition zero, but the scatter in the results does not allow one to infer such from the plot. The possible departure of the slope from unity in fitting the data in Figure 7 indicates the degree of bias in the LS-GLM station corrections when comparing to the MLE-GLM model which requires no *apriori* station corrections prior to inversion. Based on Ringdal's (1986) LS-GLM station terms, Veith *et al.* (1987) computed detection thresholds that are undistinguishable at noisy and quiet stations. The bias in LS-GLM has been demonstrated by Lilwall (1986) to be attributed to the ambiguities in keeping the detection threshold constant.

3.5 Error Analysis

The uncertainty associated with each event and station is computed with two methods. The standard deviation σ of the perturbing noise returned by the EM algorithm is believed to be a good measure of the uncertainty in any single observation. Jih *et al.* (1988) propose to scale this σ with the number of associated observations to infer the precision of each estimated parameter. The second method is by utilizing the bootstrap method (Efron, 1979, 1981), which has been extensively used in some recent network m_b estimation studies (McLaughlin *et al.*, 1986a, 1986b, 1988). Jih *et al.* (1988) propose to enlarge the pool of regular residuals with the generalized (i.e. censored) residuals for resampling to account for the fact that all the paths containing clipped or noisy data to remain so throughout the resampling iteration.

The m_b error estimates are plotted in Figure 8 using the bootstrap and EM for censored data only. Figure 9 shows the m_b error estimates obtained using censoring and no-censoring data, respectively. The EM m_b error estimates using censoring data, as shown in Figure 9a, are generally larger than the no-censoring data. The same is true for the estimates using bootstrap as shown in Figure 9b. The bootstrap method, requiring intensive computing time, does not yield correct m_b estimates and is used only for error estimation (e.g. Blandford *et al.* 1984, McLaughlin, 1988). Taking into account the fact that EM estimation indeed yields the correct m_b values together with its standard errors, we prefer to use this method over bootstrapping. The resampling scheme used in the bootstrap estimation has the drawback of assuming that all events, regardless of its size, may be censored with equal chance. This may only be true when events of essentially the same m_b level are used in the MLE-GLM. This assumption

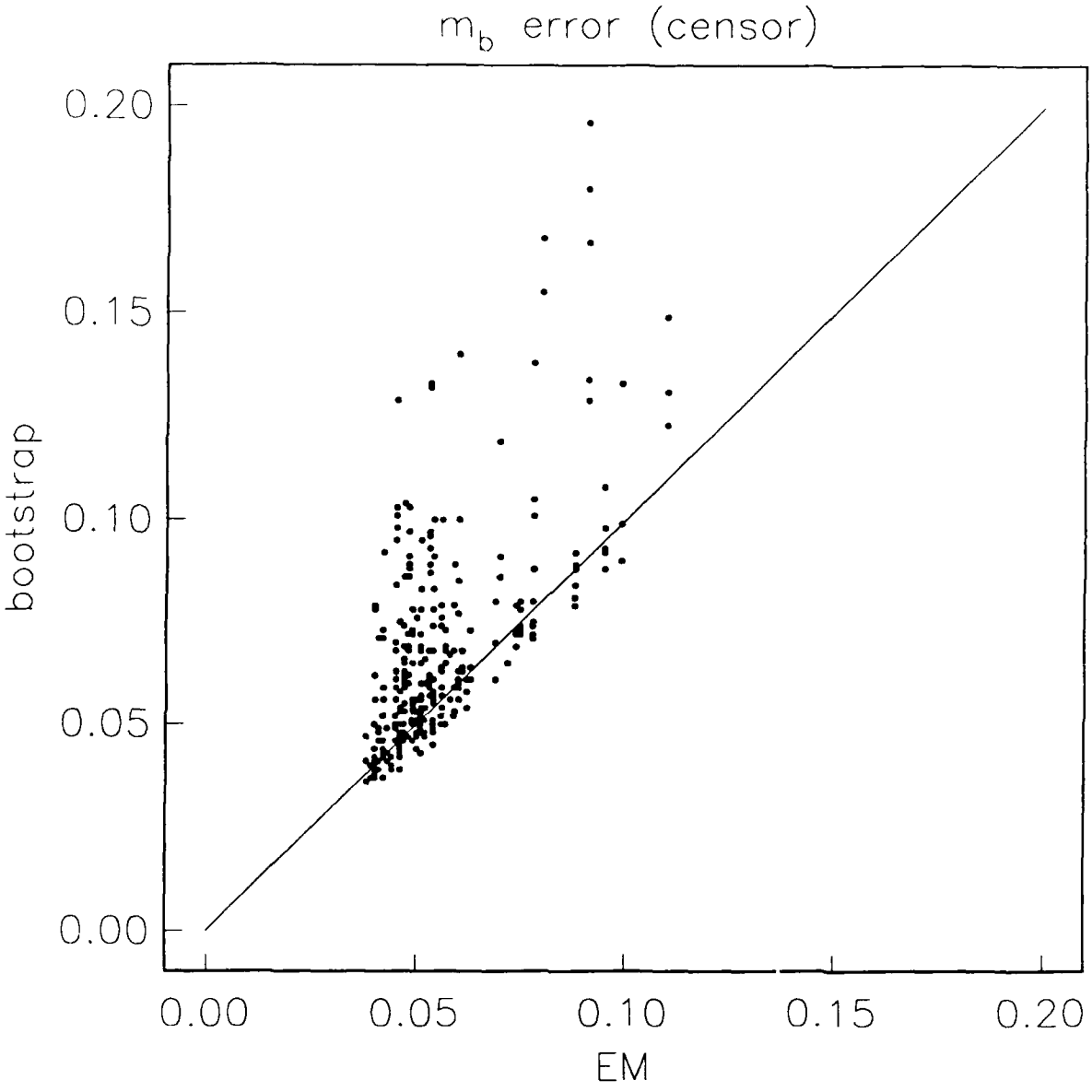

Figure 8. MLE-GLM m_b error estimates for using bootstrap versus EM. The bootstrap error estimates are biased high.

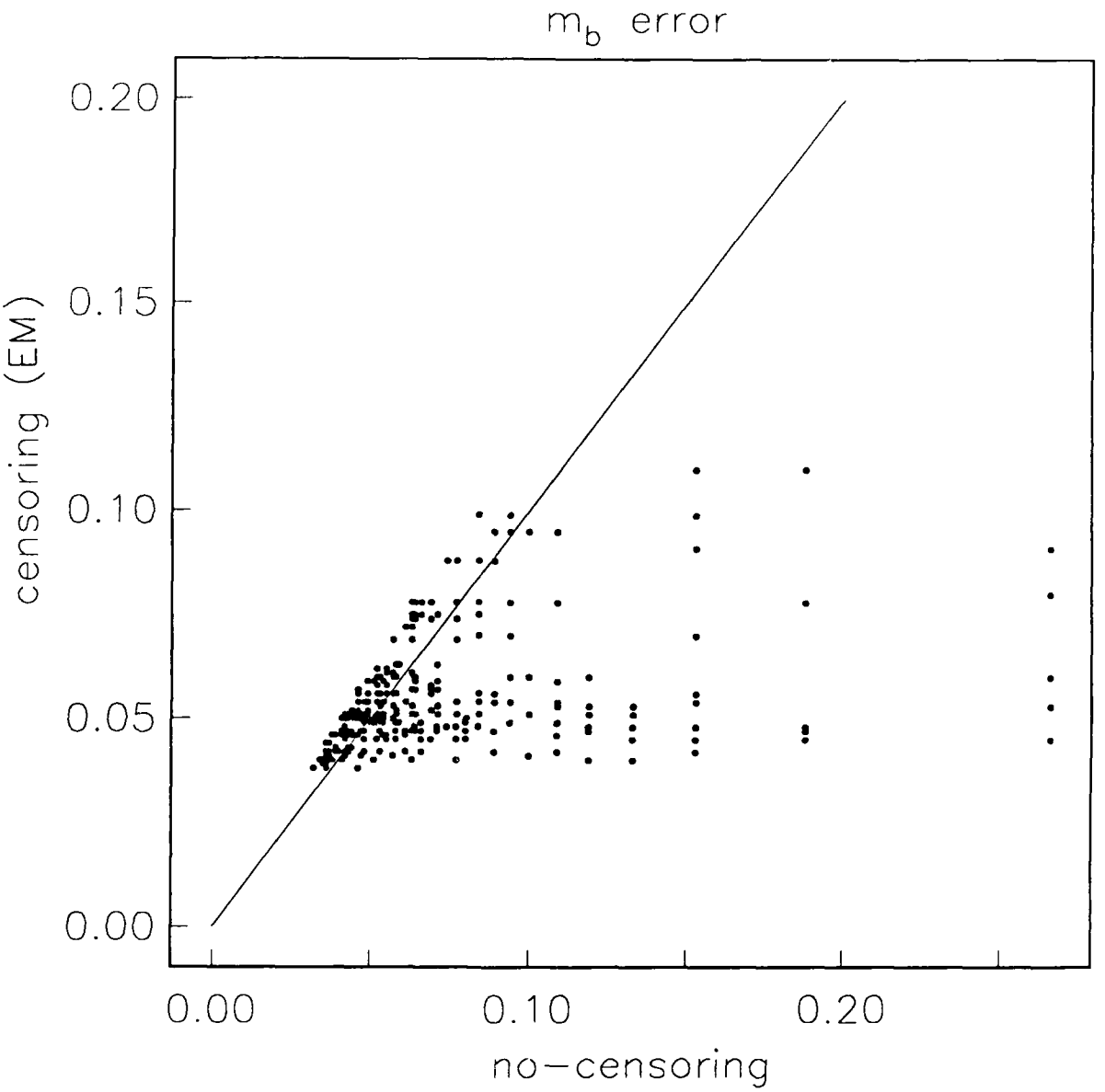

Figure 9a. LS-GLM m_b error estimates versus MLE-GLM m_b error estimates obtained from EM. The LS-GLM m_b errors computed with no-censoring information are higher than those with censoring information.

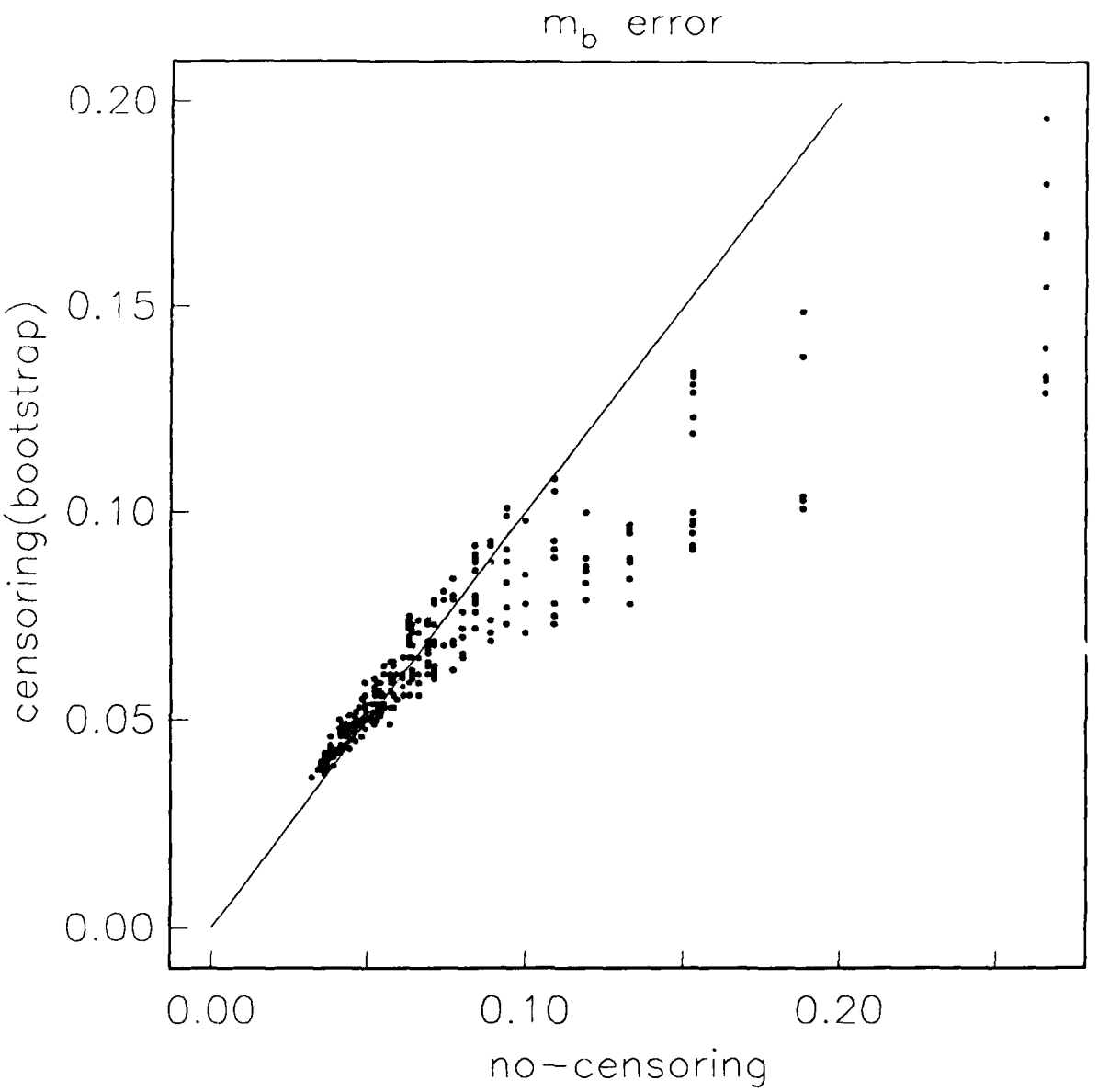

Figure 9b. LS-GLM m_b error estimates versus MLE-GLM m_b error estimates obtained using bootstrap. The LS-GLM m_b error estimates computed with no-censoring information are higher than those with censoring information.

may give rise to some of the discrepancies in the m_b error estimation using the EM and bootstrap approaches. The MLE-GLM m_b error estimates for censoring and no-censoring data are plotted in Figure 10 for all three phases separately. The larger degree of deviation from a unit slope for the error of $m_b(a)$ than for the other two phases may be attributed to the smaller number of observations for phase "a".

The error of the station effects is also computed. As in the case of m_b error estimates, the MLE-GLM error estimates of the station effects using censoring data are smaller than those for GLM using no-censoring information, as shown in Figure 11a. Using the station error estimates from bootstrap, the deviation from those obtained using no-censoring information becomes less than the MLE-GLM case, as shown in Figure 11b.

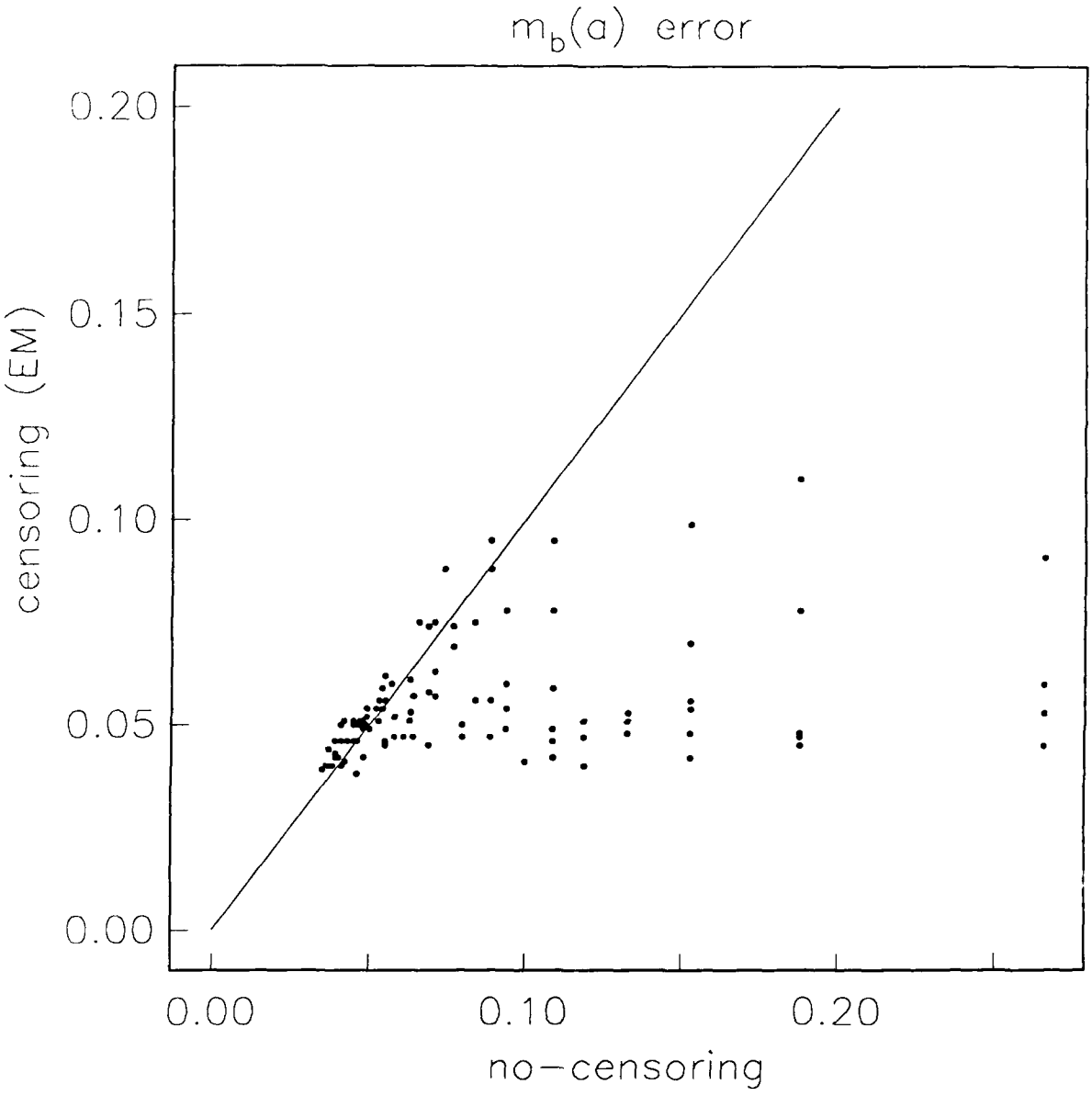

Figure 10a. LS-GLM m_b error estimates versus MLE-GLM m_b error estimates obtained from EM using just the "a" phase data. The LS-GLM m_b error estimates computed with no-censoring information are higher than those with censoring information.

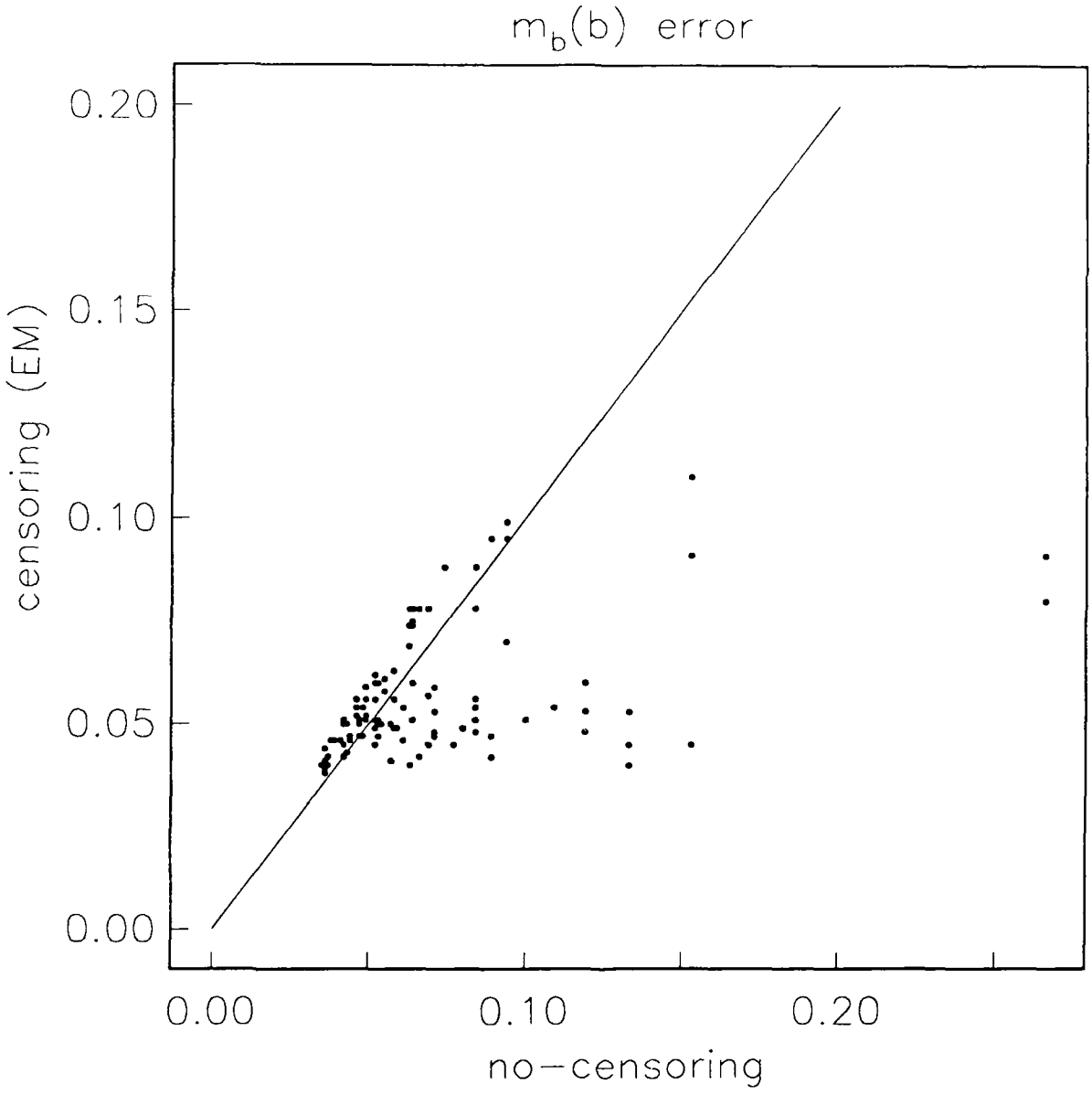

Figure 10b. LS-GLM m_b error estimates versus MLE-GLM m_b error estimates obtained from EM using just the "b" phase data. The LS-GLM m_b error estimates computed with no-censoring information are higher than those with censoring information but show smaller bias than those for phase "a".

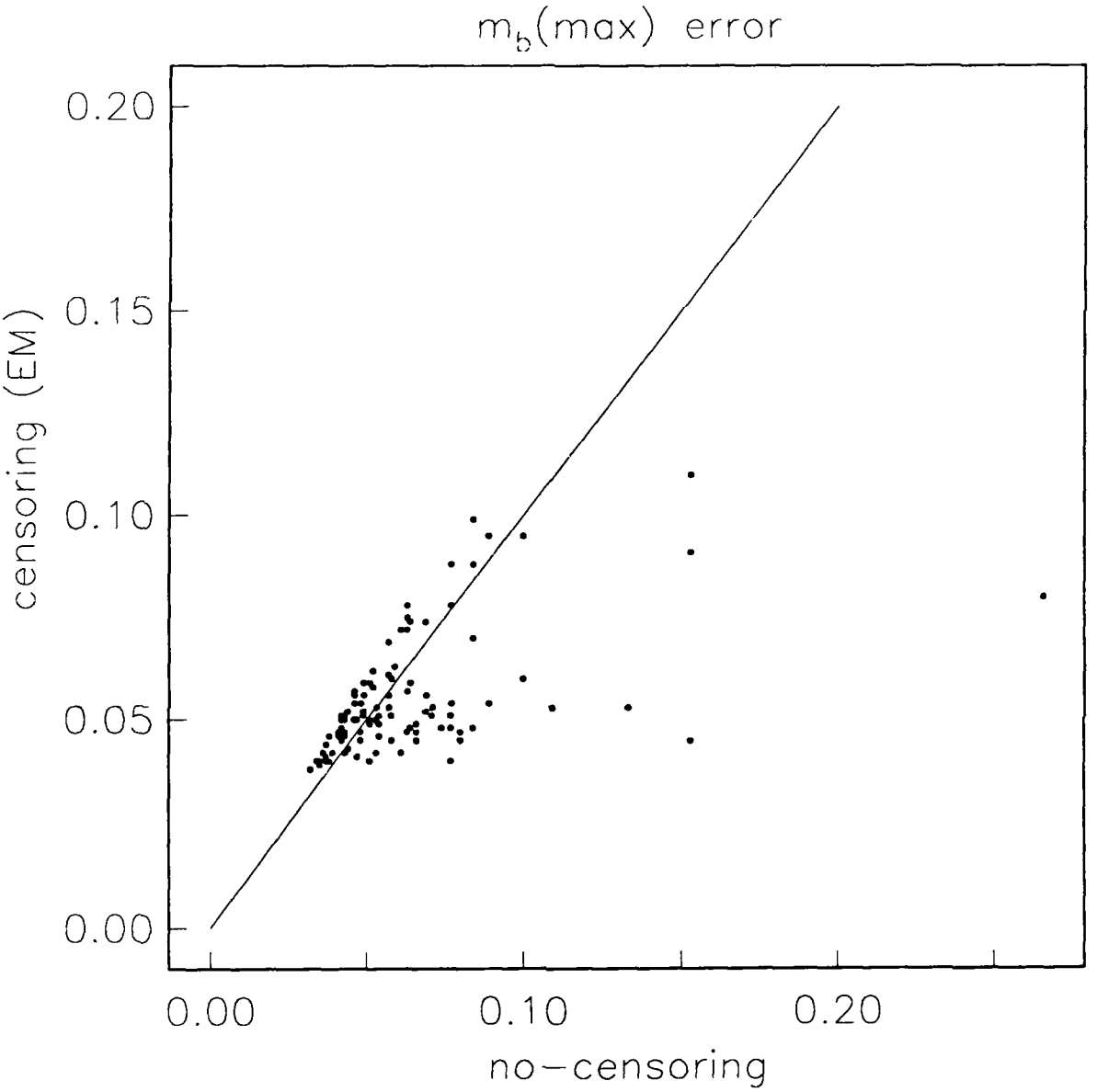

Figure 10c. LS-GLM m_b error estimates versus MLE-GLM m_b error estimates obtained from EM using just the "max" phase data. The LS-GLM m_b error estimates computed with no-censoring information are higher than those with censoring information but show smaller bias than those for phase "a".

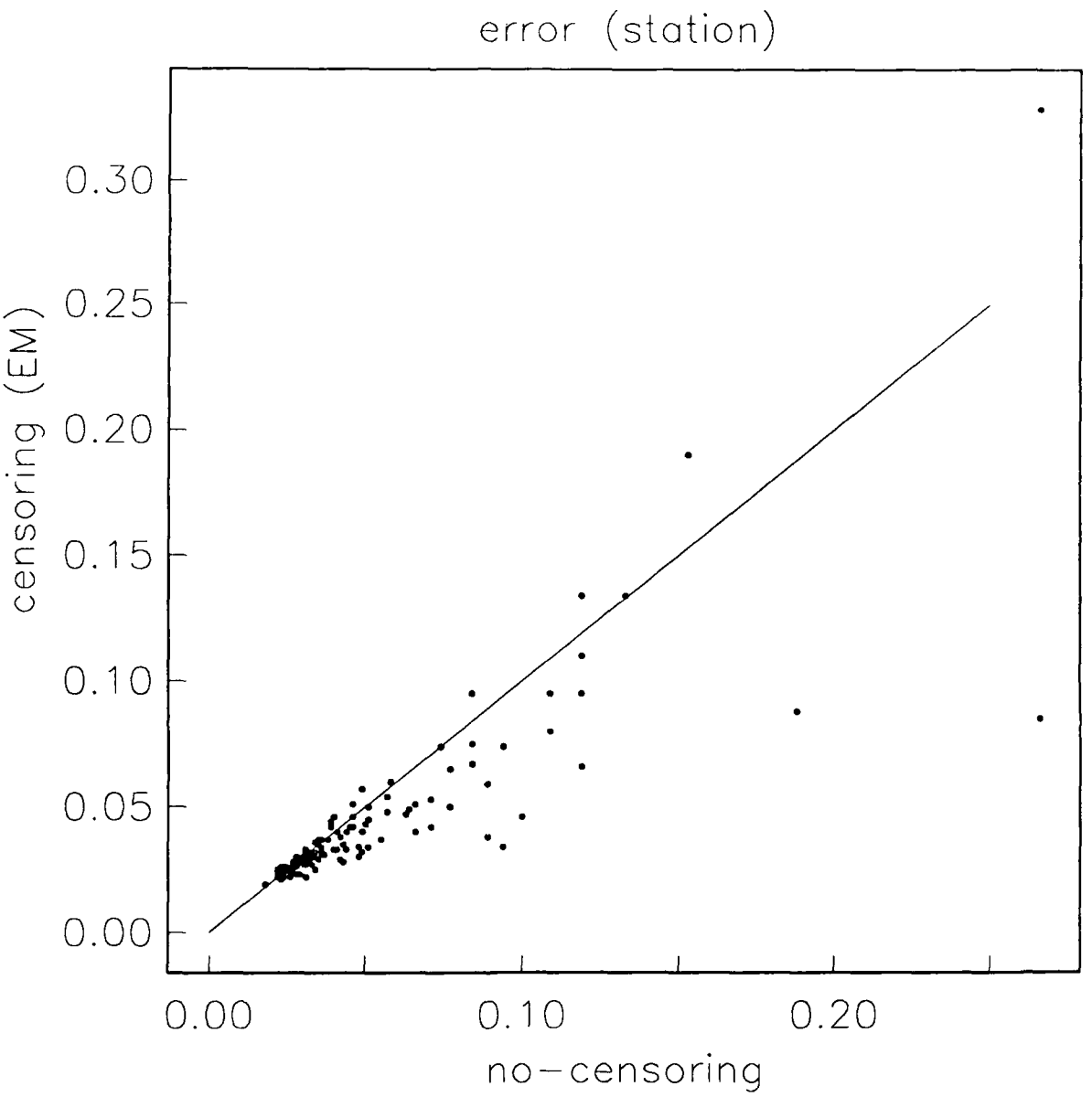

Figure 11a. LS-GLM site term error estimates versus MLE-GLM site term error estimates using EM. The error estimates for the no-censoring case are larger than those for the censoring case in agreement with the m_b error observations.

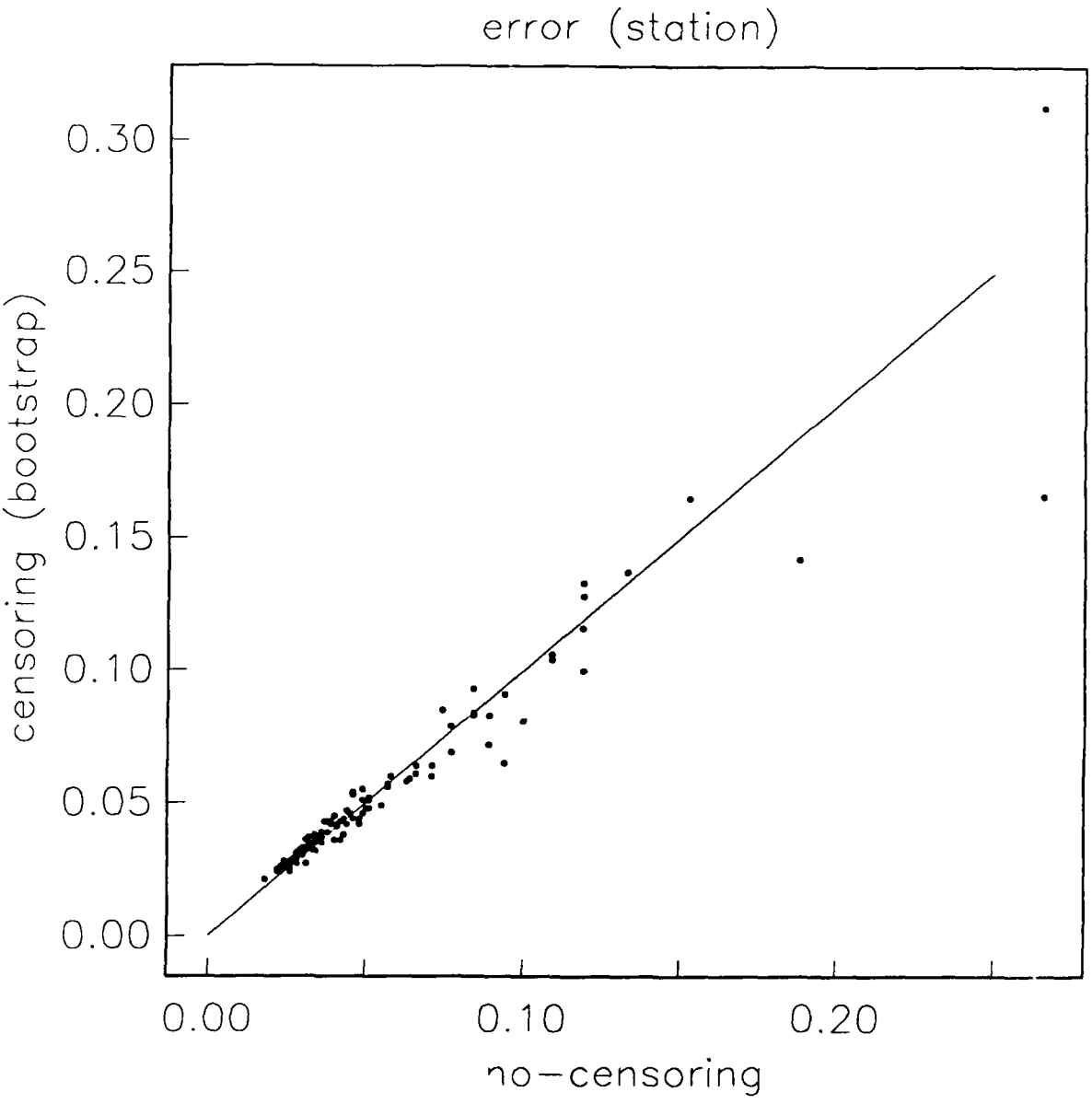

Figure 11b. MLE-GLM site term error estimates obtained using bootstrap are plotted against those obtained using EM. The error estimates using the two different schemes are in quite close agreement to each other.

4.0 PHASE DIFFERENTIAL m_b's

P and P coda arrivals are most likely affected by anomalous arrivals due to scattering, surface multiples, and cratering. The first motion P-wave amplitude measured as the "a" phase is perhaps the least affected by these later arrivals compared to the "b" or "max" phase. Therefore, comparing the "a" phase to the "b" or "max" phase may provide a calibration on the near-source effects of a nuclear explosion. By using the MLE-GLM m_b estimates from the phase-ratios of these phases, characteristics of the lateral variability of the near-source structure will be examined.

The log amplitude ratios between the "a" and "max" phase have been studied to discriminate between contained and cratering events at Shagan River and Degelen by McLaughlin *et al.* (1985, 1986a). Their findings were that the log amplitude ratios of the "max" phase over "a" phase for cratering explosions are smaller than the contained ones. The coda energy level of the teleseismic P-wave decreases dramatically for cratering shots. An example of such is the Jan 15, 1965 presumed cratering explosion at Shagan River (Rodean, 1979). Using this event as a calibration, McLaughlin *et al.* (1986a) have found two other Shagan River events which have similar amplitude ratios approaching that of the Jan 15, 1965 event.

In this study, the MLE-GLM m_b estimates for NTS and Novaya Zemlya explosions are analyzed along with the E. Kazakhstan explosions. The MLE-GLM m_b's estimates for the different test sites are used to compute the $m_b(max)$-$m_b(a)$ and $m_b(max)$-$m_b(b)$ for all events of interest and are analyzed in the context of each test site. A self-consistent set of station terms derived in the MLE-GLM is used to correct

for the site effects in the maximum-likelihood estimation.

The comparisons between the different phases made in Figure 3 for all events show that the m_b estimates for the "a" phase are on the average 0.5 magnitude unit less than those for the "max" phase. The scatter in the data indicates that biases exist among the different events, which warrants a more in-depth analysis. The δm_b's between "a" and "max" and "b" and "max" phases are plotted against m_b(max) in Figures 12a and 12b for Shagan and Degelen, respectively. Considering only those events recorded by more than 10 stations for the "a" phase, the δm_b(max-a)'s range between 0.4 to 0.68 for Shagan and 0.45 to 0.54 for Degelen events. These values are within the range presented in McLaughlin *et al.* (1985). The smaller range in δm_b's obtained for the Degelen events compared to Shagan may imply that the structure beneath Degelen is more nearly homogeneous, but the sample is too small to be conclusive.

The Jan 15, 1965 (event 29 in Table 2 and Figure 12a) presumed cratering event shows a lower than average δm_b(max-a) of 0.39, in agreement with the observation by McLaughlin *et al.* (1985). But further analysis of this event indicates that its δm_b(max-b) does not deviate statistically from the rest of the population, possibly indicating that the "a" phase is less affected by the surface reflections than the "b" and "max" phases. The Sep 15, 1978 (event 38) explosion which shows an anomalous low log(max/a) in McLaughlin *et al.* (1985) does not appear to be such in our analysis. This event has a δm_b(max-a) of 0.47 which is not statistically different from the rest of the δm_b(max-a)'s taking into account 2σ error of about 0.11 from Table 3. But in fact, the δm_b for this event is even higher than two other events, Jul 23, 1973 (event 32) and Jun 23, 1979 (event 39), that were not studied in McLaughlin *et al.*'s (1985). The scatter in

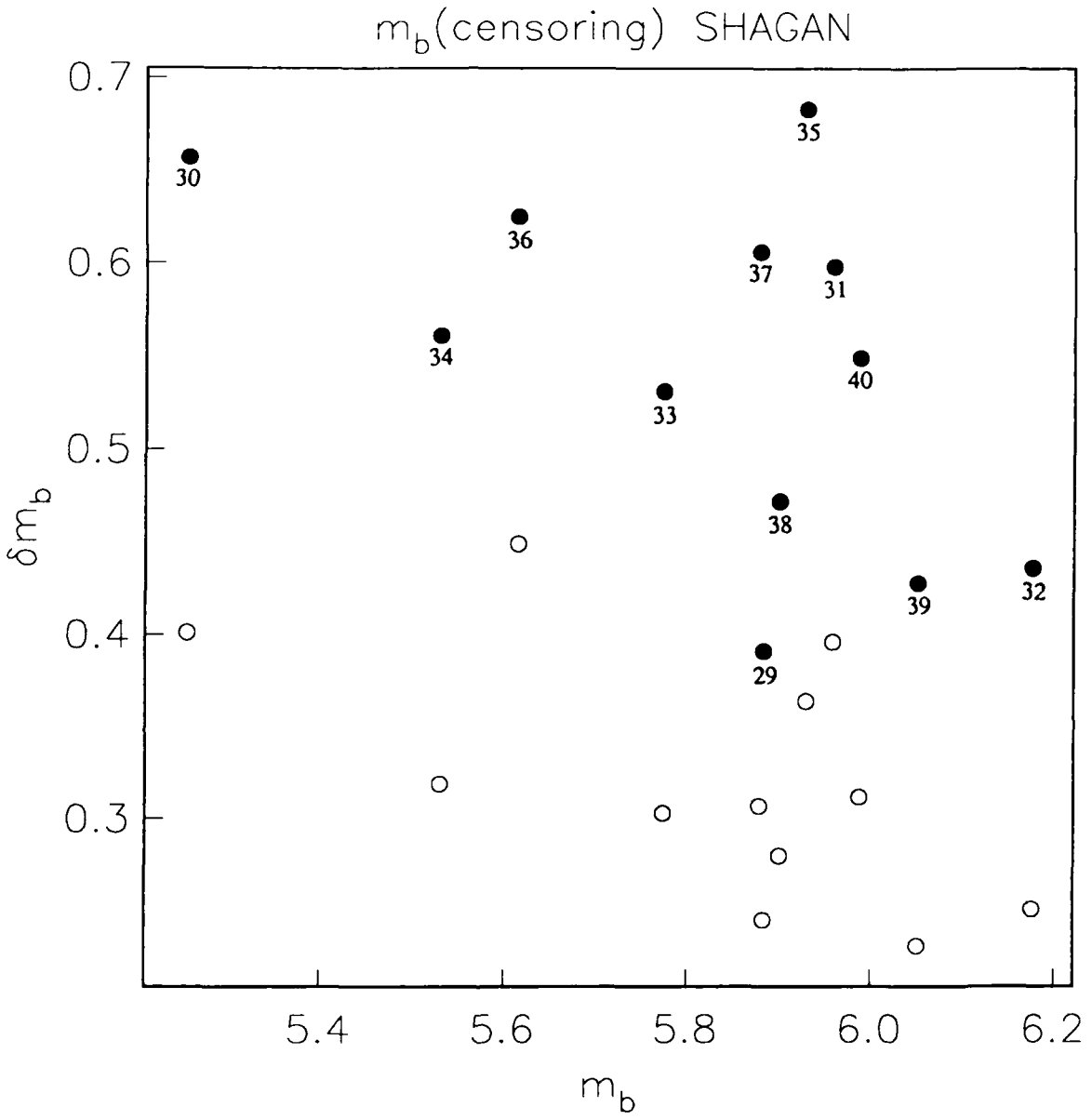

Figure 12a. m_b(max)'s plotted against δm_b's for Shagan. The m_b's are maximum likelihood estimates with the censoring information. The solid circles are m_b(max)-m_b(a) and the open circles are m_b(max)-m_b(b) for the corresponding event. The events are listed in Table 2.

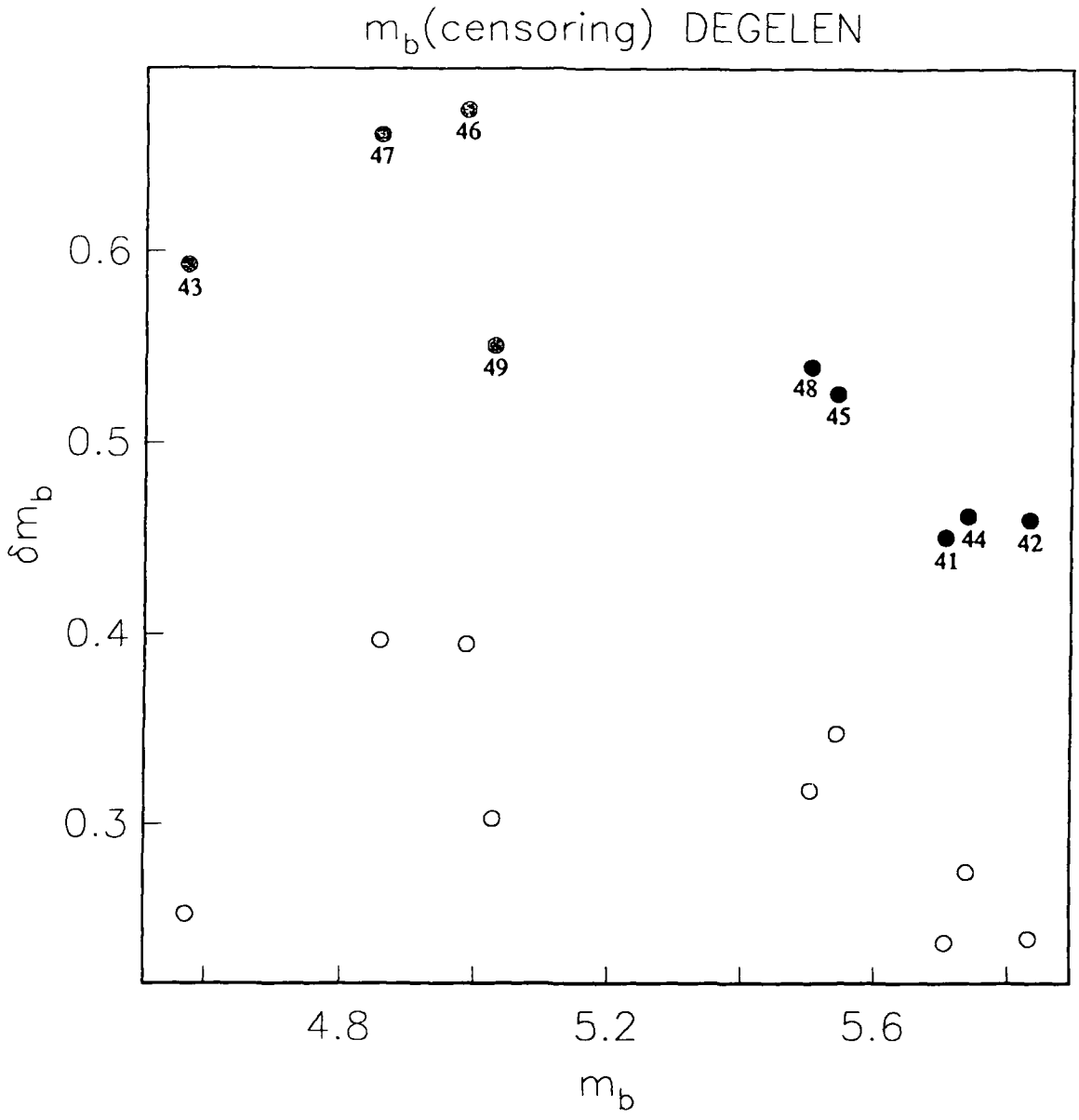

Figure 12b. m_b(max)'s plotted against δm_b's for Degelen. The m_b's are maximum likelihood estimates with the censoring information. The solid circles are m_b(max)-m_b(a) and the open circles are m_b(max)-m_b(b) for the corresponding event. The events are listed in Table 2. The hatched circles are m_b(max)-m_b(a) for which there are less than 10 "a" phase signal readings.

the data nonetheless prevents us to argue with high confidence that the low δm_b(max-a) of event 29 is directly related to the cratering effect. Moreover, the only physical interpretation of such a relationship is possibly that of an absence of surface reflected multiples causing a reduction in the "max" and "b" amplitudes. Such an effect was however not observed in a comparison of regional P_n from cratering and tamped explosions (Gupta *et al.*, 1988).

For the NTS events, most of the explosions with m_b(max) of less than 5.0 are not well detected by the WWSSN network and are not used in the analysis. The δm_b's are plotted in Figure 12c. All events with m_b(max) of less than 5.5 have low δm_b(max-a)'s between 0.3 to 0.43. The rest of the larger events have δm_b(max-a)'s of over 0.5, except for Handley (event 11). The anomalous low magnitude ratios for the smaller events (m_b(max) between 5.0 to 5.5) may be attributed to low detection levels, and they are therefore not emphasized in the analysis. Handley (m_b(max) 6.48), which is well recorded by the network with 41 signal readings, exhibits an anomalously large "a" amplitude which indicates that there may be strong heterogeneity in its source function and source medium beneath this test site compared to the rest of the NTS test sites.

The Novaya Zemlya events, divided into north and south, are plotted in Figure 12d. The presumed double event of Oct 18, 1975 (event 55) (Hurley, 1977; Chan *et al.* 1988) stands out as having large coda multiples, which contribute to the anomalous large "max" phase compared to the "a" phase. Most of the north Novaya Zemlya events have δm_b's of between 0.35 to 0.48, which are much less than the other test sites, indicating that the source structure there may be quite different from the

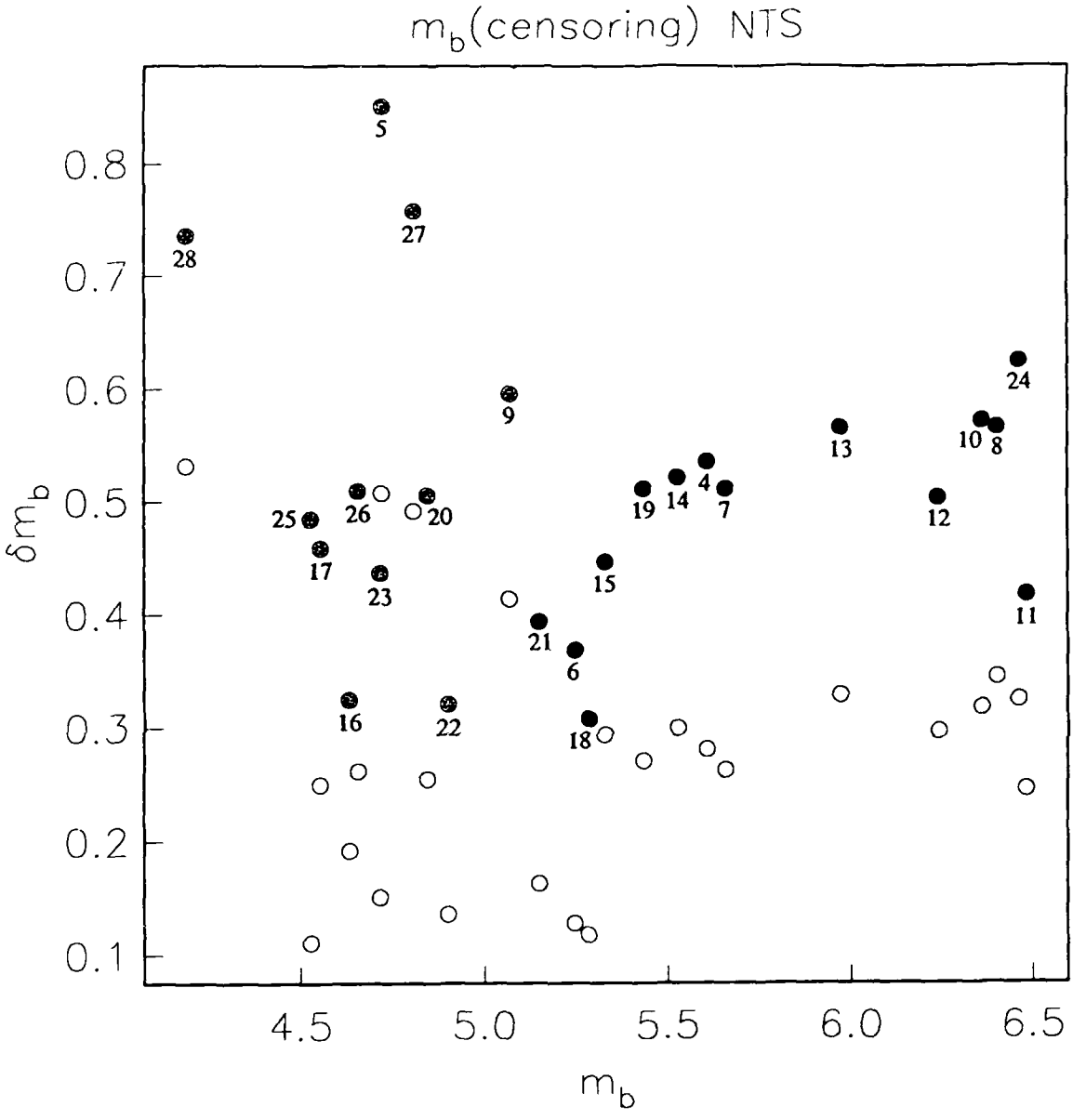

Figure 12c. m_b(max)'s plotted against δm_b's for NTS. The m_b's are maximum likelihood estimates with the censoring information. The solid circles are m_b(max)-m_b(a) and the open circles are m_b(max)-m_b(b) for the corresponding event. The events are listed in Table 2. The hatched circles are m_b(max)-m_b(a) for which there are less than 10 "a" phase signal readings.

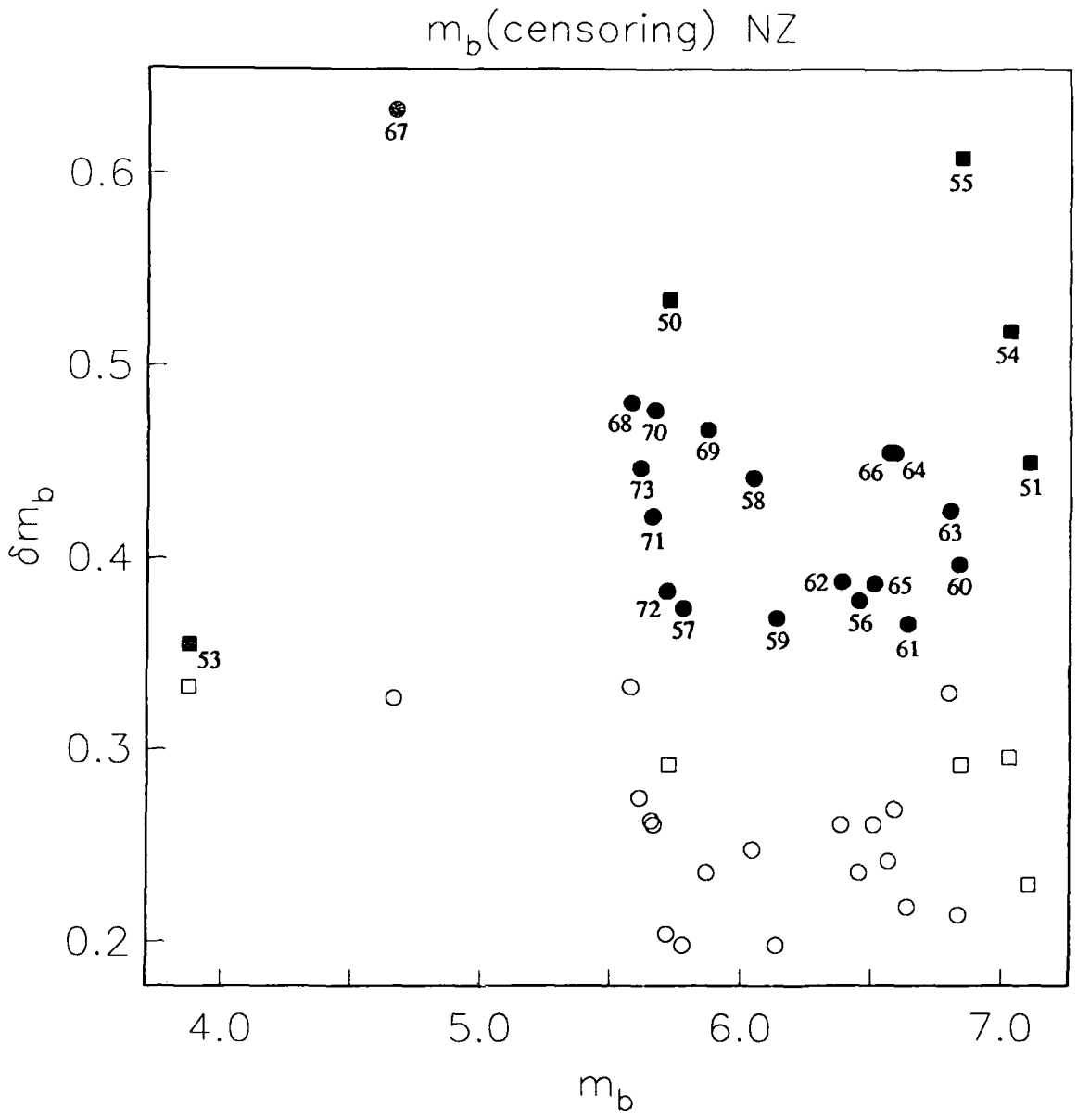

Figure 12d. m_b(max)'s plotted against δm_b's for Novaya Zemlya. The m_b's are maximum likelihood estimates with the censoring information. The solid and open circles are m_b(max)-m_b(a) and m_b(max)-m_b(b), respectively, for corresponding events in the northern site. The solid and open squares are m_b(max)-m_b(a) and m_b(max)-m_b(b), respectively, for corresponding events in the southern site. The hatched circles and squares are m_b(max)-m_b(a) for which there are less than 10 "a" phase signal readings.

others. There is a slight indication that the structure beneath the southern and northern sites may be different judging from their δm_b's levels, but more data from this test site need to be analyzed to comment further on this issue.

5.0 SINGLE TEST SITE GLM's VERSUS WORLD-WIDE GLM's

As was stated earlier, Longshot was not an adequate calibration event for Milrow and Cannikin because the composition of WWSSN stations changed for the three events and because of the clipping for Cannikin and Milrow. In order to demonstrate this, we list in Table 5 the magnitudes for these three shots as determined from an LS-GLM and MLE-GLM using only these three events, compared to the results of the full MLE-GLM for m_b(max). The results are striking in that Cannikin decreases by up to 0.105 magnitude units from a single test-site determination to the full determination, whereas Longshot increases by 0.012.

Table 5. Comparison of Single Test Site Only GLM with MLE-GLM88 Amchitka Test Site

	Amchitka Only		World-Wide		
Event	LS-GLM	MLE-GLM	LS-GLM	MLE-GLM	$\delta_{MLE-GLM}$
Cannikin	6.984	7.021	6.832	6.916	0.105
Milrow	6.565	6.583	6.433	6.497	0.086
Longshot	5.821	5.811	5.854	5.823	-0.012

This comparison points out that the common practice of choosing only a few calibration events at a single test site can and does lead to systematic errors. How does this come about? When we examine the Amchitka data set, we see that it contains 84 stations and that the RMS station effect is 0.37 magnitude units. If we were to assume that station effects are normal random variables with a standard deviation of 0.37 and zero mean, then we would expect that the mean of 84 stations drawn from the population would have a 5% probability of being either greater than 0.08 or less than -0.08. In actuality there are only 32 common WWSSN stations ($20° \leq \Delta \leq 95°$) between Longshot and the two larger shots Milrow and Cannikin. The 95% confidence bound

on the bias from these 32 stations is ± 0.13 magnitude units.

It is important to remember that the constraint equation that the station effects should sum to zero, $\sum_{k=1}^{N} C_k = 0$, has an uncertainty associated with it. In the case of the Amchitka explosions, this potential bias appears to be more acute than at other test sites since the network configuration had changed substantially between these explosions in the late 1960's.

Of course, in reality some of these biases are caused by deterministic effects that one can anticipate. The leading hypothesis for this Amchitka "bias" is the focusing-defocusing of the P-wave by the descending slab beneath the Aleutian island arc. Such effects could be predicted deterministically and corrections could be applied, as was done by Cormier (1986) using ray-tracing methods applied to a 3-D model of the source region obtained from block inversion of traveltime residuals.

We have performed the same analysis for 9 NTS events, 16 Novaya Zemlya events, and 11 Tuomotu events with the results that the event magnitudes had RMS changes of 0.038, 0.072, and 0.025 for NTS, Novaya Zemlya, and Tuomotu respectively (see Table 6). None of these test sites demonstrated substantial changes approaching 0.1 magnitude units. In each case, the data were analyzed using an MLE-GLM for the test site alone, and then the individual event magnitudes were compared to an MLE-GLM with a full complement of 106 explosions. However, when 6 southern Novaya events were used in an MLE-GLM, the average event decreased 0.05 magnitude units with an rms shift of 0.077 magnitude units. This is significant in light of the formal standard errors of the individual event magnitudes of about 0.02 units.

This implies that if magnitude calibrations are to be performed for a single test site, then uncertainties approaching 0.1 magnitude units should be attributed to the final results for purposes of inter-test site comparison.

It is interesting to note that the RMS station effect and the residual RMS error are roughly in the same proportion for each test site that was examined separately. However, there may be significant differences between some test sites in the total variance. Table 6 lists the number of events, the number of stations, the degrees of freedom, the RMS station effect, the RMS residual error, and $\sigma_{total} = \sqrt{(RMS\text{–}STA)^2+(RMS\text{–}RES)^2}$ for each major test-site specific MLE-GLM and an MLE-GLM based on 111 explosions. We see that the station effects are between 73% and 90% of the original magnitude variance. The RMS residual is smaller for smaller sets of explosions (fewer degrees of freedom) and for sets of events located in smaller test sites. For comparison, an MLE-GLM for 111 explosions and 127 stations had 2598 degrees of freedom, an RMS station effect of 0.219, and an RMS residual of 0.247. For the worldwide MLE-GLM the station effects were on average 44% of the total original variance. As events are added over a greater area of the globe, the station effects are a smaller proportion of the total variance, tending to about 40%. For example, the station effects for northern and southern Novaya Zemlya test sites treated separately are only 53% correlated; yet the two testing areas are separated by only 800 km. Amchitka (AMC) and Northern Novaya Zemlya (NNZ) have the largest total variance, and NTS has the smallest.

Table 6. Comparison of Major Test Site Specific m_b(max) MLE-GLM's

Test Site	# Events	# Stations	# Deg. Freed.	RSM STA	RMS RES.	σ_{total}
NTS	9	64	231	0.246	0.150	0.288
SNZ	6	43	45	0.273	0.138	0.306
TUO	11	53	223	0.286	0.122	0.311
NNZ	10	75	217	0.357	0.140	0.383
NZ	16	76	303	0.348	0.169	0.387
AMC	3	84	82	0.370	0.124	0.390
111EXP	111	127	2598	0.219	0.247	0.339

6.0 INTER-EVENT CORRELATION

The procedure by Blandford *et al.* (1984) for perturbing the MLE-GLM solution with an *a priori* correlation matrix is used by McLaughlin *et al.* (1986a) to construct GLM86 for a world-wide set of 53 events included in the MLE-GLM88 set. They used an event-event correlation model, so that the station corrections would not be overly influenced by a large number of events at a single test site. The model assumes that pairs of observations at a specific station are correlated if the two observations are from events that are close together. The correlation function is parameterized by two exponential decays. If two events, i and j, are separated by distance Δ_{ij}, then the observations at any station for these two events are correlated by the amount

$$C_{ij} = A_0 \left(\exp(-\Delta_{ij}/a_1) + \exp(-\Delta_{ij}/a_2)\right)/2.$$

where $A_0 = 0.8$, $a_1 = 20.0$ km, and $a_2 = 500$ km in this study. By definition, $C_{ij} = 1$ if the events are the same event, i = j.

The procedure is approximate and would not be needed if the events were evenly distributed around the world and each station were to record signals from many events with an unbiased geographic distribution. In practice, if a large number of events are selected from as many test sites as possible, the results of the perturbation could be minimal. To test this, the m_b(max) magnitudes for 111 explosions were analyzed using an MLE-GLM with and without the event-event correlation correction.

Plots of the m_b estimates derived with and without the event-event correlation perturbation are shown in Figure 13 for the three phases separately. From Figure 13, the only events that change by more than 0.075 units are the 8 Azgir events that were

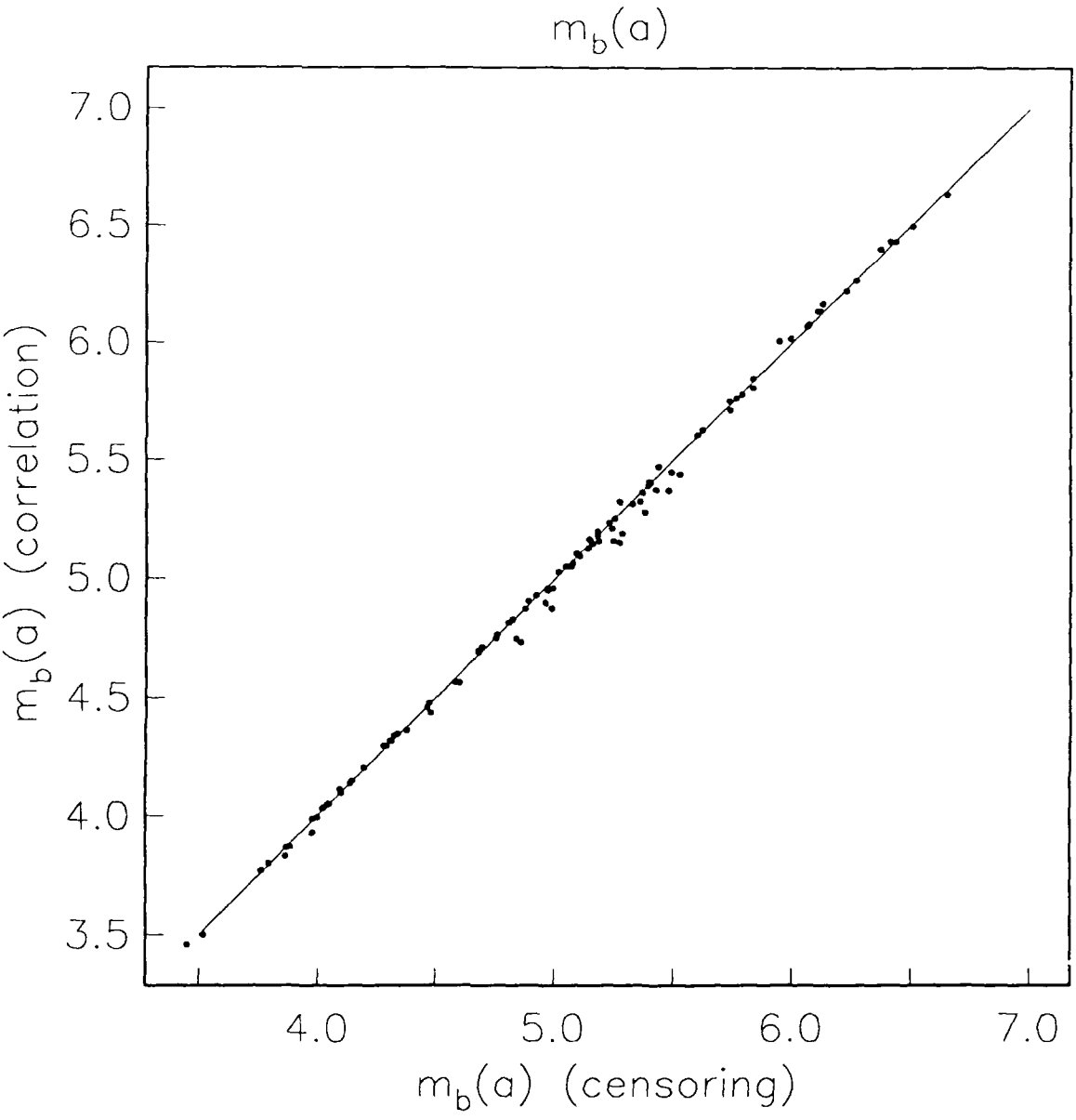

Figure 13a. Event magnitudes for phase "a", $m_b(a)$, from MLE-GLM solutions assuming event-event correlation versus no event-event correlation.

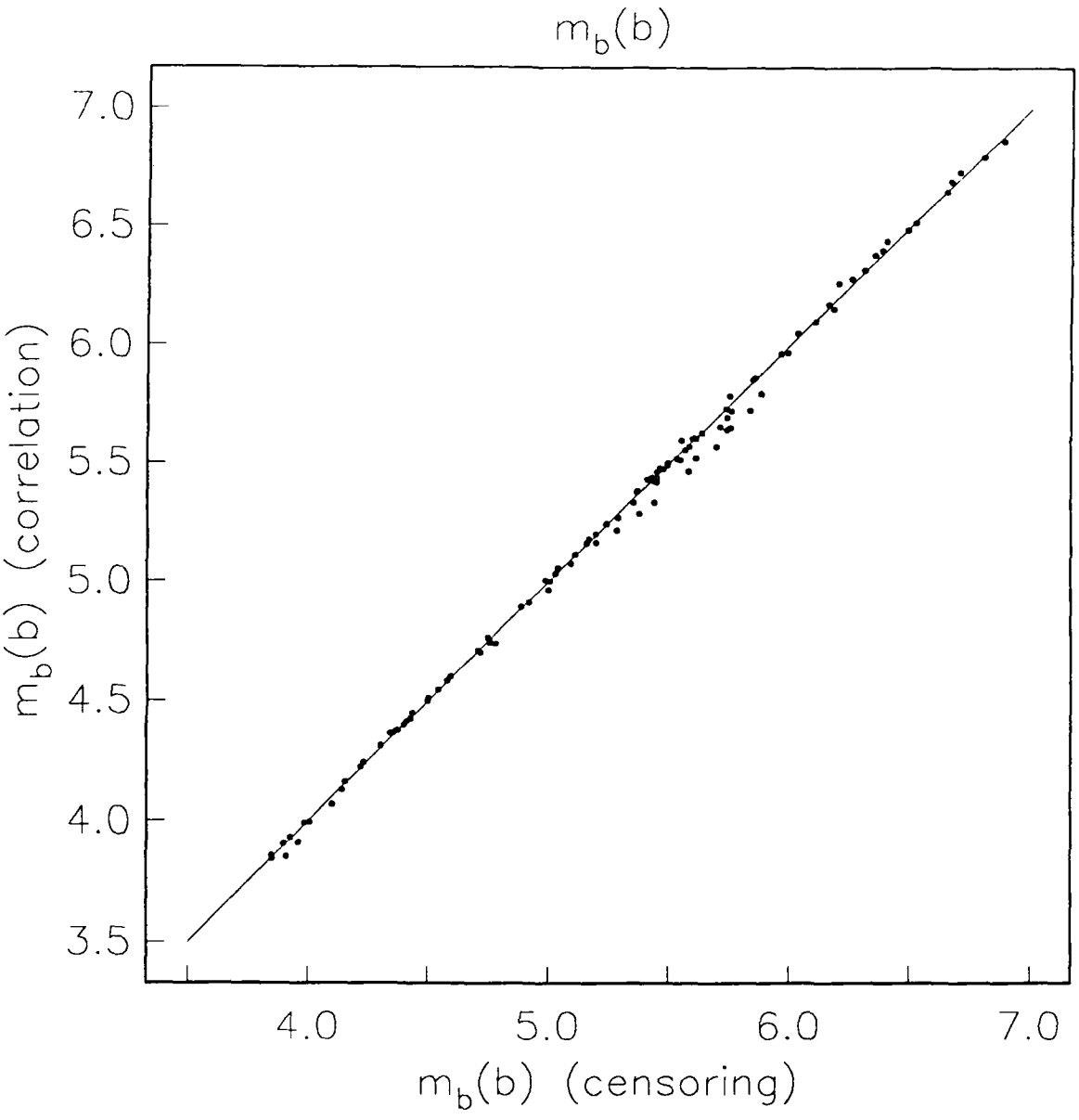

Figure 13b. Event magnitudes for phase "b", $m_b(b)$, from MLE-GLM solutions assuming event-event correlation versus no event-event correlation.

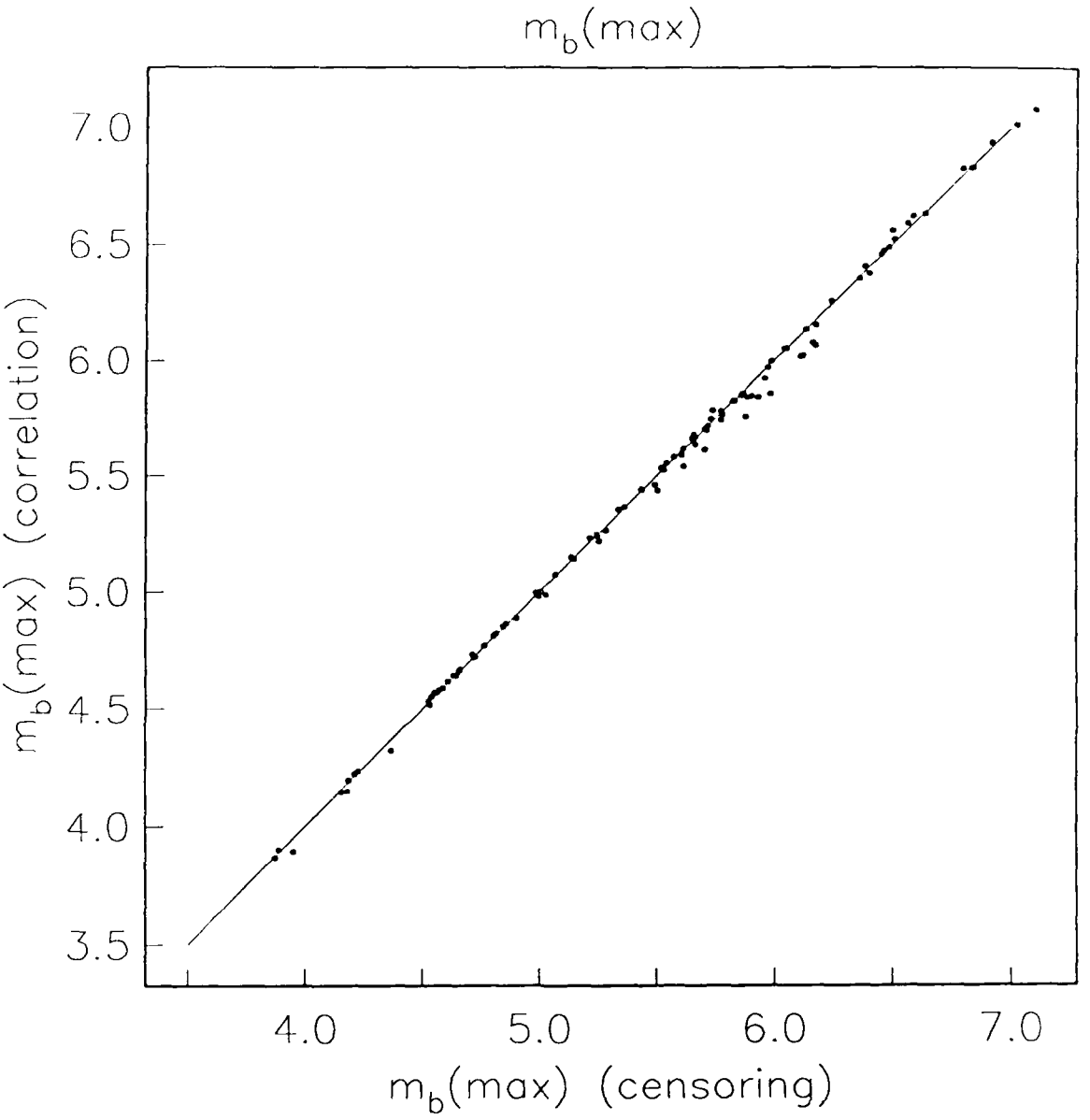

Figure 13c. Event magnitudes for phase "max", m_b(max), from MLE-GLM solutions assuming event-event correlation versus no event-event correlation.

not read at the full complement of stations. These events were read at a small number of stations, and therefore perturbations to the small set of station corrections can introduce statistically significant perturbations. The 2 Azgir events that were read at the full complement of stations did not change by more than 0.05. Again this illustrates the effects of the statistics of offsets in magnitudes from networks with small sample size. The m_b estimates for the different phases obtained with event-event correlation are also plotted in Figure 14. A similar phase bias pattern is seen here as for those in the EM case (Figure 3). The station effects derived with and without event-event correlation are plotted in Figure 15. The scatter of the station effects plotted in Figure 15a between the no-censoring case (LS-GLM) and the no-censoring event-event correlation case is very similar to that between the EM censoring and no-censoring case (Figure 7). The station effects estimates with and without event-event correlation for censoring data are plotted against each other in Figure 15b.

The resulting event magnitudes differ from the MLE-GLM tables presented above (Table 2c) without the correlation correction by an rms amount of 0.05 magnitude units. The station effects were similarly different by an rms difference of 0.05 magnitude units. The differences were generally small and comparable to the differences between the MLE-GLM88 based on "a", "b", and "max" together. Given this result, we conclude that the event-event correlation perturbation is not required for MLE-GLM88 and that the station effects are not significantly improved by the procedure.

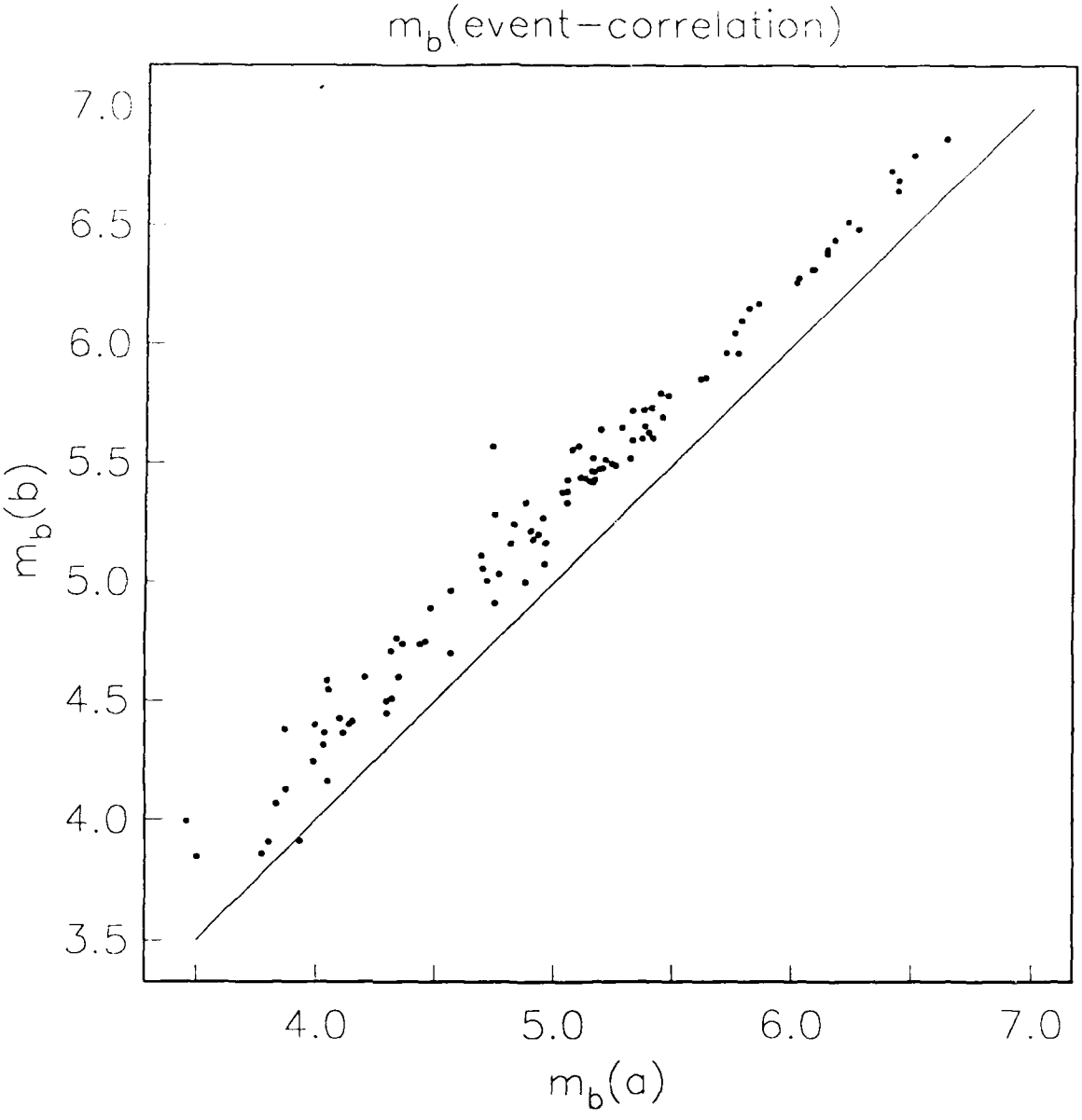

Figure 14a. m_b's estimates assuming event-event correlation for the "a" phase plotted against the "b" phase. The bias is similar to that observed for the MLE-GLM case.

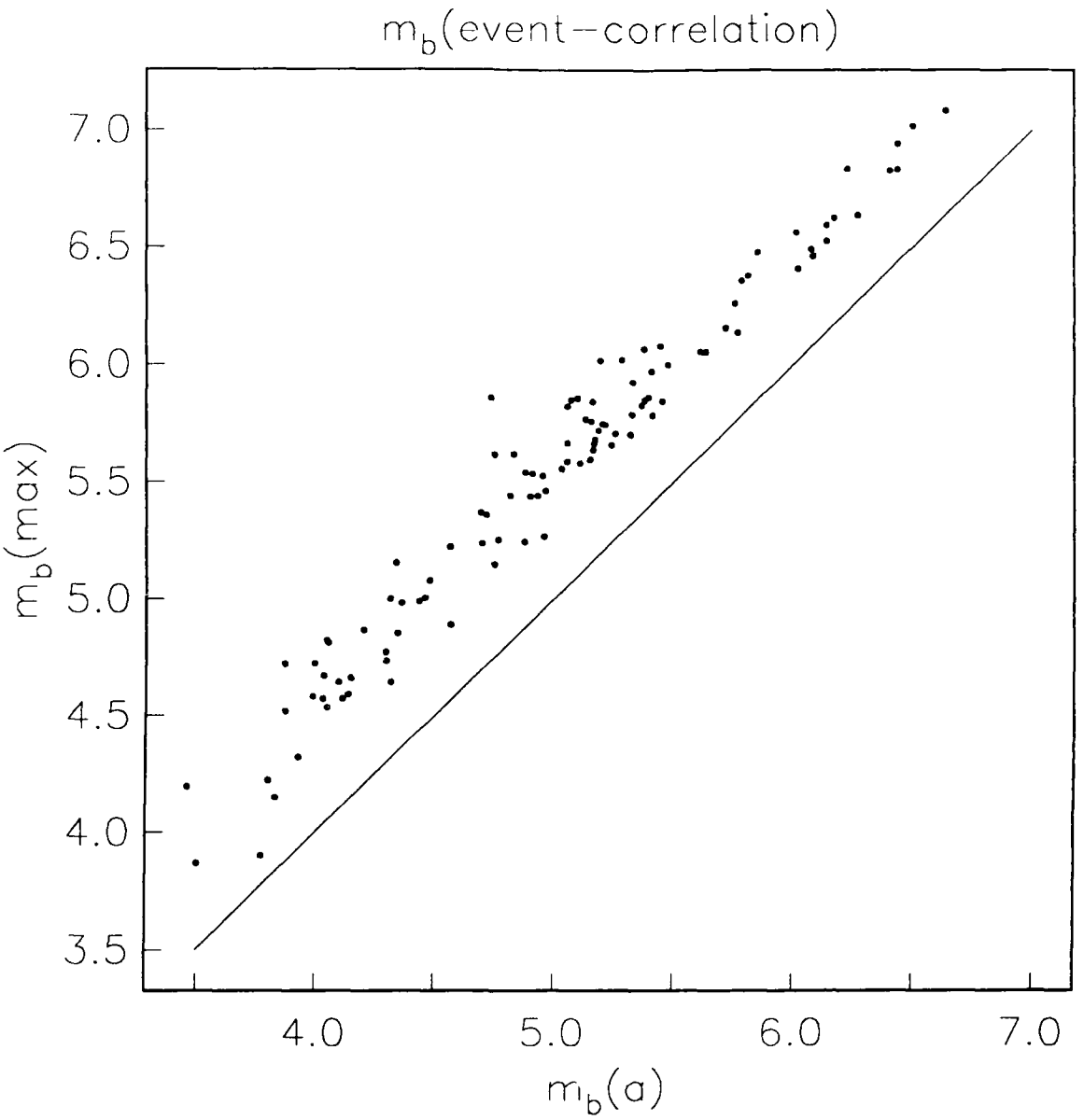

Figure 14b. m_b's estimates assuming event-event correlation for the "a" phase plotted against the "max" phase. The bias is similar to that observed for the MLE-GLM case.

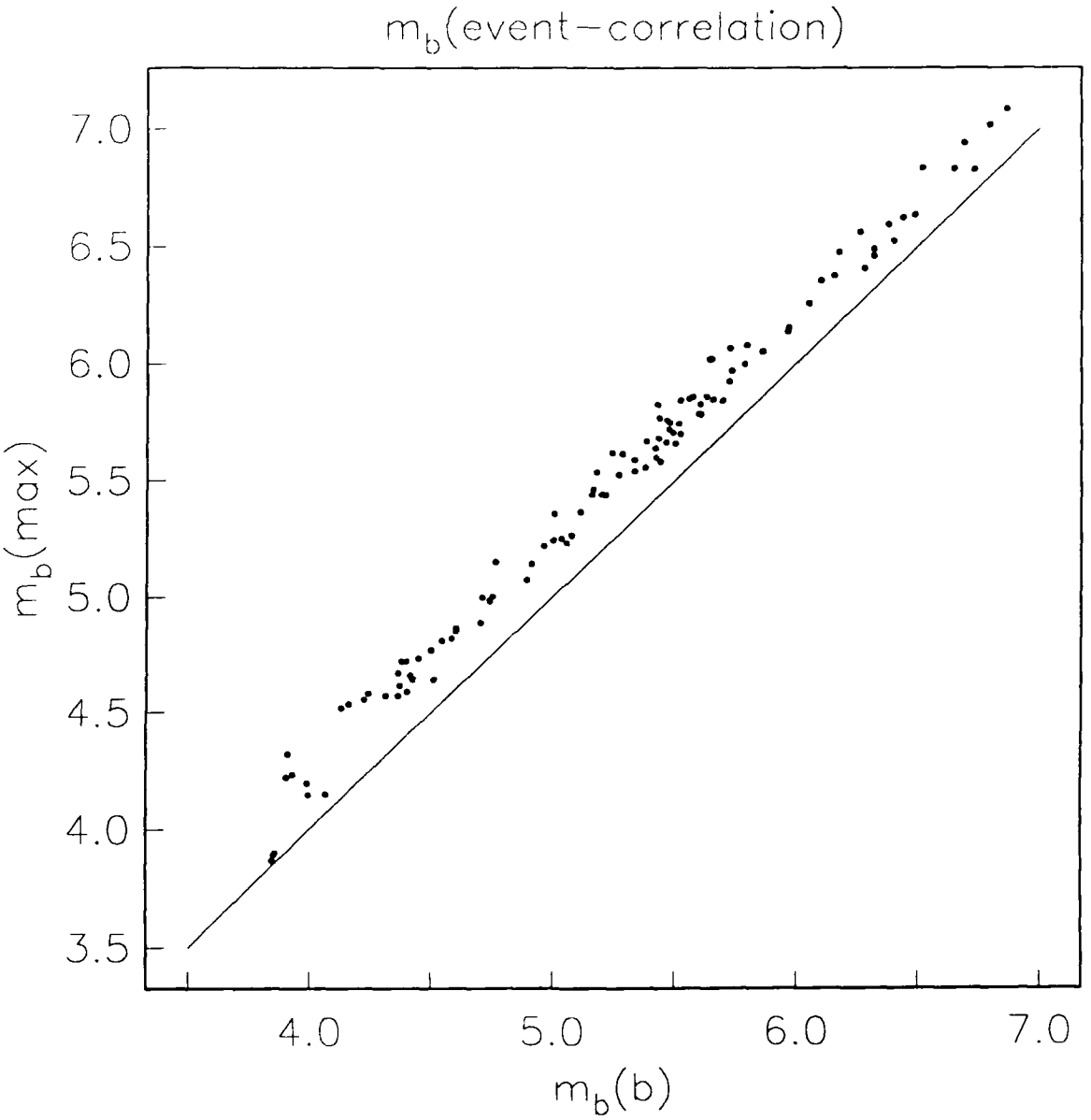

Figure 14c. m_b's estimates assuming event-event correlation for the "b" phase plotted against the "max" phase. The bias is similar to that observed for the MLE-GLM case.

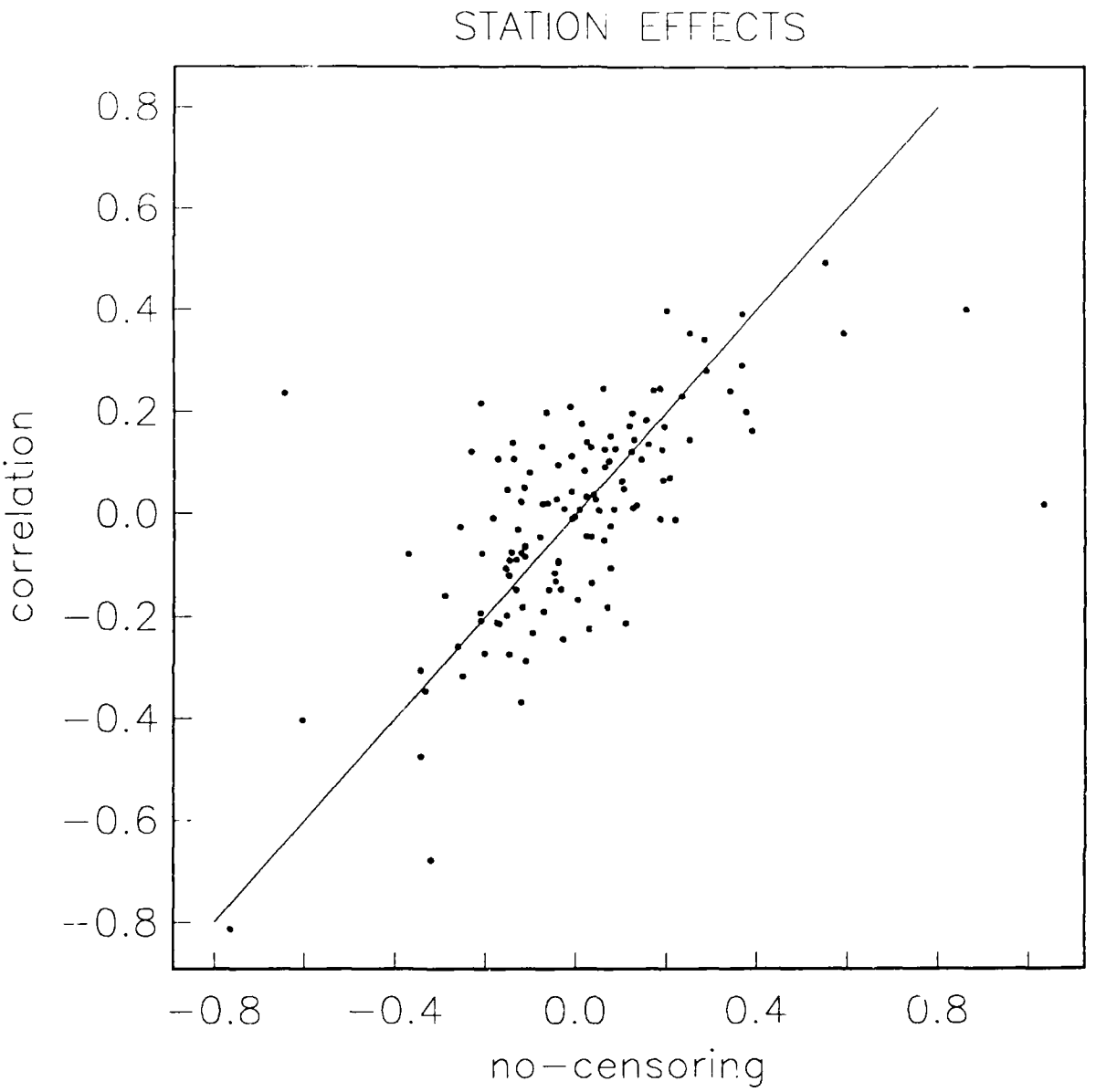

Figure 15a. Site effects for MLE-GLM solutions assuming event-event correlation versus LS-GLM with no-censoring information based on m_b's for all phases.

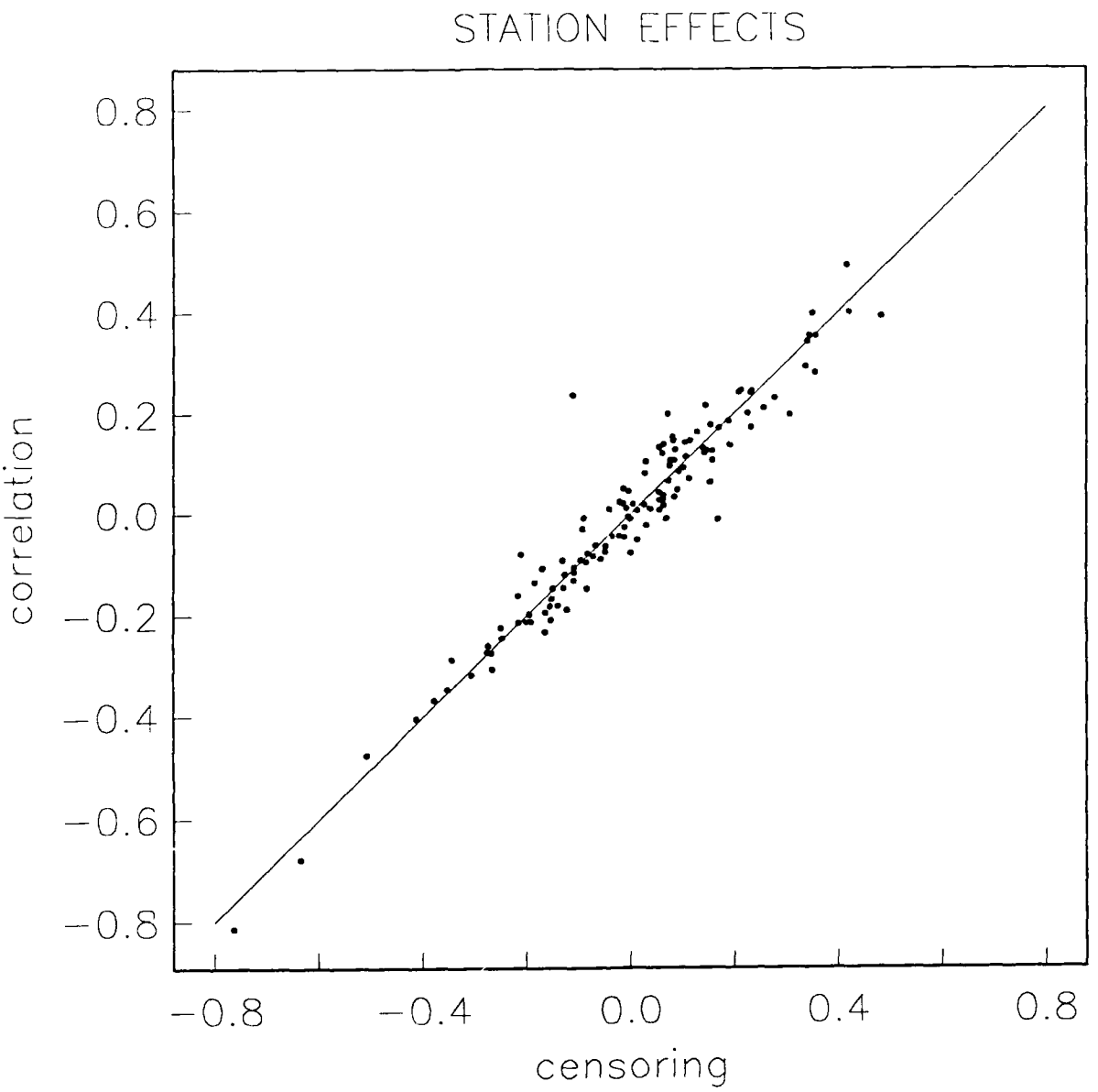

Figure 15b. Site effects for MLE-GLM solutions assuming event-event correlation versus no event-event correlation based on m_b's for all phases.

7.0 CONCLUSIONS

The event magnitudes for 111 nuclear explosions at over eight test sites worldwide are obtained using a maximum-likelihood estimation and constructed in a general linear model (MLE-GLM88). The magnitude estimates and station corrections are obtained for the "a" phase, the "b" phase, and the "max" phase of the short-period teleseismic P-wave using data from the WWSSN network.

- Taking into account the station censoring information, considerable bias is apparent for the large explosions due to censoring by clipping, and for small events due to censoring by non-detection.
- When censoring information is considered, the m_b bias is 0.28 for m_b(a) *vs* m_b(b), 0.19 for m_b(b) *vs* m_b(max), and 0.48 for m_b(a) *vs* m_b(max). When censoring information is not considered, the m_b biases are on the average lower from a more scattered distribution.
- The station corrections for 127 WWSSN stations will be useful for the estimation of seismic magnitudes for other events not included in MLE-GLM88. It would be desirable in the future not to perturb the magnitudes of each previously determined event as new events are analyzed. In this regard, the WWSSN network constitutes a basis for comparison.
- Error estimations were performed using both the bootstrap and the EM algorithms. The m_b errors estimated using bootstrap are generally larger than those obtained from EM. The error estimates taking into account censoring information are generally larger than those obtained without considering censoring

information.

- This set of 111 events can be used to calibrate smaller networks for the purposes of test-site specific station corrections. Test site specific station corrections yield more precise relative magnitudes for a test site but are susceptible to offsets between test sites. However, care should be taken in deriving station corrections from a small number of events with limited geographic extent.

- The δm_b's between the "max" and "a" phases for a presumed cratering event may be low compared to the contained ones due to the weak surface reflections associated with a cratered explosion.

- The δm_b's between the "max" and "a" phases for a presumed double event may be larger than average due to the secondary arrivals.

- The potential for bias in determining magnitudes from a single test-site LS-GLM or even a single test site MLE-GLM was demonstrated for the Amchitka test site. The magnitudes of Cannikin and Milrow may be biased by 0.11 magnitude units high due to the geometry of the WWSSN network if a reduction is performed on the Amchitka test site only. Station corrections for a world-wide data set of explosions reduce the magnitudes of the largest Amchitka explosions by about 0.12 magnitude units.

- Because the "max" phase magnitudes depend so strongly on the non-linear free-surface interaction (pP+P), the "a" and "b" phase magnitudes are useful in establishing relative sizes of events with less concern for the independent estimation of pP/P relative amplitudes and pP delay times necessary to model the m_b(max)

magnitude for a given test site.

- Based on "a", "b", and "max" phase magnitudes, the two southern Novaya Zemlya events of 02 November 1974 and 27 October 1973 are 0.1 and 0.2 magnitude units (respectively) larger than the Amchitka explosion Cannikin. All three phases are consistent in this regard, and the conclusions based on the "a" and "b" phase are not dependent upon the interpretation of pP+P interference effects on the P waveform. The two northern Novaya Zemlya events of 12 September 1973 and 14 October 1970 are within 0.06 magnitude units of the same size as Cannikin based on "a" and "b" phase magnitudes. The "max" phase magnitudes of these two events are smaller than Cannikin. Since the "max" phase magnitudes depend on P+pP interference effects, the "a" and "b" phase magnitudes suggest that these two events are the same size as Cannikin and that the lack of pP+P constructive interference is responsible for the smaller "max" phase magnitudes of the largest events at the northern Novaya Zemlya test site.
- By incorporating inter-event correlation into the MLE-GLM88, the event magnitude estimates differ by an rms of less than 0.05 magnitude units and is insignificant compared to the overall error of the model. This indicates that the inter-event correlation perturbation may not be necessary when a large database is available.

8.0 ACKNOWLEDGEMENTS

The authors would like to acknowledge Dr. R. R. Blandford, Dr. I. N. Gupta, Dr. C. Lynnes and Mr. D. W. Rivers for their critical review and suggestions. The authors are grateful to Mr. K. Hutchison for furnishing some of the regional amplitude data for Cambric which aided in the analysis process.

9.0 REFERENCES

Blandford, R. R. and R. H. Shumway (1982), Magnitude-yield for nuclear explosions in granite at the Nevada Test Site and Algeria: joint determination with station effects with data containing clipped and low-amplitude signals, *VSC-TR-82-12*, Teledyne Geotech, Alexandria, VA.

Blandford, R. R., R. H. Shumway, R. Wagner, and K. L. McLaughlin (1984), Magnitude yield for nuclear explosions at several test sites with allowance for station effects, truncated data, amplitude correlation between events within test sites, absorption, and pP, *TGAL-TR-83-6*, Teledyne Geotech, Alexandria, VA.

Chan, W. W., K. L. McLaughlin, R. K. Cessaro, M. E. Marshall, and A. C. Lees (1988), Yield estimation of Novaya Zemlya explosions from short-period body waves, *TGAL-88-03*, Teledyne Geotech, Alexandria, VA.

Cormier, V. (1986), An application of the propagator matrix of dynamic ray tracing: The focusing and defocusing of body waves by three-dimensional velocity structure in the source region. *Geophys. J. R. astr. Soc.*, **87**, 1159-1180.

Dempster, A. P., N. M. Laird, and D. B. Rubin (1977), Maximum likelihood estimation from incomplete data via the EM algorithm, *J. Roy. Statis. Soc. B.* **39** 1-38.

Douglas, A. (1966), A special purpose least squares programme, *AWRE Report No. O-54/66, HMSO London.*

Efron, B. (1979), Bootstrap methods: Another look at the jackknife, *Ann. Statist.*, **7**, 1-26.

Efron, B. (1981), Censored data and the bootstrap, *J. Am. Statist. Assoc.* **76**, 312-319.

Gupta, I. N., K. L. McLaughlin, and R. Wagner (1985), Analysis of regional data from cratering and non-cratering nuclear explosions, *TGAL-85-05*, Teledyne Geotech, Alexandria, VA.

Heasler, P. G., R. C. Hanlen, D. A. Thurman, and W. L. Nicholson (1988), Application of general linear models to event yield estimation, *PNL-CC-1801-171*, Pacific Northwest Laboratories, Richland, WA.

Hurley, R. W. (1977), Anomalous seismic signals from Novaya Zemlya, *AWRE Report No. O21/77*, HMSO, London, England.

Jih, R.-S., D. Wilmer Rivers, and R. H. Shumway (1988), Network mb determination and uncertainty estimation: comparison of LSMF, ILS, MLE, and the bootstrap in doubly censored linear models, *TGAL-88-06*, Teledyne Geotech, Alexandria, VA. (in preparation).

Lilwall, R. C. (1985), Redetermination of body-wave magnitudes (m_b) for the period 1964-81 using ISC bulletin data, AWRE Report No. O21/85, HMSO, London.

Lilwall, R. C. (1986), Some simulation studies on seismic magnitude estimators, AWRE Report No. O22/86, HMSO, London.

McLaughlin, K. L. (1988), Maximum-likelihood event magnitude estimation with bootstrapping for uncertainty estimation, *Bull. Seism. Bull. Soc.*, **78**, 855-862.

McLaughlin, K. L., and L. M. Anderson (1985), Stochastic dispersion of P wave due to scattering and multipathing, *TGAL-85-08* Teledyne Geotech, Alexandria, VA.

McLaughlin, K. L., I. N. Gupta, and R. Wagner (1985), Finite difference cratering support: Magnitude determination of cratering and non-cratering nuclear explosions, *TGAL-85-03*, Teledyne Geotech, Alexandria, VA.

McLaughlin, K. L., R. O. Ahner, and M. Marshall (1986a), Maximum likelihood event magnitudes, and log(max/a) at the Novaya Zemlya and Degelen test sites, *TGAL-86-02*, Teledyne Geotech, Alexandria, VA.

McLaughlin, K. L., R. H. Shumway, R. O. Ahner, M. Marshall, T. W. McElfresh, and R. Wagner (1986b), Determination of event magnitudes with correlated data and censoring; a maximum likelihood approach, *TGAL-86-01*, Teledyne Geotech, Alexander, VA.

North, R.G. (1977), Station magnitude bias -- its determination, causes, and effects, Mass. Inst. Tech., Lincoln Laboratory, Technical Note 1977-24, Lexington, Massachusetts.

Ringdal, F. (1977), Maximum likelihood estimation of seismic magnitude, *Bull. Seism. Soc. Am.*, **66,** 789-802.

Ringdal, F. (1984), Norsar Semi-Annual Report, Royal Norwegian Council for Scientific and Industrial Research, Kjeller, Norway.

Ringdal, F. (1986), Study of magnitudes, seismicity, and earthquake detectability using a global network, *Bull. Seism. Soc. Am.*, **76,** 1641-1659.

Rodean, H. C. (1979), ISC events from 1964 to 1976 at and near the nuclear testing ground at Kazakhstan, Lawrence Livermore Laboratory Report, *UCRL-52856,* Livermore, CA.

Veith, K., E. Giller, and L. Hamilton (1987), Detection and identification needs for low yield Threshold Test Ban Treaty, Pacific Sierra Research Report, *1758,* Arlington, VA.

von Seggern, D.H., and D. W. Rivers (1978), Comments on the use of truncated distribution theory for improved magnitude estimation, *Bull. Seism. Soc. Am.*, **68,** 1543-1548.

(THIS PAGE INTENTIONALLY LEFT BLANK)

APPENDIX

NAME

mlglm --- maximum likelihood general linear model

SYNOPSIS

mlglm < input

DESCRIPTION

mlglm simultaneously computes maximum likelihood estimate of event magnitudes as well as station effects with data set including censored information and inter-event correlation. In fact, it is applicable to any **(general) linear models** of the form: M(i,j) = E(i) + S(j) + n(i,j) where E() and S() are unknowns to be estimated and M(,) the observed data matrix.

It uses E-M algorithms of Dempster et al. (1977) twice to solve the multiparameter version of a maximum likelihood estimation problem originally considered by Ringdal in 1976. In the first loop, the maximum likelihood estimates are computed based on observations without censoring information. This result is merely for comparison purpose only. While in the second loop, program recomputes the estimates with whole data set including the censoring information due to clipping and non-detection as described in VSC-TR-82-12. It is optional to adjust the result with inter-event correlation (TGAL-TR-83-06). Efron's (1979,1981) bootstrap method is then used to compute the uncertainty in the estimates. Old versions of this code have been utilized extensively in the past four years (c.f. VSC-TR-82-12, TGAL-TR-83-06, TGAL-86-01) and current version is called **mlglm6** which has been ported to and tested on various types of computers including Celerity 12600, VAX 11/780 and SUN 3/160 at Center for Seismic Studies .

A simplified version of the code, **mlglm7,** is also available in which we always bypass the incorporation of event-event correlation function with the linear model. This is due to the urgent need of processing of large database (about 300 events) which is far beyond the capacity of **mlglm6.**

SAMPLE INPUT FILE

```
Pmax,GLM_test, 9/1/1987
A0 A1 A2 output_flag
shoal.max.AT      26oct63  shoal       39.200n  118.380w
piledr.max.AT     02jun66  piledriver  37.230n  116.060w
rubis.max.AT      20oct63  rubis       24.000n   5.000e
saphir.max.AT     27feb65  saphir      24.060n   5.030e
```

here the first 2 lines give label (format a80), event-event spatial correlation parameters (free format) as well as the output terse level control. The inter-event correlation coefficient is defined as follows: A0/2 exp(-(d/A1)^2) + A0/2 exp(-(d/A2)^2 where A0, A1, and A2 are input parameters, and d the distance between two evnts of interest. An emipirically determined parameter set (A0,A1,A2) = (0.8,20km,500km) has been used in most of late calculations. Each of the remaining lines in the input file specify the event file name, date, event name, and geodetic coordinate of the event with format (a19,1x,a7,3x,a10,3x,f6.3,a1,2x,f7.3,a1).

Each event file contains a list of stations as well as the corresponding measurement with format (a5,a1,1x,f4.2) as shown in the following sample file:

```
aae  > 5.36
aku    5.53
alq    5.62
ant  < 5.39
aqu    4.71
are  < 5.16
atu    5.28
bhp  < 5.47
lah  < 5.64
lpa  < 6.27
```

pda < 5.93
qui > 6.23

DIAGNOSTICS

Output buffer fort.38 contains diagnostic message of SVD routines which would indicate how SVD handles matrix factorization, inversion, and synthesis.

Also, larger output_flag will give detailed intermediate output.

SEE ALSO

VSC-TR-82-12, TGAL-TR-83-06, and TGAL-86-01.

Source codes are stored in ~geotech/src/cmd/magy/GLM.

AUTHORS

R. H. Shumway, R. R. Blandford, and R. A. Wagner initialized the code design during 1982-1983. K.L.McLaughlin revised and extensively utilized the code during 1983-1985. R.-S. Jih debugged/documented the code and implemented SVD routines.

BUGS

mlglm6 needs huge memory and storage to execute when large data set is to be handled and intercorrelation correction is desired. While **mlglm7** has been used lately to invert 300 events and 150 stations, current upper limit on number of unknowns (i.e. stations plus events) that **mlglm6** can handle is about 280.

(THIS PAGE INTENTIONALLY LEFT BLANK)

DISTRIBUTION LIST
FOR UNCLASSIFIED REPORTS
DARPA-FUNDED PROJECTS
(Last Revised: 26 October 1988)

RECIPIENT	NO. OF COPIES
DEPARTMENT OF DEFENSE	
DARPA/GSD ATTN: Dr. R. Alewine and Dr. R. Blandford 1400 Wilson Boulevard Arlington, VA 22209-2308	2
DARPA/PM 1400 Wilson Boulevard Arlington, VA 22209-2308	1
Defense Intelligence Agency Directorate for Scientific and Technical Intelligence Washington, D.C. 20301	1
Defense Nuclear Agency Shock Physics Washington, D.C. 20305-1000	1
Defense Technical Information Center Cameron Station Alexandria, VA 22314	12
DEPARTMENT OF THE AIR FORCE	
AFGL/LWH ATTN: Dr. J. Cipar and Mr. J. Lewkowicz Terrestrial Sciences Division Hanscom AFB, MA 01731-5000	2

AFOSR/NPG
ATTN: Director
Bldg. 410, Room C222
Bolling AFB, Washington, D.C. 20332 — 1

AFTAC/DA
ATTN: STINFO Officer
Patrick AFB, FL 32925-6001 — 1

AFTAC/TT
Patrick AFB, FL 32925-6001 — 3

AFWL/NTESG
Kirtland AFB, NM 87171-6008 — 1

DEPARTMENT OF THE NAVY

NORDA
ATTN: Dr. J.A. Ballard
Code 543
NSTL Station, MS 39529 — 1

DEPARTMENT OF ENERGY

Department of Energy
ATTN: Mr. Max A. Koontz (DP-52)
International Security Affairs
1000 Independence Avenue
Washington, D.C. 20545 — 1

Lawrence Livermore National Laboratory
ATTN: Dr. J. Hannon and Dr. M. Nordyke
University of California
P.O. Box 808
Livermore, CA 94550 — 2

Los Alamos Scientific Laboratory 2
ATTN: Dr. K. Olsen and Dr. T. Weaver
P.O. Box 1663
Los Alamos, NM 87544

Sandia Laboratories 1
ATTN: Mr. P. Stokes
Geosciences Department 1255
Albuquerque, NM 87185

OTHER GOVERNMENT AGENCIES

Central Intelligence Agency 1
ATTN: Dr. L. Turnbull
OSI/NED, Room 5G48
Washington, D.C. 20505

U.S. Arms Control and Disarmament Agency 1
ATTN: Dr. M. Eimer
Verification and Intelligence Bureau, Rm 4953
Washington, D.C. 20451

U.S. Arms Control and Disarmament Agency 1
ATTN: Mr. Alfred Lieberman
VI-OA, Rm 5726
State Department Building
320 - 21st Street, NW
Washington, DC 20451

U.S. Arms Control and Disarmament Agency 1
ATTN: Mrs. M. Hoinkes
Multilateral Affairs Bureau, Rm 5499
Washington, D.C. 20451

U.S. Geological Survey 1
ATTN: Dr. T. Hanks
National Earthquake Research Center
345 Middlefield Road
Menlo Park, CA 94025

U.S. Geological Survey 1
ATTN: Dr. R. Masse
Global Seismology Branch
Box 25046, Stop 967
Denver Federal Center
Denver, CO 80225

UNIVERSITIES

Boston College 1
ATTN: Dr. A. Kafka
Western Observatory
381 Concord Road
Weston, MA 02193

California Institute of Technology 1
ATTN: Dr. D. Harkrider
Seismological Laboratory
Pasadena, CA 91125

Columbia University 1
ATTN: Dr. L. Sykes
Lamont-Doherty Geological Observatory
Palisades, NY 10964

Cornell University 1
ATTN: Dr. M. Barazangi
INSTOC
Snee Hall
Ithaca, NY 14853

Harvard University 1
ATTN: Dr. J. Woodhouse
Hoffman Laboratory
20 Oxford Street
Cambridge, MA 02138

Massachusetts Institute of Technology 3
ATTN: Dr. S. Soloman, Dr. N. Toksoz, and Dr. T. Jordan
Department of Earth and Planetary Sciences
Cambridge, MA 02139

Southern Methodist University 1
ATTN: Dr. E. Herrin
Geophysical Laboratory
Dallas, TX 75275

State University of New York at Binghamton 1
ATTN: Dr. F. Wu
Department of Geological Sciences
Vestal, NY 13901

St. Louis University 2
ATTN: Dr. O. Nuttli and Dr. R. Herrmann
Department of Earth and Atmospheric Sciences
3507 Laclede
St. Louis, MO 63156

The Pennsylvania State University 1
ATTN: Dr. S. Alexander
Geosciences Department
403 Deike Building
University Park, PA 16802

University of Arizona 1
ATTN: Dr. T. Wallace
Department of Geosciences
Tucson, AZ 85721

University of California, Berkeley 1
ATTN: Dr. T. McEvilly
Department of Geology and Geophysics
Berkeley, CA 94720

University of California Los Angeles 1
ATTN: Dr. L. Knopoff
Department of Earth and Space Sciences
3806 Geology
Los Angeles, CA 90024

University of California, San Diego 1
ATTN: Dr. J. Orcutt
Scripps Institute of Oceanography
La Jolla, CA 92093

University of Colorado 1
ATTN: Dr. C. Archambeau
CIRES
Boulder, CO 80309

University of Illinois 1
ATTN: Dr. S. Grand
Department of Geology
1301 West Green Street
Urbana, IL 61801

University of Michigan 1
ATTN: Dr. T. Lay
Department of Geological Sciences
Ann Arbor, MI 48109-1063

University of Nevada 1
ATTN: Dr. K. Priestley
Mackay School of Mines
Reno, NV 89557

University of Southern California 1
ATTN: Dr. K. Aki
Center for Earth Sciences
University Park
Los Angeles, CA 90089-0741

DEPARTMENT OF DEFENSE CONTRACTORS

Applied Theory, Inc. 1
ATTN: Dr. J. Trulio
930 South La Brea Avenue
suite 2
Los Angeles, CA 90036

Center for Seismic Studies 2
ATTN: Dr. C. Romney and Mr. R. Perez
1300 N. 17th Street, Suite 1450
Arlington, VA 22209

ENSCO, Inc.
ATTN: Mr. G. Young
5400 Port Royal Road
Springfield, VA 22151

ENSCO, Inc. 1
ATTN: Dr. R. Kemerait
445 Pineda Court
Melbourne, FL 32940

Gould Inc. 1
ATTN: Mr. R. J. Woodard
Chesapeake Instrument Division
6711 Baymeado Drive
Glen Burnie, MD 21061

Pacific Northwest Laboratories 1
ATTN: Dr. Wes L. Nicholson
Battelle Memorial Institute
P. O. Box 999
Richland, WA 99352

Pacific Sierra Research Corp. 1
ATTN: Mr. F. Thomas
12340 Santa Monica Boulevard
Los Angeles, CA 90025

Rockwell International 1
ATTN: B. Tittmann
1049 Camino Dos Rios
Thousand Oaks, CA 91360

Rondout Associates, Inc. 1
ATTN: Dr. P. Pomeroy
P.O. Box 224
Stone Ridge, NY 12484

Science Applications, Inc. 1
ATTN: Dr. T. Bache, Jr.
P.O.Box 2351
La Jolla, CA 92038

Science Horizons
ATTN: Dr. T. Cherry and Dr. J. Minster
710 Encinitas Blvd.
Suite 101
Encinitas, CA 92024 2

Sierra Geophysics, Inc.
ATTN: Dr. R. Hart and Dr. G. Mellman
11255 Kirkland Way
Kirkland, WA 98124 2

SRI International
ATTN: Dr. A. Florence
333 Ravensworth Avenue
Menlo Park, CA 94025 1

S-Cubed, A Division of
Maxwell Laboratories Inc.
ATTN: Dr. S. Day
P.O. Box 1620
La Jolla, CA 92038-1620 1

S-Cubed, A Division of
Maxwell Laboratories Inc.
ATTN: Mr. J. Murphy
11800 Sunrise Valley Drive
Suite 1212
Reston, VA 22091 1

Teledyne Geotech
ATTN: Dr. Z. Der and Mr. W. Rivers
314 Montgomery Street
Alexandria, VA 22314 2

Woodward-Clyde Consultants
ATTN: Dr. L. Burdick and Dr. J. Barker
556 El Dorado St.
Pasadena, CA 91105 2

NON-U.S. RECIPIENTS

National Defense Research Institute FOA 290 — 1
ATTN: Dr. O. Dahlman
Box 27322
S-10254 Stockholm, Sweden

Blacknest Seismological Center — 1
ATTN: Mr. P. Marshall
Atomic Weapons Research Establishment
UK Ministry of Defence
Brimpton, Reading, Berks. RG7-4RS
United Kingdom

NTNF NORSAR — 1
ATTN: Dr. F. Ringdal
P.O. Box 51
N-2007 Kjeller
Norway

OTHER DISTRIBUTION

To be determined by the project office — 9